MUSCLE FORCE ESTIMATION AND FATIGUE DETECTION BASED ON sEMG SIGNALS

BAI FENGJUN

(*B.Eng, NEU*)

A THESIS SUBMITTED

FOR THE DEGREE OF DOCTOR OF PHILOSOPHY

DEPARTMENT OF MECHANICAL ENGINEERING

NATIONAL UNIVERSITY OF SINGAPORE

2013

DECLARATION

I hereby declare that the thesis is my original work and it has been written by me in its entirety.

I have duly acknowledged all the sources of information which have been used in the thesis.

This thesis has also not been submitted for any degree in any university previously.

Bai Fengjun

3 February 2014

Acknowledgements

First and foremost, I sincerely thank Prof Chew Chee Meng, my inspirational supervisor, for his enthusiastic and continuous support and guidance. I am grateful for his constant encouragement, suggestions, ideas and critical comments for the progress of my Ph.D. study. With his valuable supervision and personal concerns, I had a meaningful and fruitful academic journey.

I also want to thank Mrs. Ooi, Mdm. Hamidah and Mr. Sakthi, in Control and Mechatronics Lab for their help and support. I appreciate very much to Dr. Effie Chew, Dr. Teo Wei Peng and Mrs. Zhao Ling from National University of Singapore (NUH), without them, my data collection experiments from stroke patients would not be possible. Meanwhile, their constructive suggestions and ideas help me on the patients experiments, and they provide me with valuable clinical knowledge.

I am grateful to all my friends and colleagues from NUS. Especially, I appreciate the support in my research from Dr. Tomasz Marek Lubecki, Shen Bingquan and Li Jinfu. Without their help and long discussion about research, I would not have carried out this Ph.D. work smoothly. I also want to thank all students in Control and Mechanics lab who have supported me in the four years study. I am also very grateful to the examiners of this thesis for their reviews and helpful feedbacks.

Finally, I would like to thank my dear parents, for their unwavering support, encouragements and love that have provided me the strengths to move forward throughout my whole life.

Table of Contents

Summary

As command signals from the motion control system of human, transmitted to muscles through the motor nerves, surface Electromyography (sEMG) signals are commonly used in muscles relevant studies, such as sports, clinical decision-making, biofeedback, gait analysis and human-machine interface (HMI). Knowledge of internal forces and moments during movements is important to develop better active and intuitive assistive and rehabilitation devices. The ability to predict the muscle forces is beneficial to the control system by using the estimated human intention. In addition, localized muscle fatigue occurs after prolonged and relatively strong muscle activity. Therefore, muscle force estimation and fatigue detection are considerably important for biofeedback and HMI of assistive device and rehabilitation.

The aim of this study is to investigate the relationships between the sEMG signals features and muscle force using a time-frequency analysis method, and to explore novel approaches to predict muscle force and detect muscle fatigue. In addition, real-time implementation of the force estimation and fatigue detection methods are carried out to test and validate the feasibility of the algorithms using online sEMG signals.

Three relationships, sEMG amplitude-force relationship, mean frequency (*MF*) and force relationship, and the relationship between frequency parameters and signal energy distribution (*MF*-power relationship) are first investigated in this thesis. The results show that these relationships are nonlinear from both time-domain method and time-frequency analysis method with high regression correlation coefficients R^2 values. In addition, the influence of electrode locations on these relationships is studied, since the sEMG signal amplitude and frequency features are very sensitive to small electrode displacements. Statistical analysis results demonstrate that the electrode locations affect these

relationships with different regression fitting R^2 values. In addition, the relationships established from the electrode located in the innervation zone shows higher R^2 values.

Several approaches are explored to predict muscle force/torque in this study. The time-domain force estimation method (windowed RMS) is based on the amplitude-force relationship, while the time-frequency analysis method is based on the MF-force relationship using continuous wavelet transform (CWT). When comparing the two methods, force estimation results from off-line sEMG signals show high correlation coefficients from the CWT-based method between the estimation force and measured force. T_f is also calculated which describes the time difference between the estimated force and the measured force. Longer T_f is found from the proposed frequency domain method, and the estimated force leads the measured force by a few milliseconds. This long T_f ensures the prediction of the muscle force in advance or concurrently to the actual applied force, which is important if sEMG signal is used in rehabilitation device as the control signal. Another force prediction method is developed based on CWT and artificial neural networks (ANN). The filtered *MF* and measured force are the input signals for network training. Results also show high correlation coefficients between the estimated force and measured force for both healthy subjects and stroke patients.

A novel muscle fatigue detection approach is explored using a time-frequency analysis method from sEMG signals during various muscle contraction conditions for both the healthy and stroke subjects. General fatigue levels are first obtained indicating the fatigue changes in muscles. These fatigue levels are quantified to the muscle maximal capacity based on linear regression and statistical analysis, which enables the proposed algorithm to describe the fatigue progresses as close as the changes of the real physiological fatigue.

The proposed methods are finally implemented and tested using the on-line sEMG signals in real-time. When the CWT-based force estimation approach is implemented with the lower limb rehabilitation robot, real-time experimental results illustrate that the assistive device assists the subjects with proper torque according to their intention. In real-time, fatigue detection results are generally in line with the off-line results, which provide significant potential of implementation in rehabilitation device.

List of Tables

List of Figures

Acronyms

sEMG	Surface Electromyography
HMI	Human machine interface
AP	Action potential
CNS	Central nervous system
MU	Motor unit
MUAP	Motor unit action potential
CMRR	Common mode rejection rate
RMS	Root mean square
MAV	Mean absolute value
MF	Mean frequency
PDS	Power density spectrum
CC	Correlation coefficients
RMSE	Root mean square error
ANN	Artificial neural networks
MVC	Maximum voluntary contraction
CWT	Continuous wavelet transform
ANOVA	Analysis of variance

List of Symbols

m	End point of the window
k	Beginning point of the window
n	Window length
x	Sample of sEMG signal
$s(t)$	Input signal example
T_f	Average time difference between the estimated force and the measured force
T_m	Average time difference between the filtered *MF* and the measured force
$\varphi_{a,\tau}(t)$	CWT window function (daughter wavelet)
$W_s(a,\tau)$	CWT output (CWT coefficients)
a	Scale parameter
b	Temporal translation parameter
$\varphi(t)$	Mother wavelet
f_s	Sampling frequency
f_0	Center frequency of the wavelet at scale a=1
f_a	Pseudo frequency corresponding to wavelet scale a
$E(a,b)$	Scalogram
P	Signal power
$P*$	Estimated signal power

ω	Frequency variable
F	Nyquist frequency
L_a	Scale length
E_m	Threshold value (Maximum value of the scalogram)
R^2	Square of the coefficient of multiple correlations
y_i	Measured force
$\hat{y}_i$	Estimated force

CHAPTER 1

INTRODUCTION

1.1 Background and Motivations

Human movements such as walking, squatting or lifting heavy loads are accomplished by contracting skeletal muscles. Measurements on contracting muscles of interest are very important in many fields of application such as sports, clinical decision-making [1], biofeedback [2], gait analysis and human-machine interface (HMI) [3]. In assistive device or rehabilitation robotic devices, HMI is commonly used as the interaction between human and device. Thus, measuring the forces applied to a joint and predicting the force generated by the muscles are vital for an intuitive HMI, since they are the commonly used ways to detect human intention. However, to record force generated by muscles directly is currently infeasible. Currently, special force sensors are required to measure the individual forces exerted by muscles. In addition, most of the commercial force or torque sensors are bulky, expensive, inconvenient and not user friendly. Therefore, a muscle force estimation method should be developed to avoid using such force sensors. Nevertheless, muscle fatigue occurs when muscles are under a prolong contractions.

Muscle fatigue is the reduction in the ability of a muscle to generate force or to maintain a target force [4, 5]. Generally, localized muscle fatigue occurs after a prolonged and relatively strong muscle activity. Consequently, the accumulation of long periods of fatigued contractions can lead to muscle pain and even an increased risk of injuries [6].

Such sudden accidents and injuries can be avoided by continuously monitoring the progression of muscle fatigue, which is able to inform the users in advance. Moreover, in application field, if human muscles are involved in the HMI for rehabilitation device, it is essential to detect muscle fatigue and estimate the fatigue levels to moderate the output torque of such devices.

Electrical currents are produced by muscle fibers prior to the generation of muscle force. These small currents are generated by exchanging the ions across muscle fiber membranes, which is a part of the signal processing for the muscle fibers to contract [7]. The signal associated with muscle contraction is called the electromyography (EMG). Generally, the EMG signals can be measured by applying conductive elements or surface electrodes to the skin surface, or intramuscular measurements. To measure intramuscular EMG, needle electrodes or a needle containing two fine-wire electrodes is inserted through the skin into the muscle tissues invasively. Physiotherapists must be involved to observe the electrical activities while inserting the electrodes. In order to minimize the risk to the subjects and to simplify the signal measurement procedures, surface EMG (sEMG) is the more commonly employed measurement method. Since sEMG signal is unique in revealing what a muscle actually does at any human movement or posture [8], it has been widely employed in recent decades to predict human limb movements and the amount of force required to accomplish a task, and to track muscle state, from non-fatigue to fatigue [9]. There are many variables that can influence the signal at any given time: velocity of shortening or lengthening of the muscle, rate of tension buildup, fatigue, and reflex activity [10].

Currently, sEMG signals generated from healthy humans are widely investigated. However, the analysis of sEMG signals from stroke patients for predicting muscle force and estimating fatigue has not been studied comprehensively. In recent years, stroke has become a leading cause of chronic and serious disabilities. Most of the stroke patients' movements are abnormal, and there are dramatic structural changes in skeletal muscles after stroke. Due to the hemiparesis and one-side motor impairment of the body, the patient's daily activities are usually affected. Shaughnessy et.al [11] found that nearly

two thirds of stroke survivors experience a limitation in walking. Stroke also leads to long-term complications of falls, osteoporosis, contractures, depression and cardiovascular complications. Hence, to develop a lower limb rehabilitation device is significant for stroke patients gait training. An active and intuitive assistive device where sEMG signals play an important role in the HMI, especially enables a more efficient gait training. However, muscular atrophy due to stroke reduces the amplitude of sEMG signals measured from the stroke patients. Therefore, it is still a great challenge to estimate muscle force generated from the affected side muscles of stroke patients using sEMG signal. In addition, it is necessary to understand and investigate the changes of sEMG characteristics during muscle fatigue processes for stroke patients.

1.2 Objectives and Scope

From current research studies, different approaches have been proposed to estimate the force/torque generated by muscles and assess muscle fatigue. However, there are still some issues to be resolved, they are as follows:

- The relationships between force and sEMG features during muscle voluntary contractions, so far, have not been studied comprehensively. The sEMG amplitude-force relationship was found to be linear or parabolic curves. However, the relationships between sEMG spectral parameters and force, especially for both healthy subjects and stroke patients, are not well understood. Furthermore, in frequency domain, to the author's knowledge, there is no intensive research study that correlates the change in signal frequency to the energy distribution of the sEMG signal.

- If the human intention detected from sEMG is used for HMI in assistive device or rehabilitation robotics, it is essential to predict muscle force in advance or concurrently to the actual exerted force. Currently, most of the research works investigate muscle force estimation without considering the prediction of muscle force before the force is measured. If proper signal processing method is

developed, the force generated by muscles can be predicted in a few milliseconds before the actual force is applied. Moreover, most of the current force estimation approaches are based on time domain analysis, whereas, the time-frequency analysis method for muscle force prediction has not been investigated, even though time-frequency analysis method is proved to be more suitable for extracting features from non-stationary signal.

- Due to the variability of the muscle characteristics from person to person, there is no simple or suitable function based on muscle load and timing that can describe muscle fatigue progress precisely between subjects. Therefore, how the muscle fatigue progress changes from non-fatigue state to fatigue state is still unclear. In addition, for the types of muscle contraction aspect, most of fatigue detection studies concentrate on constant force contraction, while varying force is hardly comprehensively investigated. Meanwhile, only few studies have documented fatigue assessment methods in persons with hemiparesis due to stroke.

A detailed survey of relevant literature works and specific gaps will be covered in Chapter 2.

The main purpose of this thesis is to develop novel methods for muscle force estimation and fatigue detection based on continuous wavelet transform (CWT) using sEMG signals, and implement the proposed algorithms in real-time.

There are many factors influencing the experimental protocol and results. In this thesis, the focus will be on investigating both muscle force estimation method and muscle fatigue assessment approach with single and specific muscles. Other aspects such as muscle co-contractions will not be considered. Meanwhile, some other factors such as gender, age, weight are not taken into account. In this thesis, the muscle groups of interest are the main muscles that are relevant to elbow and knee flexion/extension, namely, biceps brachii, triceps brachii, rectus femoris, and triceps femoris.

The specific objectives of this research are to:

- Establish the relationships between sEMG features and force using linear regression. These relationships are the sEMG amplitude-force relationship, and sEMG spectral frequencies and force relationship, respectively. Another relationship will only focus on the sEMG frequency domain features, sEMG spectral frequency and signal power relationship. Furthermore, the influences contributed by difference electrode locations on these relationships are also investigated. This will help the selection of the most suitable electrode location.

- Investigate possible approaches which can predict force/torque exerted by muscles for healthy subjects and stroke patients. T_f describes the average time difference between the estimated force and the measured force from force sensor. The T_f value, correlation coefficients, root mean square errors between the measured force and estimated force are calculated to evaluate the efficiency of the force estimation methods.

- Explore possible approaches which can detect muscle fatigue using sEMG collected from muscles under constant and varying force contractions. General estimated fatigue levels are marked to track the progress of muscle fatigue. sEMG characteristics changes during fatigue process is also to be investigated. In addition, the same approach with modified parameters is applied to detect stroke patients muscle fatigue of stroke patients with sEMG signals from the affected leg muscles during isometric contraction and varying force contraction.

- Implement the force estimation method and fatigue detection approach in real-time and test with online sEMG signals. The CWT-based force estimation method is implemented in a new wearable lower extremity assistive device for rehabilitation. Proper assistive torque will be provided according to the user's intention to control the knee joint in real-time. In addition, isometric and force-

varying contractions until fatigued are performed to validate the feasibility of the fatigue detection method in real-time.

1.3 Thesis Contributions

The results of this study contribute to the development of novel force estimation methods and fatigue assessment approaches for both healthy subjects and hemiplegic patients after stroke. Specifically, the contributions of this thesis are summarized:

- Establish the relationships between sEMG features and force, and relationships between frequency parameters and signal energy distribution for healthy subjects and stroke patients. The relationships with frequency domain features are able to interpret the association between sEMG and force from a new point of view. The influence on these relationships from different electrodes locations are also detailed studied in detail.

- Explore new methods of muscle force estimation for healthy subject and stroke patients. A long T_f value ensures the force is predictively in advance or concurrent to the measured force, implying that there is a high potential for application in a rehabilitation device.

- Propose new approach which can detect muscle fatigue based on continuous wavelet transform for healthy subjects and stroke patients. Quantified fatigue levels make the fatigue assessment much closer to the real physiological fatigue changes.

- Successfully implement the proposed force estimation on a lower limb rehabilitation robotics. The proposed fatigue detection algorithm works well in tracking the muscle fatigue states by showing the general estimated fatigue levels.

1.4 Thesis Organization

This thesis is organized as follows:

Chapter 2 first gives a general introduction of sEMG signal. Then, a detailed literature review of different sEMG analysis methods for estimating muscle force and detecting muscle fatigue is presented.

Chapter 3 establishes the relationships between sEMG features and force with time domain and frequency domain analysis, respectively. Meanwhile, the relationships between the frequency parameters and signal energy distribution are also established. Newly developed based-line noise removal algorithm will be presented first. Then, the detailed description of the experimental protocol for collecting sEMG signal is provided. The methods to establish these relationships are mentioned in the following section. Lastly, results of the effects of different electrode locations on these relationships will be illustrated and discussed.

Chapter 4 provides a comprehensive description of the proposed muscle force estimation method for healthy subjects and stroke patients. The experimental protocol of sEMG signal collection for force estimation is first described in detail. Evaluation on the feasibility of the proposed methods will be carried out by calculating the root mean square error and correlation coefficients. The proposed CWT-based method is also compared with the traditional time-domain method. The ability to estimate the muscle forces in healthy subjects and patients following stroke will benefit the development of assistive device for rehabilitation.

Chapter 5 gives a detailed description of the proposed fatigue detection approach. First, different fatigue experimental protocol is presented. The sEMG data from the experiments are employed to test the feasibility of the proposed method. The results and statistical analysis shows the discrete fatigue levels keep increasing with the raising progress of fatigue. These fatigue levels are quantified using regression and statistical

analysis methods. The same fatigue assessment method is also applied to detect fatigue for stroke patients, which is presented in the rest section of this chapter.

Chapter 6 presents the results of implementing the force estimation method real-time on a lower extremity rehabilitation device. The results of the real-time implementation are yielded by performing different muscle contraction tasks. In addition, the fatigue detection algorithm is implemented in real-time, the results show that the subjects fatigue levels keep increasing, which are in line with the off-line performance.

Chapter 7 concludes the contributions of this thesis and outlines the directions for future studies.

CHAPTER 2

LITERATURE REVIEW

2.1 Introduction

This chapter covers in detail the research studies mentioned in the introduction. Utilizing sEMG signals to predict muscle force and assess fatigue requires a deep understanding of muscles and the way they generate bioelectrical signals. Thus, the review starts with the elaborate knowledge of sEMG signal. This part includes the basic principle of sEMG signal generation, physiology mechanisms, the factors and phenomena that contribute to this signal, and the wide spread application of this signal. Section 2.3 reviews some developed approaches towards estimating the muscle force using sEMG signal. In Section 2.4, different advanced signal processing methods to detect muscle fatigue will be introduced. The physiological changes in sEMG signals for both the healthy subjects and stroke patients under muscle fatigue will also be highlighted in this section.

2.2 EMG Signals

2.2.1 Physiology Mechanism of Signal Generation

EMG signal is one of the electrophysiological signals, which is extensively studied and applied in clinic and engineering. The basic use of EMG signal is in physiological and biomechanical studies. In addition, it is also widely employed in sport training, gait &

posture analysis [12], physical therapy [13], and rehabilitation [14]. This signal represents the electrical activity generated when skeletal muscles contract after an action potential (AP) stimulated by the muscle fibers [8].

The central nervous system (CNS) controls all the muscle activities in the human body (be its contraction or relaxation). This system, which is responsible for the activation of muscle fibers, carries the electrical pulses from the brain to the muscles [15]. Motor neuron, situated in the spinal cord, has a long axon,combines with other axons in a nerve to the muscle. A skeletal muscle is composed of thousands of tiny muscle fibers, groups of which are innervated by a single alpha-motor neuron. These two components, a single motor neuron and all the muscle fibers it innervates, compose a motor unit (MU) which is the smallest functional unit to describe the neural control of the muscular contraction process [16].

Figure 2.1 illustrates the simplified schematic diagram of the CNS and the background concept of MUs [17, 18]. When a MU is electrically activated, a measurable electrical potential called action potential (AP) is carried down from the motor neuron to the muscle [17, 19, 20]. The generated APs emerge at the neuromuscular junction in the middle of the muscle body, and propagate along the muscle fibers to both directions towards the muscle tendons. The superimposition of all the electrical activity is called the motor unit action potential (MUAP) [21]. In one MU, all the muscle fibers are fired when the MU fires. The repetitive firing of a MU creates a train of pulse which is known as the motor unit action potential train. The temporal summation of electrical activity created by each MU is the EMG signal.

EMG signal can be detected by invasive electrodes or surface electrodes. The invasive electrodes, which are also known as intramuscular electrodes since they are inserted directly into the muscle, allow for the electrical potentials detection close to the source. However, in order to choose the most accurate electrodes locations for inserting the electrodes, a well-trained physical therapist should be involved in data collection experiments. Conversely, surface electrodes which are attached to the skin surface, are easy handling and enable us to simplify the data measurement procedures. Due to these

benefits, surface electrodes are commonly used in research studies. Most of the important limb and trunk muscles can be measured by surface electrodes. The basic diagrams of the main muscles are shown in Figure 2.2.

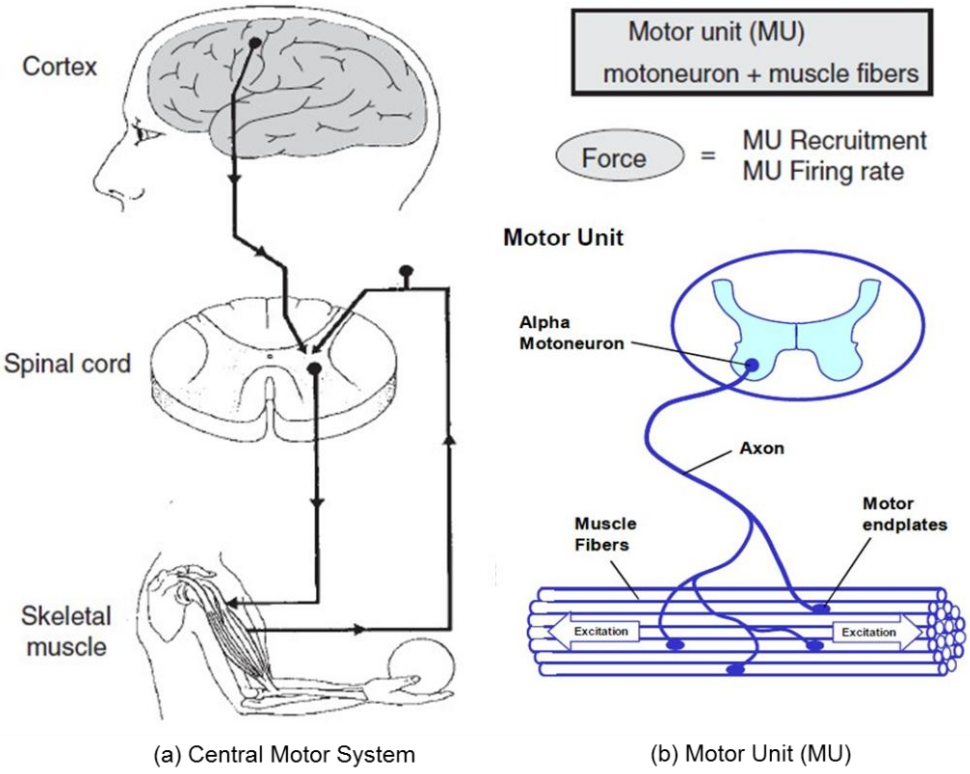

Figure 2.1 Simplified schematic diagram of the basic motor control mechanism, motor unit and its components (Modified from [17, 18]).

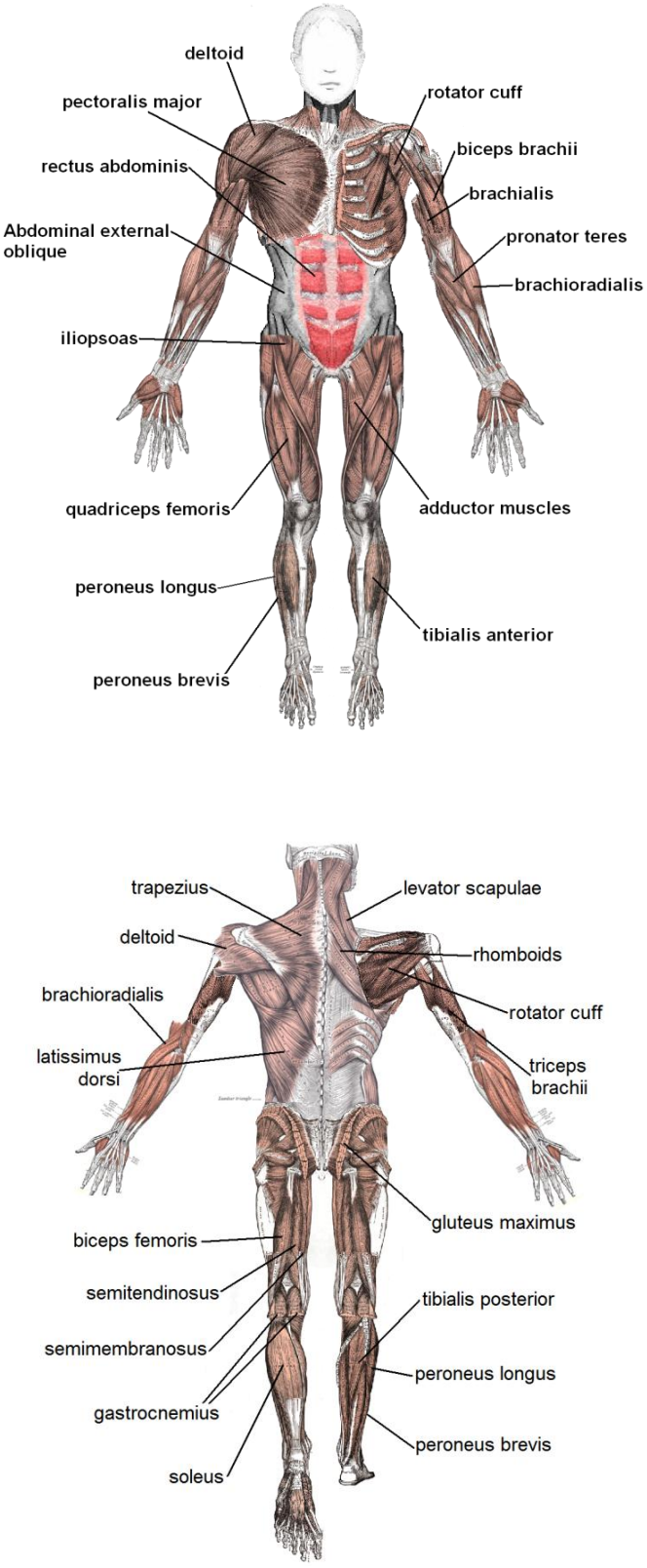

Figure 2.2 Basic diagrams of the human main muscles.

2.2.2 sEMG Signal Characteristics and Measurements

Raw sEMG signal is an unfiltered and unprocessed signal generated from the superimposed MUAPs [17]. By its nature, raw sEMG spikes are of random shape. The amplitude of the raw signal is about 0 to 10 mV (peak-to-peak) [8, 22]. The usable energy of the signal is limited typically to around 6 to 500 Hz frequency range, and most of the sEMG frequency dominant power is located between 10 to 250 Hz.

Since the approximate usable frequency range of this signal is 6-500 Hz, the sampling rate is usually at least twice as high as the maximum expected frequency of the signal. This sampling frequency ensures that the signal frequency spectrum is translated completely by the processing unit. Accordingly, the minimum sampling frequency is typically set to be 1 KHz or higher [19, 22].

When working with sEMG signal, several external factors which alter its shape and characteristics should be taken into account. Konrad [17] summarized the basic influencing factors as follows:

1) Tissue characteristics;
2) Physiological crosstalk;
3) Changes in the geometry between muscle belly and electrode site;
4) External noise;
5) Electrode and amplifiers;

Most of these influencing factors can be minimized or controlled by well-designed circuit and skin preparation. sEMG signal is easily affected by various sources of noise. First, all electronics equipment generates electrical noise which cannot be eliminated. It can only be reduced by applying high quality electronic components, intelligent circuit design and good construction techniques. Another noise is the ambient noise which originates from sources of electromagnetic radiation, such as televisions, computer monitors, motors, electrical power lines, fluorescent lamps or light bulbs. This kind of noise cannot be avoided. The ambient noise frequency occurs primarily within the range of 50 Hz or 60

Hz [22], while the amplitude of the ambient noise is about one to three times greater than that of an sEMG signal. Lastly, the interface between the detection surface of electrodes and skin, the movement of the cable connecting the electrodes to the amplifier, are another two main sources contributing to the motion artifacts. Since the dominant energy of the motion artifacts is distributed in a frequency range from 0 to 20 Hz, it can be reduced by using low-pass filters.

Currently, the advent of modern electronics and differential amplification have enabled the measurement of sEMG signals with low noise and high signal fidelity. In practice, it is possible to measure the full effective bandwidth of the signal with differential amplifier. Generally, the signal should be amplified using high common mode rejection rate (CMRR), and the high input impedance in the analogue circuit [22]. Typically, the band-pass filter ranges are from between 10 and 20 Hz (high-pass filtering) to between 500 and 1000 Hz (low-pass filtering) [23].

2.2.3 Stroke Patients sEMG Signals

The affected muscles in stroke patients are commonly very weak. This muscle weakness can be related to both the interruption of the corticospinal tract and muscle atrophy [24]. The impairment and disability affect the muscle strength in a group of chronic stroke survivors. This neurological disorder is accompanied by a diminished ability to sustain voluntary contractions. The damaged CNS of the post-stroke patient causes a lack in the central drive of the muscle during muscular contractions. Consequently, the contractions in muscle itself are limited, and the detected output sEMG signal are limited as well [25]. Meanwhile, muscular atrophy due to stroke reduces the amplitude of sEMG signals measured from the stroke patients, which makes the muscle force estimation be a great challenge. The physiology of muscle fatigue in post-stroke patients will be discussed in fatigue section (Subsection 2.4.4).

2.3 Muscle Force Estimation Methods

To utilize sEMG signal to detect human intention and to command motors of rehabilitation devices, the force generated from muscles are the key information contributed to the control scheme. However, currently, muscle force cannot be easily measured in vivo, because it is inside the human body, and it is difficult to be assigned to a specific muscle due to complex actions in which involve a large number of muscles [26]. In addition, special force sensors might be able to measure the force exerted by muscles, but most of the commercial force transducers are bulky, expensive, inconvenient and not user friendly. Moreover, solely using sEMG signal to predict muscle force directly does not yield accurate results. Therefore, the force exerted by muscles must be assessed, calculated and modeled. To access the force generated by muscles, it is necessary to investigate the relationship between force generated by muscles and the corresponding sEMG signals. Based on these relationships, muscle force can be estimated or predicted.

2.3.1 sEMG Features and Force Relationship

The electrical activity associated with a muscle can be observed using electrodes on the skin surface. This electrophysiological activation of a muscle initiates the production of mechanical force. Considering most of the applications of sEMG signal for muscle force prediction, assumptions are made that there is a relationship between sEMG signals and underlying muscle forces. Generally, the relationship between sEMG features and force is divided into two fundamental branches, sEMG amplitude and force and sEMG spectral frequencies and force.

2.3.1.1 sEMG Amplitude and Force

Two main mechanisms contribute to the control of muscle force: the recruitment of additional MUs and the increasing firing rate of the already active MUs. For different muscles, these two mechanisms are presented in different proportions, which may have

different effects on both sEMG signal amplitude and force [27]. The sEMG signal amplitude depends on both the number of active MUs and their firing rates. sEMG amplitude features are commonly extracted using root mean square (RMS) or mean absolute value (MAV).

Since both sEMG amplitude and force changes because of the same mentioned mechanisms, there is a very high correlation between force and sEMG signal amplitude. Most of the sEMG amplitude-force relationship research studies are based on the early work of Inman et.al and Bigland [28, 29]. Their investigations demonstrate that there is a linear relationship between force and sEMG amplitude. Some literatures concluded that, for various muscles, the magnitude of the sEMG signal is directly proportional to muscle strength for isometric contractions with a constant speed [30-32]. While others found that this relationship is nonlinear [19, 33-37], [38].

More specifically, Hof and Van Den Berg [39] found a linear association between triceps surae muscle sEMG and ankle plantar moment, when the weighted sum of all heads of the triceps muscle was considered. On the other hand, when they analyzed the sEMG signal of each head separately, nonlinear relationship was obtained. In some skeletal muscles that control fingers, the relationship between force and sEMG amplitude was found to be linear [40]. Bell and Eloranta et.al [41, 42] investigated the individual muscles of the quadriceps femoris during isometric knee extension. Their results illustrated that the relationship is nonlinear, such that sEMG amplitude increases out of linear proportion to force. Figure 2.3 shows a typical case of force testing with static force. A highly reproducible relationship between the forces exerted at the wrist and the sEMG activity of the biceps muscle is curvi-linear is shown. At the higher force portions, more sEMG is needed to generate higher force [43].

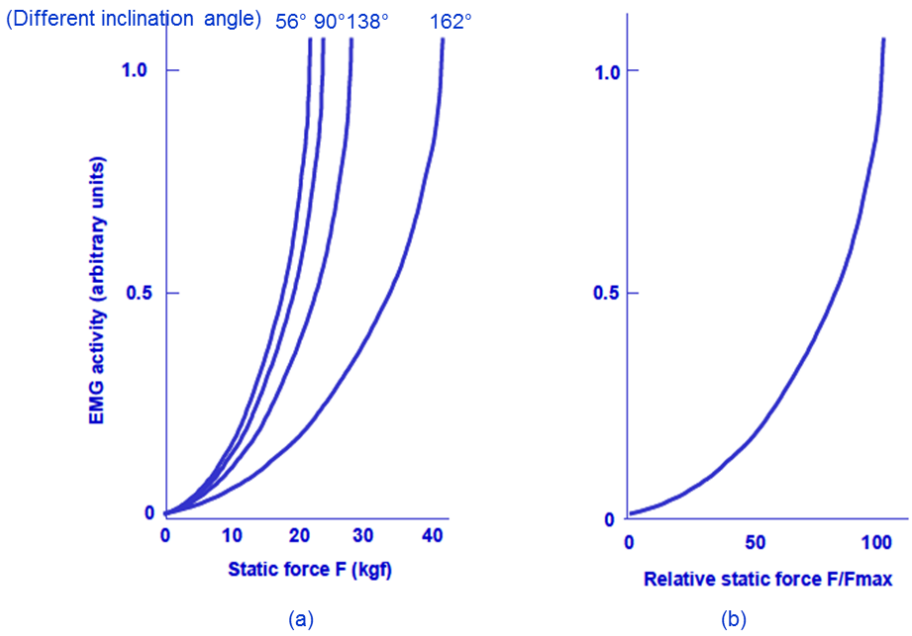

Figure 2.3 (a) sEMG activity as a function of force *F* under isometric conditions. The different curves related to different arm angles meaning different muscle length of biceps. (b) The normalized F/F_{max} in relation to the sEMG activity values [43].

2.3.1.2 sEMG Spectral Frequencies and Force

Most studies on the sEMG-force relationship focus on the associations between the sEMG signal amplitude and force. In contrast, the relationships between force and sEMG frequency domain features are not widely investigated. The superposition of the spectral densities of the MUAP represents the power spectral density of the interference sEMG signal [27]. Alternatively, when the force increases, the activation frequency of the muscle fiber recruitments will be increased. In non-fatigued muscle state, some literature studies found that there is an increase of spectral variables (e.g. mean frequency) with increasing force target [33, 44-47], while others showed no increase or even decrease of mean frequency (*MF*) [33, 48].

Solomonow et al. [49] reproduced the natural recruitment process in the cat's gastrocnemius muscle experimentally using electrical stimulation. The results demonstrated a linear increase in the median frequency (*MDF*) of the power density spectrum (PDS) when the motor units were recruited progressively. Bilodeau et al. [50] investigated the changes of sEMG frequency contents with the increasing force generated

from the quadriceps femoris muscles of both male and female. The increasing mean power frequency (MPF) was observed with the ramp up muscle contraction force.

Generally, most studies aim to develop a suitable method to estimate the force exerted by muscles using sEMG-force relationships. Multiple studies can be found in [26, 36, 38, 51, 52] and good force estimation results can be observed. However, for these force estimation methods, most sEMG signals features are derived in the time domain, while the force estimation approaches using frequency-domain features are quite few. In addition, only a few current studies consider the T_f values between the estimated force and the measured force. Whether the frequency domain method provides longer T_f values than the time-domain method has never been investigated comprehensively. Here T_f describes the average time difference between the estimated force and the measured force from force sensor.

2.3.2 Other Methods

Instead of investigating the relationship between sEMG features and force for force estimation, some other force estimation methods have been developed by applying musculoskeletal models. These models consider the effects of muscle length and muscle contractile speed on the force, and extract a function to transfer the activation to the force. Muscle models explain how the muscles act together to produce the exerted force. They have been developed to estimate force for knee [9, 53, 54], elbow [55] and lower back [56] specifically. Lloyd and Besier [9] developed an modified Hill-type muscle model to estimate knee moments and muscle forces, using activation and muscle tendon lengths as the inputs for healthy subjects during dynamic tasks. The results illustrated that it is a possible way to estimate muscle forces and predict the knee joint moment for a range of tasks.

The development of muscle models requires validation from some external kinematic or dynamic data measured by dynamometers or other sensors. Moreover, during muscle movements, time and frequency features of the signals are influenced by muscles and the

activation manners of muscle fibers. At the same time, problems may be induced by making assumptions about some unknown nonlinear parameters that cannot be measured experimentally. Under different circumstances, the unknown properties may lead to undesirable influences on the force estimation. Currently, musculoskeletal models have been used to investigate movement dynamics for healthy individuals. It is still unclear if this approach could be used to estimate muscle forces produced by post-stroke patients.

Artificial neural networks (ANN) is another commonly applied approach for estimating muscle force. ANN has been used to map complicated relationships successfully in biomechanics research studies [57-59]. It is able to extract features from complicated signals and acts as a black box model to approximate the complex nonlinear mappings directly from the input signals. Furthermore, no detailed information such as the mathematical expression that relates the sEMG signals to the muscle force is involved when using ANN. Thus, no need to derive any complex functions to describe the relationships. The first use of ANN for muscle force estimation was reported in [58]. Savelberg et al. [60] employed multi-layer perceptron artificial neural networks (MLPANN) with back propagation (BP) training for cat leg dynamic tendon force estimation, using recorded EMG data and kinematic information (joints angle and velocity). Palmar pinch force was estimated in real-time by Choi et al. [61] with ANN, and good estimation results were obtained. The training target was the measured force during palmar pinch, while the amplitude of sEMG worked as the training input data. Luh et al [62] constructed a three-layer feed-forward network with an adaptive learning rate to map the relations between the isokinetic elbow joint torque and the sEMG activity.

Nevertheless, in most of these studies, the characteristics extracted from sEMG signals are limited to the time domain, while the frequency domain features, such as *MF*, *MDF* are seldom involved for muscle force estimation. Moreover, most of these present works are carried out with healthy subject muscles, there should be significant and meaningful outcomes if post-stroke patients sEMG signals are studied.

2.4 Muscle Fatigue Detection Methods

As being one of the most common phenomena with substantial impacts on human daily life, muscle fatigue has attracted much attention since the beginning of last century. Recent advances in physiological studies have demonstrated the significance of detecting or predicting muscle fatigue in various aspects of our lives, including sports, rehabilitation and ergonomics. Various signal analysis methodologies are developed to assess fatigue non-invasively using sEMG signals recorded from muscles under different contraction conditions.

Nevertheless, most current research studies focus on the myoelectric manifestations of fatigue during constant force conditions, which is easy to be studied, but cannot reflect the muscle functions of daily life. In addition, to date, research on localized muscle fatigue mainly focuses on clinical side and detecting the occurrence of fatigue. Very little research is carried out on detecting muscle fatigue in real-time and tracking the continuous muscle state from non-fatigue to fatigue. Meanwhile, few works are reported to track the muscle state using discrete fatigue levels. The estimated fatigue levels could be incorporated in assistive devices, to reduce the risk of injuries and to track the patient participation during gait training by modulating the assistance torque level.

Special individuals, such as stroke patients, experience functional deficits induced by the muscle weakness and fatigue. So far, little is known concerning the changes in neuromuscular fatigue after stroke. In the following sections, the general definition of fatigue and fatigue physiological phenomenon are first introduced briefly. Then the prevalent research studies on detecting fatigue are reviewed.

2.4.1 Definitions and Physiological Phenomenon

“Fatigue” is a commonly used term to describe the decrease in physical performance associated with an increase in difficulty of a task or exercise. During muscle contractions, fatigue is a long lasting reduction of the ability to contract and exert force, or to maintain

the required level of strength [4, 5]. Generally, localized muscle fatigue occurs after a prolonged, relative strong muscle activity, and develops progressively over time [63]. Also argued by Barry and Enoka [64], the fatigue definition indicates that fatigue occurs fast after the onset of a sustained period of exercise, although the subjects may still be able to sustain the activity. Another description of fatigue deals with the inability to reach the same initial level of maximal voluntary contraction (MVC) force. The evolution progress of muscle fatigue may be fast or slow, depending on the effort performed, and leads to mechanically detectable performance changes eventually.

Commonly, muscle fatigue is divided by central fatigue and peripheral fatigue based on sustained time of muscle contraction [65]. Central fatigue designates a decrease in voluntary activation of muscle, such as a decrease of the MUs firing rate. Peripheral fatigue indicates a decrease in the contractile strength of the muscle fibers, which represents the changes in mechanisms underlying the transmission of APs [66].

During isometric fatiguing contractions, some biochemical and physiological changes in skeletal muscles can be observed. As a result of the biochemical changes, muscle fiber conduction velocity decreases and directly induces changes in the shape of the MUAP waveform. Eventually, the properties of sEMG signal will be an interference signal of all the generated MUAPs [8, 67]. The direct result of this phenomenon is the decrease of MF or MDF. Therefore, the decrease of muscle fiber conduction velocity is one of the causes of signal power spectral shifting toward lower frequencies. Meanwhile, this change also leads to the increase of sEMG signal amplitude.

2.4.2 Time Domain and Frequency Domain Analysis

As mentioned in the previous section, myoelectric manifestations of muscle fatigue can be summarized to the changes in signal frequency, amplitude and the muscle conduction velocity for various types of muscle contractions. However, due to the variability of muscle characteristics for different persons, there is no simple function that can precisely

describe muscle fatigue progress or the fatigue levels. In general, changes in the sEMG signals caused by fatigue are either measured in time or frequency domain.

Integrated EMG (iEMG), RMS and MAV are frequently used as the time domain features, and an increase can be observed in the fatiguing period for isometric muscle contractions [68, 69]. These amplitude features reflect the combination of MUs recruitment and muscle fiber firing rate [70]. However, sEMG signal amplitude is rarely used as a fatigue indicator solely. One method, named joint analysis of sEMG spectrum and amplitude (JASA) [67, 71] is generally developed based on signal amplitude and spectral changes under fatigue. In this method, the fatigue state is distributed into four different cases, force increase, force decrease, fatigue and recovery, which corresponds to the changes in sEMG amplitude and spectrum. Luttmann et al. [71] found that it is possible to reach precise conclusion with this simple and easy implemented four-case method. In addition to the above approaches, zero-crossing rate of the signal is also studied by [72], which illustrated close properties to *MF*. At the onset of fatigue, the zero-crossing rate drops dramatically due to the decrease in conduction velocity in the muscle. However, zero-crossing rate is strongly dependent on the signal-to-noise ratio of sEMG.

When analyzing fatigue in frequency domain, the total band power (THP) was estimated by Welch [73] in the early studies. This method has been proven to be useful in fatigue analysis by calculating the sEMG signal power [67]. Two of the most common frequency-dependent features in sEMG analysis are the *MF* and *MDF*. *MF* is the frequency where the product of the frequency value and the amplitude of the spectrum are equal to the average of all such products throughout the complete spectrum. While *MDF* is the frequency which divides the power spectrum in average [67]. For constant force muscle contraction, these two spectral features decrease during the fatiguing process attributed by the decrease in MUAP conduction velocity, which are strong indication of fatigue [8, 70, 74] [48]. A development of muscle fatigue correlates with the changes in sEMG amplitude and *MDF* was observed by [75].

Another newly defined spectral frequency parameters to represent the frequency content or the instantaneous frequency are the instantaneous median frequency (IMDF) and

instantaneous mean frequency (IMNF) [76]. These two features demonstrate a significant decline for isometric contraction, which are indicators of fatigue occurrence.

With the above-mentioned approaches, to detect precise fatigue occurrence seems to be feasible for isometric muscle contractions. During constant force contractions, sEMG signal is assumed to be wide-sense stationary over a contraction period of 0.5-2.0 seconds [77, 78]. Under such circumstance, time domain or frequency domain characteristics are reliable fatigue indicators. However, most of the human daily activities are carried out under dynamic muscle contractions. Additionally, if the fatigue detection studies are to be extended to other applications such as sports, rehabilitation or assistive devices, it is essential to adapt a proper signal processing method to deal with the non-stationary signals.

During force-varying muscle contractions, changes in the exerted muscle force, muscle lengths, the electrode locations and the movement velocity have strongly influences on the fatigue evaluation results [76]. Under such conditions, the generated sEMG signals cannot be considered as a stationary process. Hence, the power spectrum parameters obtained from fast Fourier transform (FFT) [79] and other traditional signal processing methods may not be suitable for the analysis of sEMG signals from such muscle contractions.

In order to overcome these issues in the non-stationary muscle contraction analysis, many time-frequency or time-scale methods have been employed to assess fatigue. Cohen's class of distribution, a general time-frequency representation, was first introduced by Cohen [80] using bilinear transformations. However, the Cohen's class can be affected by cross-term contamination.

Due to the variation of the sEMG signals, applying FFT to extract the frequency features would lose the information about time. Short time Fourier transform (STFT) is derived from FFT, which is calculated on a sliding short time window. This approach provides an insight into variations of the spectrum as a function of time [67], and it is commonly employed to determine the frequency and phase evolution of sEMG over time [81]. STFT

is able to estimate the spectral variation with time in a relatively short time window, the resolutions of the time and frequency for the non-stationary signal is traded-off for the shorter time window. STFT was used to evaluate fatigue during cyclic flexion-extension movements of the quadriceps muscle [82]. *MF* as a fatigue indicator was calculated from the spectrogram. The slope of regression fitting of the maximum values of *MF* was considered as the fatigue index.

The Wigner-Ville distribution (WVD) [83] is an optimal approach to analyze non-stationary signals, which overcomes some limitations of the spectrogram with high resolution representation in time and frequency. Duchene, J., et al. [84] applied the WVD method to analyze the electrical activities of uterine muscle and to track its instantaneous frequency. However, this time-frequency method is limited by severe cross-terms or interference terms between the components in different time-frequency regions.

The Choi-Williams distribution (CWD) attenuates the interference terms without influencing the auto-terms of the time-frequency distribution significantly. Knaflitz et al. [76] discussed the electrical manifestations of muscle fatigue during cyclic dynamic contractions. They extracted the instantaneous spectral parameters suited to track the changes arisen by muscle fatigue. The results highlighted that this method allows the assessment of muscle electrical manifestations during fatiguing contractions.

Wavelet transforms is an alternative method for time-varying signal analysis. It replaces the frequency shifting operation in STFT by a time scaling operation [85, 86]. It not only can be used in non-stationary conditions as they vary the time-frequency aspect ratio, but also leading to good frequency localization at low frequencies and good time localization at high frequencies [87]. The fundamental concept comparison of STFT and wavelet transform is illustrated in Figure 2.4. STFT has a fixed time and frequency resolution, and it is unable to have good time resolution along with good frequency resolution inherently. However, wavelet transform ensures good time resolution at high frequencies and good frequency resolution at low frequencies [87, 88]. Karlsson et al. [89, 90] compared several time-frequency analysis methods, including WVD, CWD, STFT and continuous wavelet transform (CWT), to analyze the sEMG signal during dynamic

muscle contractions by extracting time-dependent spectral parameters. They found that the *MF* and *MDF* estimated by CWT is more accurate and precise than the other three time-frequency methods. Meanwhile, CWT offers a high and flexible resolution for scale and time when compared with others.

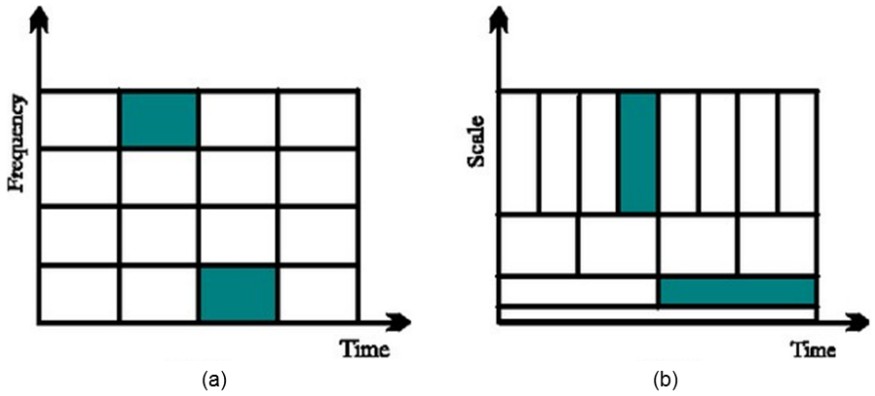

Figure 2.4 Fundamental concept comparison, time resolution and frequency resolution. (a) STFT; (b) Wavelet transform.

However, during force-varying muscle contractions, the MU recruitments and muscle fibers firing rate change according to the force exerted by muscles. As a result, the *MF* or *MDF* and amplitude of sEMG signal vary according to the applied force. Under such conditions, it is inaccurate to track the fatigue progress exclusively by simply extracting time or frequency spectral parameters.

2.4.3 Other methods

Briefly, the time domain, frequency domain, and time-frequency analysis methods in the previous section are applied to extract features which are relevant to indicating fatigue. Other than these mentioned methods, other methods based on the time and frequency analysis method have been developed to assess muscle fatigue.

Gonzalez-Izal et al. [91-93] assessed peripheral fatigue during dynamic contractions by comparing different sEMG parameters. Based on discrete wavelet transforms (DWT), they developed new spectral indices. These spectral indices were compared to different parameters, such as MAV, MDF and ratios between different scales obtained by DWT.

The results demonstrated that the spectral indices was a useful tool in indicating changes in muscle power output during fatiguing dynamic contractions, and can be used as predictors of changes in muscle power output. sEMG signals features are also extracted based on the use of wavelet packet in combination with neural networks to identify and classify muscle fatigue [94, 95].

Entropy is a nonlinear, statistical measurement of the complexity of a signal. Sung et al. [96] claimed that entropy reveals sEMG features that are not included in the power spectrum. More fatigue studies can be found in [97, 98]. Approximate entropy (ApEn) was first developed by Pincus [99] based on the theory of entropy. It is believed to provide quantitative information about the complexity of experimental data which are usually corrupted with noise and short data length. Xie et al. [100, 101] applied ApEn with fuzzy logic to detect fatigue with biceps muscles under isometric contraction. Results suggested that the proposed fuzzy ApEn has the potential to be a reliable method for fatigue assessment and it is applicable to other short noisy physiological signal analysis.

Autoregressive (AR) model is a random process applied in statistics and signal processing to model and estimate the natural phenomena. It was used to measure muscle fatigue in the truck muscle by [102], and the results demonstrated the capability of assessing fatigue for isometric contractions.

Some other fatigue studies are based on ANN models. In these methods, the commonly used sEMG features were extracted and combined as the inputs of the ANN model. MacIsaac et al. [103-105] extracted four time-domain features and four frequency-domain characteristics, and combined them into the training data set and the testing data set. A mapping function tuned by ANN yielded a generalized mapping index that assessed fatigue effectively.

Al-Mulla et al. [106] developed an algorithm for automated muscle fatigue detection in sport related scenarios. They labeled the sEMG signals in two classes, non-fatigue and fatigue. The labels were determined by a fuzzy classifier, and the inputs were the elbow

angle and its standard deviation. A genetic algorithm was employed to evolve a pseudo-wavelet function for optimizing the detection of muscle fatigue on any unseen sEMG signals. From their updated research studies, the labeling had been extended to three types, non-fatigue, transition-to-fatigue, and fatigue [107].

Most of developed fatigue detection approaches have accomplished efficient fatigue assessment. However, many complicated algorithms, such as genetic algorithm, fuzzy logic, wavelet decomposition etc. integrated in one approach may increase the burden of computation and storage. In addition, few of these methods are applicable for real-time implementation.

2.4.4 Stroke patients muscle fatigue

Most current fatigue studies focus on the sEMG signals from normal subjects. While only a few studies have reported sEMG characteristics of fatigue and fatigue detection approaches for persons with hemiparesis due to stroke [24] [108]. Individuals following stroke experience altered muscle activation and movement patterns. Many changes within the motor system following a stroke could potentially alter specific responses of the neuromuscular system to fatigue. Significant changes in the ability to activate muscles were observed from the hemiparetic patients. Some literatures reported that there is a dramatic decrease in the ability to achieve maximum muscles activation at knee joint and elbow joint. Thus, fatigue after stroke is common and distressing to patients. To track the muscle state of post-stroke patients, it is essential to understand the cause of fatigue in stroke patients.

Some new evidence reveals dramatic structural and metabolic changes in skeletal muscle after stroke. These muscle changes include gross atrophy and shift to fast myosin heavy chain in the hemiparetic leg muscles [109]. The impairments will eventually lead to total fatigue, where it is impossible for the patients to continue performing task [110].

Typically, fatigue studies on stroke patients compare and observe the features changes between the affected side and healthy side. The paretic and non-paretic muscles in stroke

patients were studied to compare the changes of sEMG characteristics under fatiguing contractions for lower limbs [24, 111, 112]. The results demonstrated that the changes in *MDF* for affected side and non-affected side were statistically different, with the values on healthy side much higher than the affected side. In addition, a greater decrease in *MDF* was found for healthy side when comparing with the paretic side. Riley et al. [112] evaluated the effects of stroke on fatigue related changes in upper limb torque patterns and sEMG signals. Compared with the healthy side, the affected side showed a lower level of voluntary activation and higher relative torque at the forearm and shoulder. For the changes in *MDF*, roughly same changes were found as presented in [24] and [111]. The reasons of these changes, the decrease in the ability to activate muscles and declined motor unit synchronization in stroke patients were pointed out by [113-115].

2.5 Summary

This chapter provides a general introduction of sEMG signals and a review of past works on estimating human muscle force and assessing muscle fatigue, giving a specific classification of the most prevalent research that has been done in detail.

As the command signals from the human motion control system, transmitted to the muscles through the motor nerves, sEMG signal is commonly used in muscles relevant studies. In its application fields, sEMG signal is widely used for the control of assistive devices. The sEMG signal features are typically used to predict the intended limb movement or the amount of force required to execute a task, and human muscle fatigue.

Different algorithms for estimating the force exerted by muscles have been reviewed. The most popular methods are generally based on the sEMG and force relationship. Linear or nonlinear relationships between sEMG amplitude and force have been found. While the relationship between sEMG frequency domain features and force has not been examined comprehensively. Few studies argued an increase and decrease of spectral variables with increasing muscle force. The results of recent studies of different sEMG spectral features and force relationships are still equivocal. Most of the force estimation methods are

accomplished with the sEMG amplitude-force relationship, the ambiguous spectral variables and force relationship has not been examined comprehensively and applied to estimate muscle force.

Another aspect reviewed in this chapter is the approaches for muscle fatigue detection. Generally, time domain, frequency domain, and time-frequency analysis methods are used to extract fatigue related features. Most of the studies focus on isometric contractions, while only a few works concentrated on dynamic contractions are reported. Meanwhile, muscle fatigue levels describing the fatigue progress have not been investigated.

Based on the above literature survey, some advantages but also limitations have been shown in these methods. In this thesis, the relationships between sEMG time domain features and force, and the relationships between spectral features and force will be investigated comprehensively in the following chapter. Two muscle force estimation approaches will be described in Chapter 4, one is based on sEMG-force relationship, and another is based on the CWT and ANN. In addition, a novel fatigue detection method will be presented for isometric contractions and force-varying contractions. Real-time implementation will also be accomplished to evaluate the efficiency of these methods.

CHAPTER 3

RELATIONSHIPS BETWEEN sEMG FEATURES AND FORCE

3.1 Introduction

The relationships between sEMG features and force exerted by muscles are the direct way to estimate the force information from sEMG signal. Like in time-frequency analysis, sEMG spectral frequencies and signal power are also correlated with some mathematical associations. This chapter is the fundamental for Chapter 4, Chapter 5 and Chapter 6.

In this chapter, we first describe the experimental protocol for data collection. sEMG signal is collected from four muscles, biceps brachii, triceps brachii, quadriceps femoris and rectus femoris of fourteen subjects under separate experiment trials. The forces applied by subjects' muscles are measured by a load cell. Then, we propose the method to establish the relationships between sEMG signal features and force. These sEMG features will be extracted using time domain and time-frequency analysis, respectively. In time domain, windowed RMS is a quadratic mean of the sEMG signal, which is widely used as the amplitude feature. While in time-frequency analysis, *MF* will be calculated from time-scale analysis method, CWT. Since another objective is to establish the relationship between MF and signal power, the signal power describing the energy distribution of power spectrum will also be extracted from CWT.

In the rest of this chapter, the influence on the relationships of different electrode positions obtained from biceps brachii muscles will be investigated in detail. A summary on the established relationships results and the electrode location influences is provided at the end of the chapter.

3.2 Experimental Protocol

In this section, the experimental protocol is presented. The information about the subjects is first described. In Subsection 3.2.2, the experiment setup and the data collection instruments are shown. Lastly, we highlight the experiment methods for collection sEMG signals.

3.2.1 Subjects

Fourteen subjects (10 males and 4 females) voluntarily participated in this study. Each subject agreed and signed the written informed consent documents before participating in the experiments. None of the participants reported any current or ongoing neurological disorders or musculoskeletal problems specific to the wrist, elbow, shoulder and legs. The subjects' mean ± standard deviation age, weight and height are 26.3±2.9 years, 65.6±12.3 kg and 170.3±7.0 cm respectively. The experiments were approved by the institutional review board of National University of Singapore.

3.2.2 sEMG and Force Measurements

sEMG signals were recorded from the biceps brachii, triceps brachii, rectus femoris and biceps femoris muscles of the dominant side of the subjects separately, using self-adhesive pre-gelled Ag/AgCl surface electrodes (Noraxon USA, Inc.). The sEMG electrodes and the pre-amplifier are shown in Figure 3.1. The recorded voltage waveform is the difference in potential between the two red electrodes. Another black electrode is the ground.

Before electrodes were attached to the skin, the underlying skin at the targeted areas was prepared by shaving the excess hair and cleaned with alcohol to reduce the electrical impedance between skin and electrodes. The electrode placement and locations onto the target muscles were done according to SENIAM guidelines [116]. All electrodes pairs were placed parallel to the general direction of muscle fibers, and along the longitudinal axes of the short head of the target muscles. Electrodes pairs were placed with the distance between the electrode's centers of 20mm. For female subjects, the electrodes were placed by a female staff. Contraction tests were carried out by contracting and relaxing the target muscles. The acquired sEMG signals activity correlated to the contraction and relaxation of the target muscle was checked to ensure good contact between electrodes and skin.

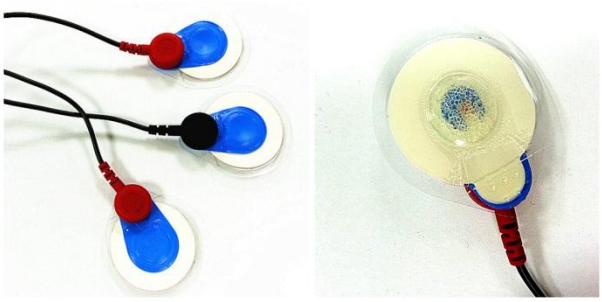

Figure 3.1 Surface Electrodes and pre-amplifier.

sEMG signals were pre-amplified and the common mode rejection ratio (CMRR) of the pre-amplifier was over 95 dB. The data was recorded with a 12 bit analog to digital convertor at a sampling rate of 10 KHz. The recorded signal was subsequently stored in a computer for off-line analysis.

A force-measuring setup with handles was used to measure the force exerted by human muscles generated by elbow and knee joints. During the experiments, the positions of the handle are in the middle of forearm and the middle of shank, respectively. The force sensor is able to measure bidirectional force with a measurement range of 30 kg. The measured force data were amplified with a strain gauge amplifier. Before the experiments, the force and output voltage relationship of the force measurement setup was calibrated using a digital force gauge (IMADA, DS2-50N). Figure 3.2 depicts the experimental

setup for measuring the force and recording sEMG signals. The measured force signal was sampled at 10 KHz and synchronized with the sEMG signal recordings. The sEMG and force signals were recorded simultaneously with a data acquisition system (USB-DAQ 6009, National Instruments, US).

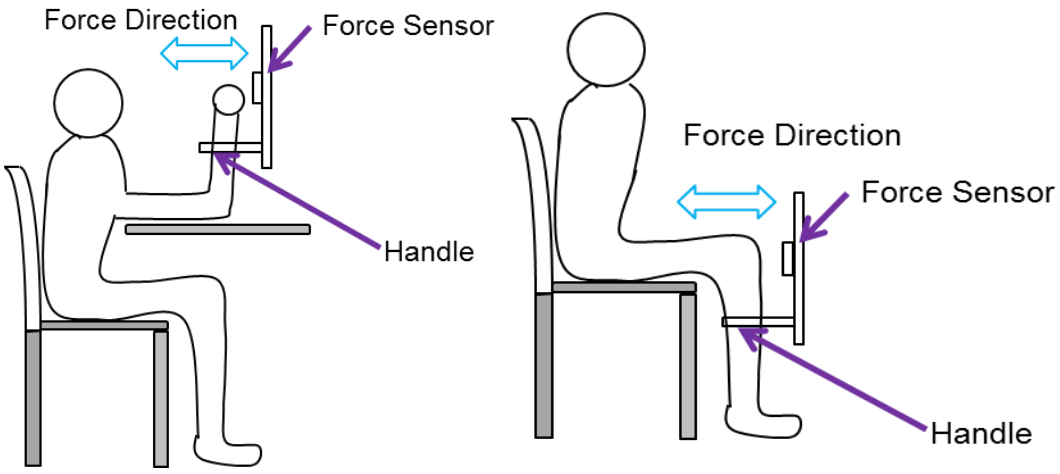

Figure 3.2 Illustration showing the force measurement.

3.2.3 Experiment Methods

During the experiments, the subjects were seated comfortably on a chair with their back in a vertical position. To help the subjects familiarize with the setup and the experimental tasks, warm-up exercises were performed by slowly performing elbow and knee joint flexion/extension. Since the sEMG features and force relationships depend strongly on the type of the force dynamics, the changes of muscle lengths, and joint angles during muscle contraction trials are fixed. All the flexion/extension muscle contractions were performed by elbow or knee joint at a 90 degrees joint angle. The elbow flexion/extension angle was defined as the angle formed by the intersection of the forearm and upper arm, while the knee flexion/extension angle was defined as the angle between thigh and calf.

Graphs depicting the target force, actual applied force and sEMG signals were displayed in real-time on a computer screen facing the subjects to provide a visual biofeedback

while they performed their muscle contractions. Three different contraction trials were performed by each subject using per muscle, and each trial was conducted on different days to avoid the influence from muscle fatigue.

- ***Trial 1: MVCs measurements***

  The subjects were asked to contract biceps brachii muscles to the maximal voluntary contraction (MVC) while pulling the handle of the force measurement setup with the elbow joint angle at 90 degrees. Each MVC value was held for at least 3-5 seconds. After a two minutes rest, same contractions were repeated at least two more times to ensure the recorded signals represent the maximum force of each subject. The subjects were encouraged verbally to exceed previous maximum force level. The averaged MVC value was considered as the non-fatigue maximum voluntary force. This value was used in the following trials as the reference to set the submaximal force level for each subject.

  The same procedures were performed by triceps brachii, rectus femoris and biceps femoris in the subsequent separate trials. However, the MVCs were measured by pushing the setup handle for triceps brachii and rectus femoris, namely, elbow and knee joint extension.

- ***Trial 2: Ramp up contractions***

  The subjects exerted their muscle force from a relax state to MVC slowly within approximate 10 seconds. The computer screen displayed a ramp up function illustration as a guide for subjects to follow.

- ***Trial 3: Ramp down contractions***

  The subjects exerted their muscle force from 100% MVC to a relaxed state slowly within approximate 10 seconds. The computer screen displayed a ramp down function illustration as a guide for subjects to follow.

3.3 sEMG Amplitude and Force Relationship

To establish the amplitude-force relationship, the time domain feature, windowed RMS was calculated using the sEMG signals recorded under ramp down muscle contraction. The recorded sEMG signals and the measured force were downsampled to 2500Hz. The signal flow diagram describing the procedures to establish this relationship is illustrated in Figure 3.3.

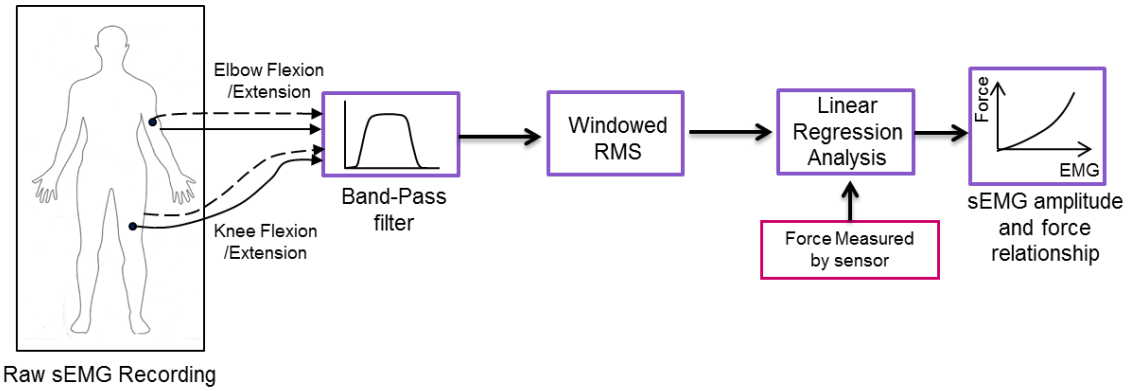

Figure 3.3 Sign flow diagram for establishing relationship between sEMG amplitude and force (Dashed arrows depict elbow/knee joint flexion, while solid arrows show the elbow/knee joint extension).

Raw sEMG signals from each muscle of per subject under ramp down muscle contractions were the input to the proposed method. The raw sEMG signal was first band-pass filtered using a 4^{th} order Bessel IIR filter with the cut-off frequencies at f_1=35Hz and f_2=650Hz. These cut-off frequencies were chosen such that the motion artifacts and higher frequency signals without correlating to the muscle activation have to be removed [117]. The Bessel filter is observed to have a linear phase response and maximally flat group delay. Meanwhile, since this filter has constant and controllable group delay across the whole pass-band, it ensures the filtered signal shape in the pass-band and provides effortless choice of the overall delay introduced by the filter. Subsequently, the signals were rectified and smoothed using windowed RMS which is defined as,

$$RMS_m = \sqrt{\frac{1}{n}\sum_{k=m-n}^{m} x_k^2} \quad (3.1)$$

where x_k is the input signal sample, n is the window length, k is the windowing running index and it starts from m-n and ends at m. For windowed RMS, the longer window length, the smoother the output signal, but the larger time delay. Thus, a properly selected window length has a strong influence on the signal processing results. In this method, n is chosen to be 250 samples which corresponds to 100 ms.

For different subjects and different muscle groups, the skin impedance at the electrode sites is different. Meanwhile, the force target values vary from subject to subject. In addition, a prominent characteristic of windowed RMS is its variability, which makes it inherently difficult to compare signal amplitude across different individuals, different muscles or even across different sessions within the same individual. To compensate the variability of these factors, the windowed RMS signals have to be normalized to 1. Meanwhile, the measured force is normalized and expressed as a percentage of MVC.

The sEMG amplitude-force relationship was established using linear regression method, curve-fitting tool in MATLAB. The two input data sets are the output signals from windowed RMS as x-axis and the measured force from force sensor as y-axis, respectively.

3.4 sEMG Spectral Frequency and Force Relationship

The manifest property of sEMG signal is its variation with respect to time, however, typically, the temporal variation of sEMG signal alone is not enough to present all the physical processes involved. For this reason, various forms of transforms have been developed to analyze sEMG signals. One of extensively studied aspects of sEMG signals is in frequency domain. sEMG signal has the energy distributed around 6 to 500 Hz frequency range, and the most dominant power is located between 10 to 250 Hz. This frequency range contains the characteristics relevant to force exerted by muscles.

The FFT of sEMG signal cannot depict how the spectral contents of the signal with time, which induces the information loss in many non-stationary signals in practice. Commonly, to extract frequency information from sEMG signals, time-frequency analysis method is applied. Time-frequency representations provide direct information about the frequency components occurring at any given time by combining the information of temporal behavior of the signal. It avoids the problems arisen by FFT. The basic goal of time-frequency analysis is to determine the energy concentration along the frequency axis at a given time instant [118].

3.4.1 CWT and Spectral Features Extraction

Time-frequency analysis is more appropriate for analyzing non-stationary signals, as it provides direct information about the frequency components occurring at any given time. To investigate sEMG signals with time-frequency representations, CWT is regularly applied to extract frequency parameters, which has been proven to be computational efficiency and better to estimate the frequency variables.

CWT was first introduced by Morlet in 1982 as an alternative approach to the STFT and specifically to overcome the resolution limitation of the STFT [85]. STFT is derived from FFT working on a short time windowed signal which is assumed to be stationary. When using STFT, the time-bandwidth product is constant in the whole time-frequency plane, once the window is chosen, the time-frequency resolution is fixed at all time and frequencies. Narrow window length results in good time resolution but poor frequency resolution. Meanwhile, wide window induces good frequency resolution but with poor time resolution. On the contrary, in the case of CWT, the time-frequency resolution varies according to the frequency of interest. High frequency resolution for low-frequency signal and good time resolution for high-frequency signal can be achieved simultaneously in CWT.

The CWT analysis is done in a similar way to the STFT analysis, in the sense that the signal is multiplied with a function. Similar to the window function in the STFT, CWT is

calculated separately for different segments of the time-domain signal [119]. Given the input signal $s(t)$, the CWT of the signal $s(t)$ is defined as the integral transform of $s(t)$ with a family of window function $\varphi_{a,b}(t)$:

$$W_s(a,b) = \int_{-\infty}^{\infty} s(t)\, \varphi_{a,b}^*(t)dt \tag{3.2}$$

where $a > 0$ represents the scale parameter, b is the temporal translation parameter (time shifting). The output of the CWT is the wavelet coefficients. These wavelet coefficients yield information as to the correlation between the wavelet (at a certain scale) and the data array (at a particular location). Larger positive amplitude implies a higher positive correlation, while large negative amplitude implies a high negative correlation. Meanwhile, the superscript $*$ in Equation (3.2) refers to the complex conjugate. $\varphi_{a,b}^*(t)$ is obtained by scaling the mother wavelet $\varphi(t)$ at time b and scale a [87],

$$\varphi_{a,b}(t) = \frac{1}{\sqrt{a}}\varphi(\frac{t-b}{a}) \tag{3.3}$$

The function $\varphi(t)$ is commonly called the mother wavelet, whereas the family of functions $\varphi_{a,b}(t)$ are called daughter wavelets since they are derived from scaling and shifting the mother wavelet [87]. The mother wavelet function is limited in time domain, and has values in a certain range. Two dominant properties of mother wavelet are zero-mean and the normalization is constant,

$$\int_{-\infty}^{\infty} \varphi(t)dt = 0 \tag{3.4}$$

$$\|\varphi(t)\|^2 = \int_{-\infty}^{\infty} \varphi(t)\varphi^*(t)dt = 1 \tag{3.5}$$

Unlike STFT, the temporal width of $\varphi_{a,b}(t)$ of CWT is not a constant. It changes as the transform is computed for every single spectral component, scale parameter a.

If the localization properties of the CWT filter characteristic are combined together, CWT performs a local filtering of the input signal $s(t)$ both in time and in scale. Therefore, commonly, wavelet transform can also be seen as a bank of filter.

The relationship between wavelet scale parameter a and its center frequency is defined as

$$\omega = \frac{f_0}{a} f_s \tag{3.6}$$

where f_s is the sampling frequency, f_0 is the center frequency of the mother wavelet at scale a=1, ω is the pseudo-frequency (Hz) corresponding to wavelet scale a. Based on this relationship, it can be observed that large scales corresponds to low frequencies, while small scales correspond to high frequencies. For the resolution property, lower scales have a better scale resolution, which means that it is less ambiguous about the exact value of scale. While, higher scales correspond to better frequency resolution of lower frequencies.

Most widely used way to determine CWT energy distribution within the data array is to plot the wavelet power, which is equivalent to the square of the absolute value of CWT,

$$E(a, b) = |W_s(a, b)|^2 \tag{3.7}$$

This $E(a, b)$ is called Scalogram which represents the energy distribution of the sEMG signal over the entire time-scale plane. Since the wavelet coefficients consist of i columns (i is the input data points index) and j rows (j is the wavelet scale index), Scalogram calculated from MATLAB is a two-dimensional ($j \times i$) matrix of squared wavelet coefficients, but with the signal energy distributed at specific time and scale.

In MATLAB implementation, the wavelet scale length was selected to be 196 to calculate the Scalogram. Morlet wavelet was selected as the mother wavelet from the suggestion given by Karlsson et al. [89, 120]. The wavelet Morlet wavelet is a complex analytic function and has been commonly used in signal processing. Figure 3.4 illustrates real-valued Morlet wavelet in the time domain.

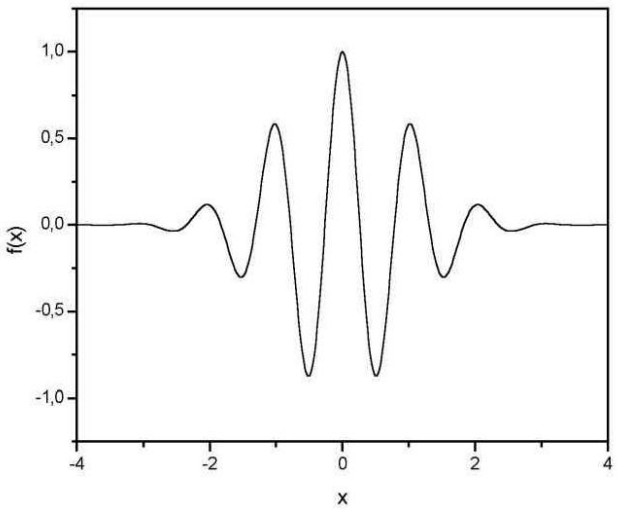

Figure 3.4 Morlet wavelet in the time domain (Real-valued).

In this thesis, two spectral parameters have been extracted with time-frequency analysis, namely *MF* and the signal power *P*. Signal power *P* is able to describe sEMG signals spectral energy distribution with time. Meanwhile, *MF* is a useful frequency-domain features [121] that is frequently used for muscle fatigue assessment with sEMG signals [67]. Using scalogram, *MF* representing the signal frequency domain characteristics is defined as the average frequency of the signal power spectrum. It is calculated as [67]

$$MF_i = \frac{\sum_{j=1}^{La} \frac{f_0}{a_j} f_s E(a_j, b_i)}{\sum_{j=1}^{La} E(a_j, b_i)} \tag{3.8}$$

where $a_j > 0$ represents the scale parameter, b_i is the temporal translation parameter (time shifting). f_s is the sampling frequency, f_0 is the center frequency of the mother wavelet at scale a=1. $E(a_j, b_i)$ is the Scalogram. The Scalogram is a two-dimensional ($j \times i$) matrix, where i is the input data sample index and j is the wavelet scale index. L_a is the length of scale.

The signal power *P* is the average energy distribution along the scale for sample i is calculated as

$$P_i = \frac{\sum_{j=1}^{La} E(a_j, b_i)}{L_a} \tag{3.9}$$

where L_a is the length of scale, $E(a_j, b_i)$ is the Scalogram .

3.4.2 Baseline Noise Elimination

In sEMG time-frequency analysis, the major sources of variability that influence the signal are the diverse noises associated with sEMG recordings. Several intrinsic and extrinsic sources of noise contaminate the sEMG signals. Modern advance electronics technology and appropriate designed circuits can attenuate some extrinsic noise, such as the power line noise and the cable motion artifacts [122]. However, despite noise reduction is done at the source by proper skin preparation, and the use of well-designed electrodes and signal recording equipment, some noise always accompany the desired signal [117].

Intrinsic noise, like baseline noise, is detectable whenever the electrodes are attached to the skin. It is one of the major sources which can be observed at some zero contraction force sections. Figure 3.5 shows a trial of ramp up force and sEMG signals measured from biceps brachii during elbow flexion. It is easy to observe the baseline noise (see the red dashed circle) from the sEMG signal at the end of the trial, where the muscle contraction force is zero. When calculating *MF* and *P* of the power spectrum, the power spectrum contributed from quiet epoch should be discarded rather than ignored, since it contaminates the sEMG signal in the whole trial. Eliminating the effect of zero contraction force (quiet epochs) on the sEMG signal power spectrum makes the signal power spectrum parameters estimation more accurate. For this reason, the baseline spectrum diminishing is essential.

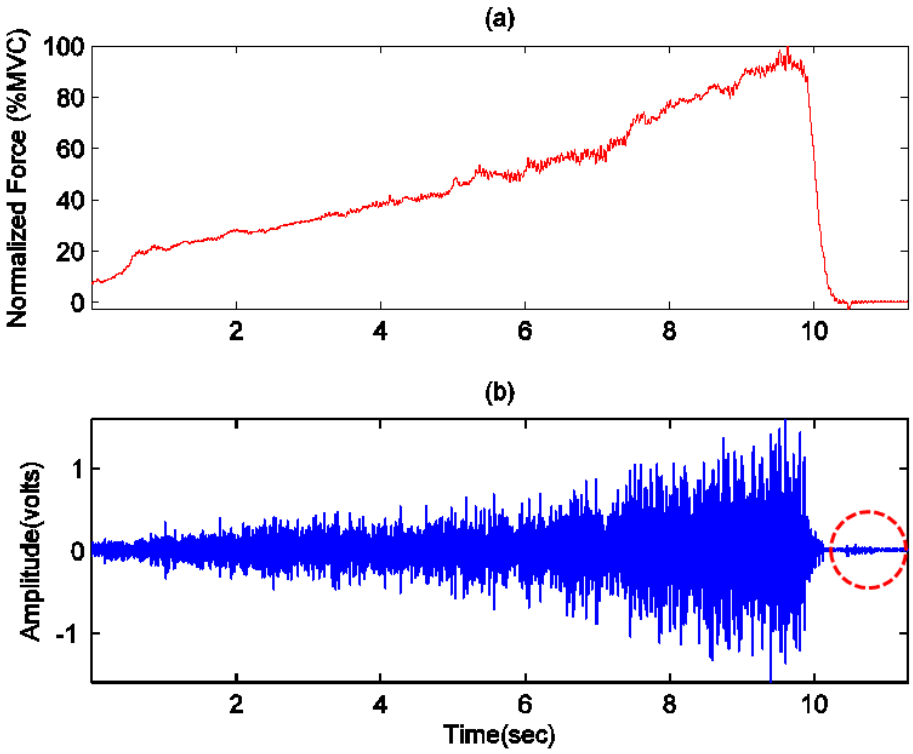

Figure 3.5 (a) Normalized force measured during a ramp up biceps brachii muscle contraction in approximate 10 s period; (b) the corresponding sEMG signal.

To remove the baseline noise, scalogram of the silent period (zero muscle contraction force) was first calculated. The energy of the silent period is very small. A maximum value E_m of the power spectrum for this section was obtained and set as the threshold. To avoid contaminating *MF* and *P* calculation, when calculating *MF* and *P* for the active contraction, if the scalogram value at time *t* is smaller than E_m, the signal power spectral density will be set to zero. Otherwise, continue to calculate the *MF* and signal power *P*. Mathematically, the calculation can be expressed as Equation 3.10,

$$E(a_{j,}b_i) = \begin{cases} 0, & if\ E(a_{j,}b_i) \leq thershold\ E_m \\ E(a_{j,}b_i), & otherwise \end{cases} \tag{3.10}$$

Where $E(a_{j,}b_i)$ is the scalogram at signal sample *i* and scale *j*, while E_m is the threshold value.

With this method, *MF* (Equation 3.8) and *P* (Equation 3.9) will be calculated much more accurately. Figure 3.6 illustrates an example of *MF* calculated with and without this baseline variability elimination algorithm. It is evident that the power spectrum of the quiet period signal influences *MF* dramatically by contaminating the baseline level. For those parts where the muscle contraction force are zero, the *MF* contents should be zeros or very low frequencies, however, from Figure 3.6 (b), the lower frequency components are shifted to higher part due to the effects from baseline noise.

Since the signal power spectrum in the silent period has been eliminated, *MF* decreases to low frequency level when the exerted force is small, and it changes with the muscle active contraction progressively. Using the baseline elimination algorithm on the signal power spectrum, more accurate *MF* and signal power *P* can be obtained and they vary with the force exerted by muscles correctly.

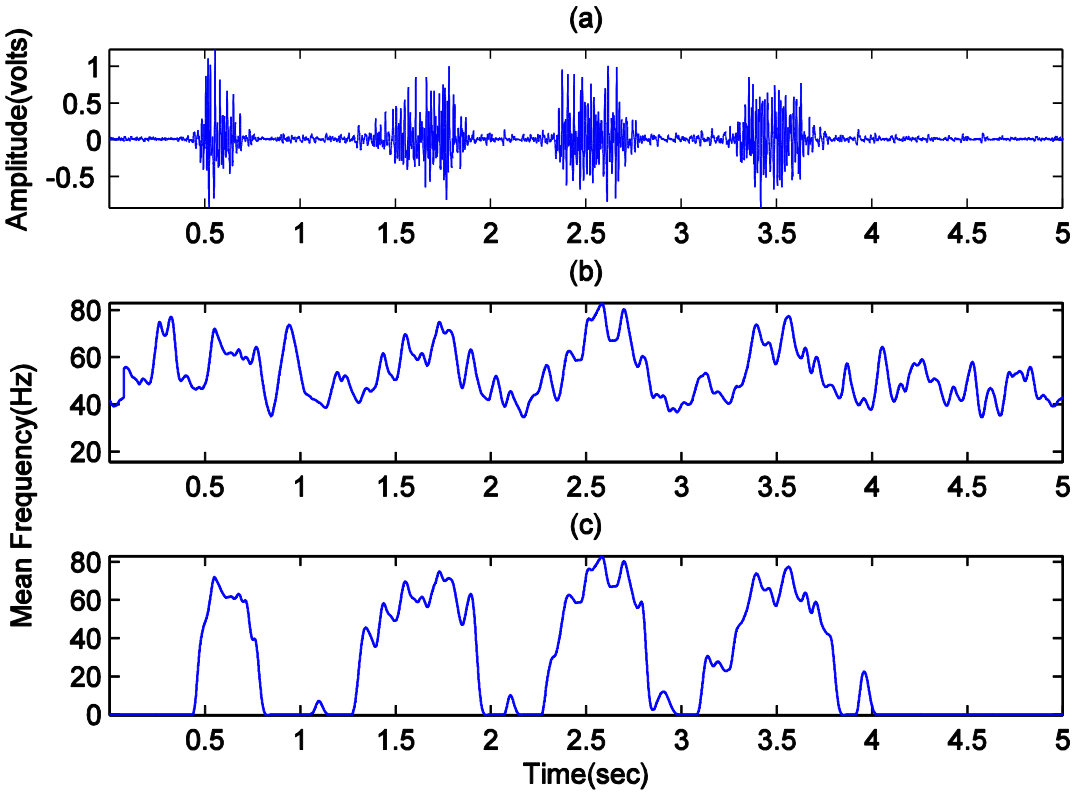

Figure 3.6 (a) sEMG signal recorded from rectus femoris with force-varying contraction; (b) MF is calculated without baseline variability elimination algorithm; (c) MF is calculated baseline variability elimination algorithm.

For each muscle contraction trial, the quiet period is unavoidable and strongly influences the calculation accuracy of *MF* and signal power *P*. Without setting the threshold E_m on the power spectrum leads to inaccurate results in *MF*. The proposed eliminating method is an effective way to obtain the accurate estimation of *MF* and *P*. Therefore, in the following chapters, for any calculation on *MF* and *P*, the algorithm will eliminate the baseline noise first. However, attributed by the changes in electrode positioning, different muscle groups and different muscle contraction trials, the noise characteristics of the zero force contraction vary significantly. Therefore, it is essential to set the threshold E_m trial by trial to ensure the accuracy.

3.4.3 Relationships Establishment

Figure 3.7 depicts the procedures to establish the relationship between *MF* and force using the sEMG signal from ramp down muscle contractions. *MF* obtained from CWT was first low-pass filtered. A 4th order low-pass Bessel filter with a 5Hz cut-off frequency was used to smoothen the *MF* signal by removing the spurious peaks. Then the measured force and the filtered *MF* were analyzed with linear regression. The measured force and filtered *MF* have to be normalized due to the variation from different individuals and different muscle groups. The filtered *MF* is normalized to 100 Hz, while the measured force is normalized and expressed as a percentage of MVC. In MATLAB implementation, two input data sets to curve fitting tool are the normalized *MF* as the x-axis and the measured force as the y-axis, respectively.

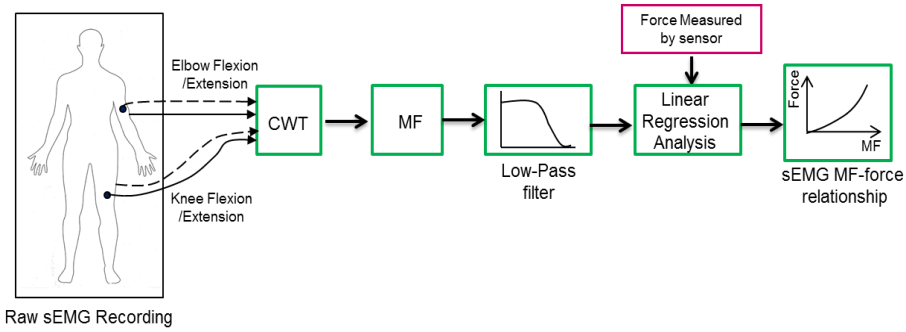

Figure 3.7 Signal flow diagram for establishing sEMG *MF*-force relationship (Dashed lines depict elbow/knee joint flexion, while solid lines show the elbow/knee joint extension).

The development of relationship between *MF* and signal power *P* is illustrated in Figure 3.8. The sEMG signals collected under ramp down muscle contractions are used to establish this relationship. *MF* and *P* were filtered by 4th order Bessel filters with a 1.5 Hz cut-off frequency to simultaneously remove the noise which are shown as the high frequency spurious peaks. This also ensures that two paths were performed with the same signal bandwidth and group delay. Then the filtered *MF* was normalized to 100 Hz, while *P* was normalized to 1. In MATLAB implementation, two input data sets to curve fitting tool are the normalized *MF* as x-axis and signal power *P* as y-axis, respectively.

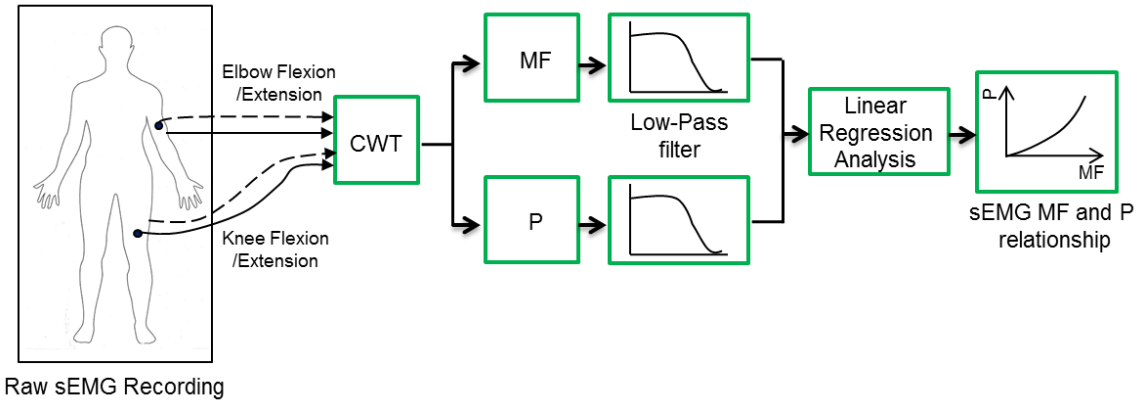

Figure 3.8 Signal flow diagram for establishing *MF-P* relationship (Dashed lines depict elbow/knee joint flexion, while solid lines show the elbow/knee joint extension).

3.5. Relationships Results

The recorded sEMG under ramp down muscle contractions were used to obtain the sEMG amplitude-force relationship, *MF*-force relationship and *MF-P* relationship. Figure 3.9, Figure 3.10 and Figure 3.11 illustrate the amplitude-force relationships, *MF*-force relationships and the *MF-P* relationships, respectively, from the four measured muscle groups. These relationships were fitted with polynomial models. All available polynomial models were selected during curve fitting estimation, such as linear, quadratic, cubic and higher order polynomial. For each muscle, a polynomial model was obtained from each subject. The best polynomial estimator for each muscle group was selected by comparing which gives the highest R^2 value and lowest root mean square error (RMSE). R^2 value is the square of the coefficient of multiple correlations. It is used to check the goodness of

fit. The closer this value is to 1, the higher goodness of fit is between the two signals. The level of significance value alpha was set at $p \leq 0.05$ in this study. Even though there might be some other models like exponential, power, logarithmic etc. describing the relationships relatively accurate, considering the computational efficiency when implementing in real-time system and to simplify the implementation process, only polynomials are employed in the thesis.

For the sEMG amplitude-force relationship, the windowed RMS values increase slowly at low-level exerted force, and they increase dramatically when the exerted force is increased to higher level. It is evident that relative more muscle fibers are fired to generate more contraction force.

For the *MF*-force relationship, the general trends of the two upper arm muscles are slightly different from the rectus femoris and biceps femoris, but they are still in parabolic shapes. At low-level muscle force, *MF* increases rapidly, whereas the growth is slower when a very high muscle force level is exerted by biceps brachii and triceps brachii. In the rectus femoris and biceps femoris, the changes in *MF* are almost same as the amplitude-force relationship when the force is increasing. This can be attributed to the increasing firing rates of muscle fibers, which results in the rapidly increasing rate of *MF* at high muscle force. This phenomenon also can be observed in the relationships between *MF* and signal power *P*.

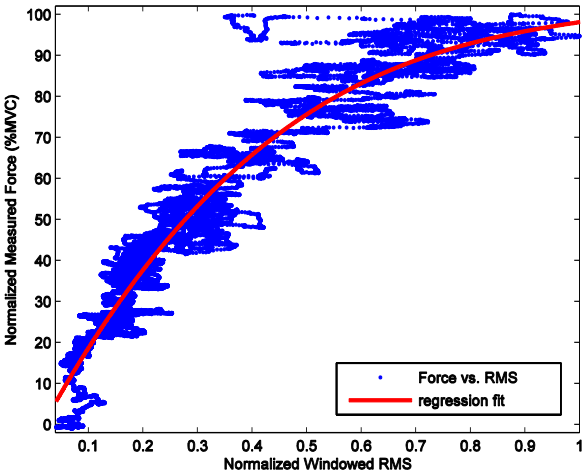

(a) Curve fitting example with input data (Biceps brachii)

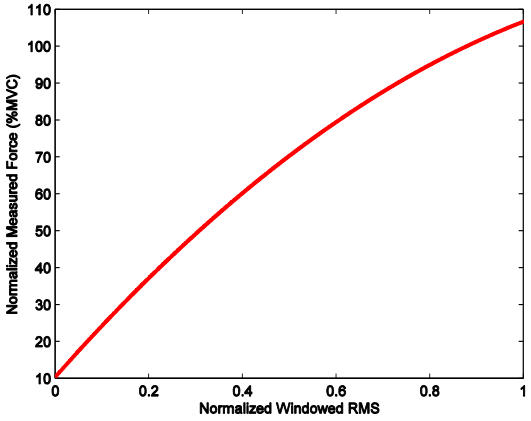

(b) Biceps brachii

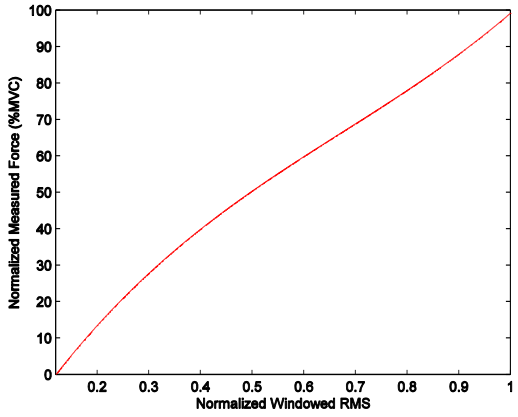

(c) Triceps brachii

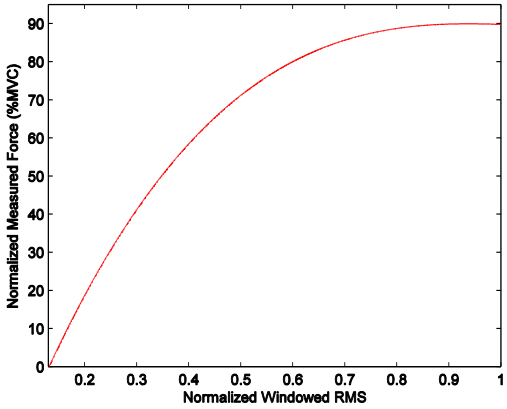

(d) Rectus femoris

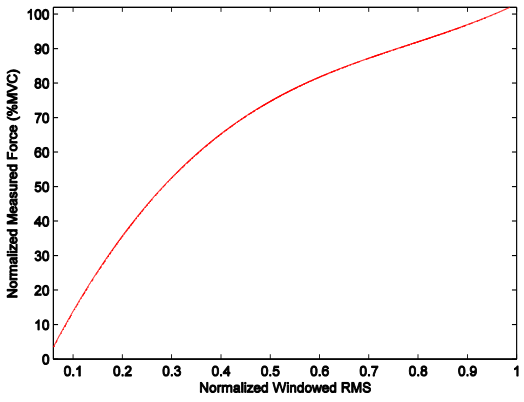

(e) Biceps femoris

Figure 3.9 sEMG amplitude-force relationships. (a) Curve fitting example with input data (Biceps brachii); (b) Biceps brachii (3rd order polynomial); (c) Triceps brachii (3rd order polynomial); (d) Rectus femoris (4th order polynomial) (e) Biceps femoris (4th order polynomial).

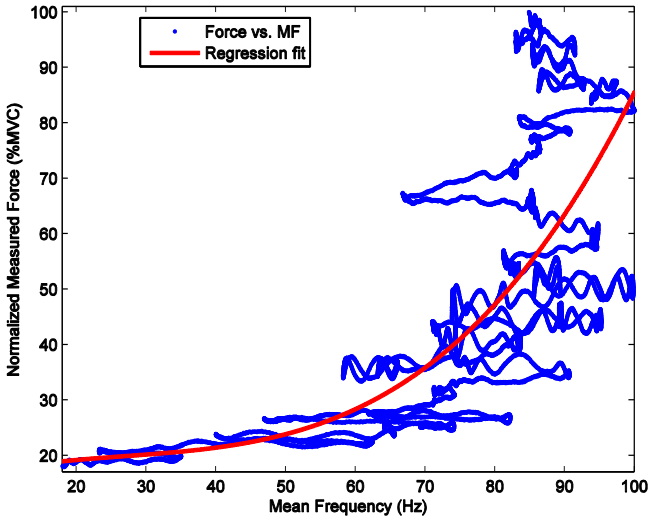

(a) Curve fitting example with input data (Biceps brachii)

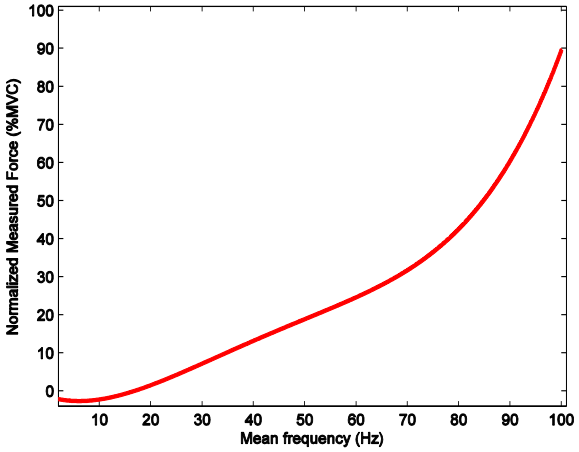

(b) Biceps brachii

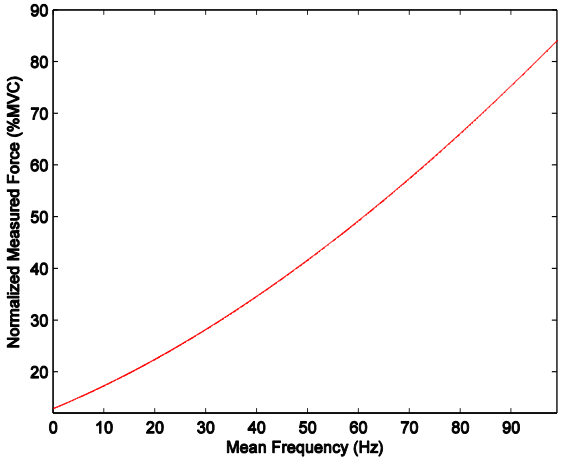

(c) Triceps brachii

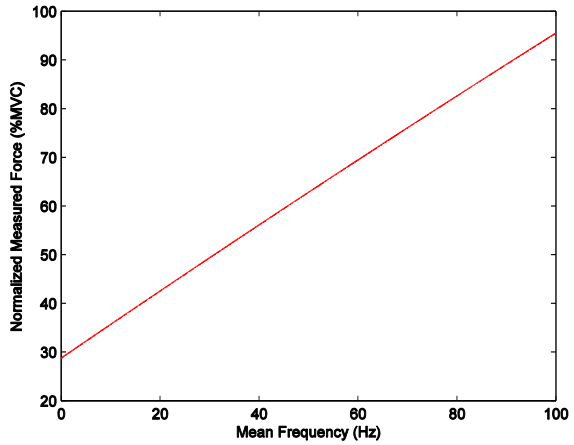

(d) Rectus femoris

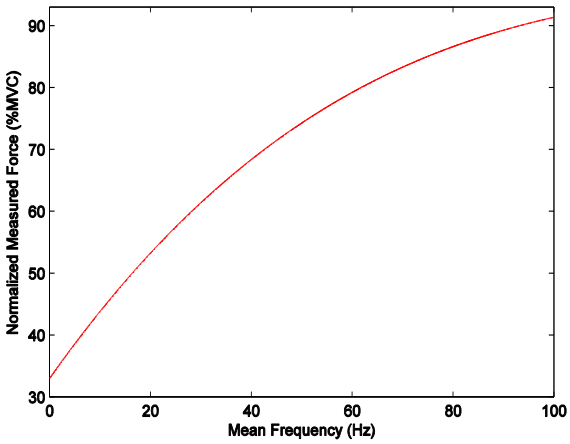

(e) Biceps femoris

Figure 3.10 sEMG *MF*-force relationships. (a) Curve fitting example with input data (Biceps brachii); (b) Biceps brachii (3rd order polynomial); (c) Triceps brachii (3rd order polynomial); (d) Rectus femoris (4th order polynomial) (e) Biceps femoris (4th order polynomial).

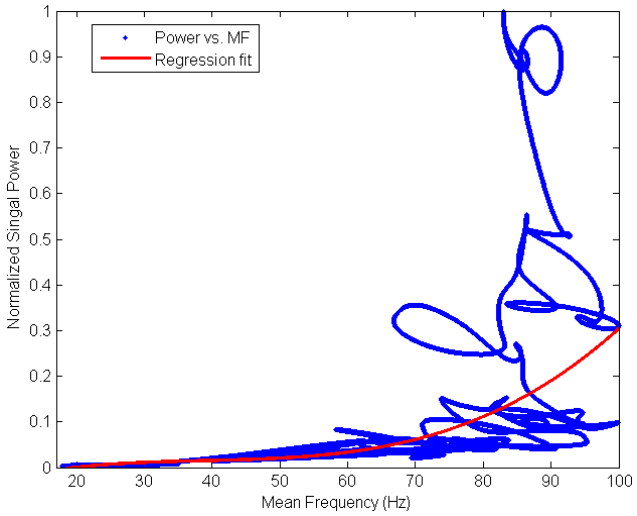

(a) Curve fitting example with input data (Biceps brachii)

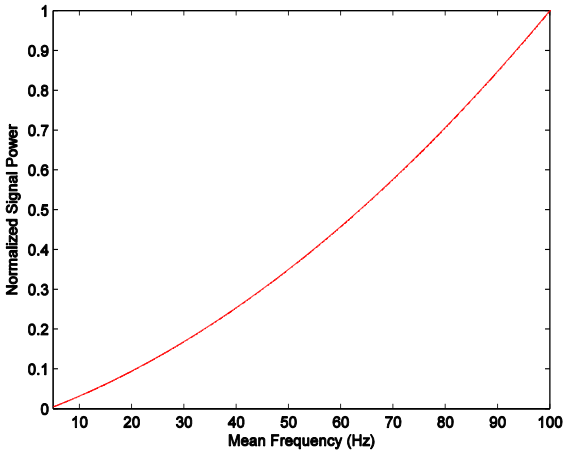

(b) Biceps brachii

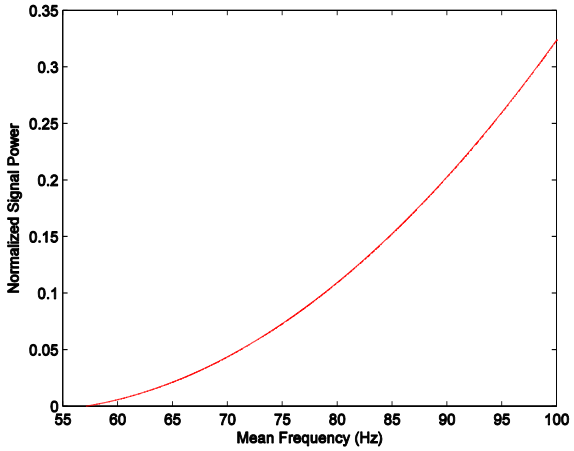

(c) Triceps brachii

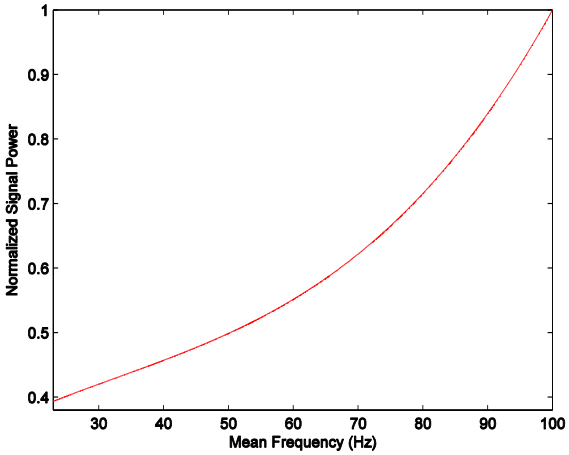

(d) Rectus femoris

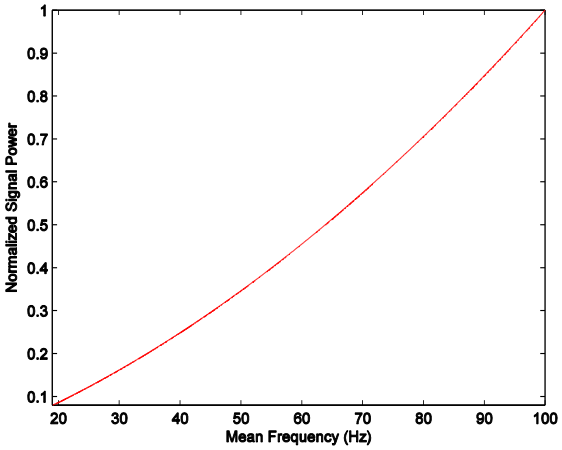

(e) Biceps femoris

Figure 3.11 sEMG *MF-P* relationships. (a) Curve fitting example with input data (Biceps brachii); (b) Biceps brachii (3rd order polynomial); (c) Triceps brachii (3rd order polynomial); (d) Rectus femoris (4th order polynomial) (e) Biceps femoris (4th order polynomial).

Table 3.1 lists the R^2 and RMSE values of the selected polynomials given by the regression fitting from each muscle for the amplitude-force relationship and *MF*-force relationship. The high R^2 values indicate that there are strong correlations not only between the force and sEMG with time domain features, but also between the force and the spectral frequency features.

Analysis of variance (ANOVA) is employed to analyze the differences between group means and their associated procedures [123]. In this study, a single factor ANOVA was performed to compare the R^2 values between these two sEMG features and force relationships, for the results from all measured muscle groups. The ANOVA in this study was calculated using Microsoft Excel. In addition, ANOVA was performed among the four muscles to determine any significant difference in measured muscles for each established relationships. *P*-values less than 0.05 were considered significant. In this study, the ANOVA was calculated using Microsoft Excel.

ANOVA results indicate that the difference between the *MF*-force and amplitude-force relationship are not statistically significant since the *p*-value is larger than 0.05. This also demonstrates that the association varies relatively small for both sEMG amplitude feature and the spectral frequency. On the other hand, for the relationships, amplitude-force and *MF*-force, the single factor ANOVA reveals that there were no significant difference among all the measured muscles.

Table 3.1 Selected Polynomial R^2 and RMSE Values for Each Muscle (*MF*-force relationship and Amplitude-force relationship).

Muscles	MF-force relationship		Amplitude-force relationship	
	R^2	RMSE	R^2	RMSE
Biceps Brachii	0.9233	0.0756	0.8195	1.066
Triceps Brachii	0.8601	0.2786	0.8858	0.3862
Rectus Femoris	0.7685	0.3772	0.9033	0.2270
Biceps Femoris	0.8041	0.3823	0.9071	0.2495

3.6 Influence of Electrode Locations on the Relationships

When discussing the relationship between sEMG features and force, numbers of factors should be taken into account. One of the factors is the electrode location. In numbers of methodological and clinical publications, the effects of electrode locations on the estimation of sEMG amplitude or the spectral variables have been studied in recent years. However, the influence of electrode locations on the relationships between sEMG features and force are hardly comprehensively investigated. It is widely known that the sEMG amplitude and spectral parameters are very sensitive to small electrode displacements and they depend on the electrode locations strongly. Jensen et.al [124] examined the effects of electrode positions on the sEMG amplitude-force characteristics for the upper trapezius muscles. Results indicated that in the region with high sEMG amplitude, a linear amplitude-force relationship was observed, whereas highly variable relationships were found in the lateral and dip region. They also highlighted that an almost linear relationship could be observed for electrode locations far from the innervation zone.

The different electrode locations not only affect the sEMG amplitude, but also influence the frequency spectral parameters. To locate the electrode more accurately and precisely, and investigate the effects of electrode positions on the relationships, some muscle contraction trials and relationship results from different electrode locations are presented in this section.

3.6.1 Experimental Methods

Five subjects were involved in this investigation. The five subjects are random selected from the fourteen subjects that are mentioned in Subsection 3.2.1. The five subjects' mean ± standard deviation age, weight and height were 23.5±1.6 years, 66.4±10.6 kg and 171.6±5.2 cm respectively. sEMG and force signals were recorded using the same equipment as mentioned in Subsection 3.2.2. sEMG signals were collected from biceps brachii of the subjects' dominant sides by performing elbow flexion. The electrode pairs

were placed with the distance between the electrode's centers of 20mm. To distinguish the three target electrode locations on the skin surface, they were marked with circles and named as location 1 (L_1), location 2 (L_2) and location 3 (L_3). The three target electrode locations were chosen with 10mm center distance between each set of electrodes. For each electrode location, Trial 1 and Trial 2 mentioned in Subsection 3.2.3 were performed by each subject. Figure 3.12 shows the three different electrode locations. A single factor ANOVA was performed among the subjects by comparing the R^2 values to investigate any significant difference in the three electrode locations for the three established relationships (p<0.05).

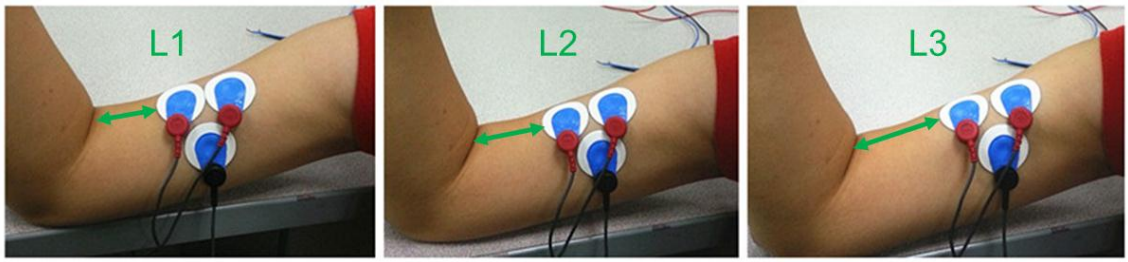

Figure 3.12 Three different electrode locations on biceps brachii.

3.6.2 Statistical Analysis Results

The sEMG amplitude-force relationship, *MF*-force relationship and the *MF-P* relationship were calculated using the same methods as Section 3.3 and Section 3.4 for the three different electrode positions. Linear, quadratic, cubic or higher order polynomial regression was fit for each subject with each set of electrodes position. The example of relationship curves from one subject with different electrode locations are shown in Figure 3.13, Figure 3.14 and Figure 3.15, respectively.

All the relationships are found to be non-linear. As shown in Figure 3.13, no much difference can be observed from the sEMG amplitude-force relationship under the three electrode locations. For the *MF*-force relationship, in L_3, the *MF* increasing rate is much faster than the other two locations as the force increases. The signal power increases very slow at low *MF* for L_1 in the *MF-P* relationship. When we change the electrode location

to L_2 and L_3, the increasing trends are very rapid, but the relationship curves show no much difference between the two locations.

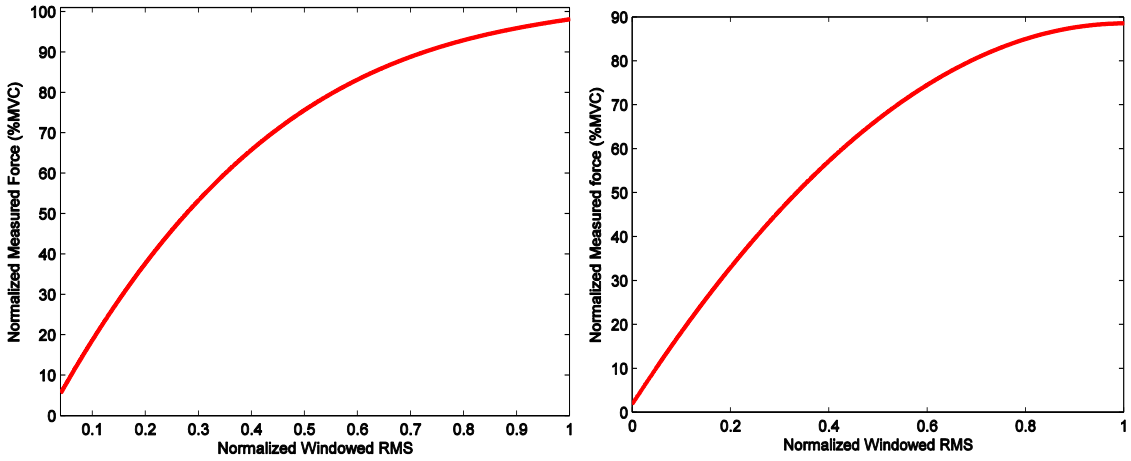

(a) (b)

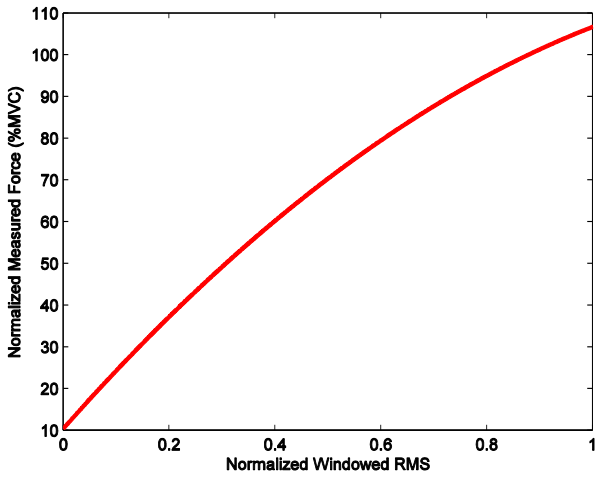

(c)

Figure 3.13 Relationship between sEMG amplitude and the exerted force. (a) L_1; (b) L_2; (c) L_3.

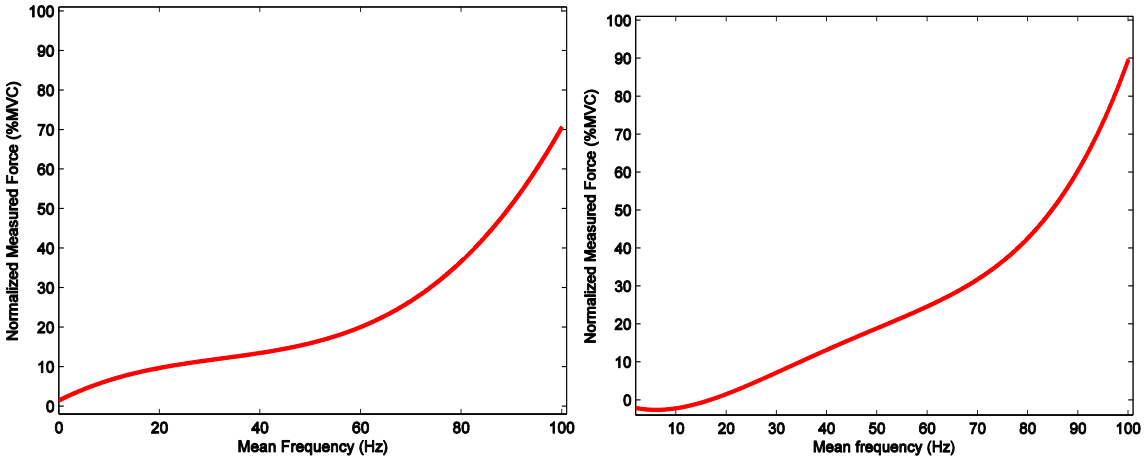

(a) (b)

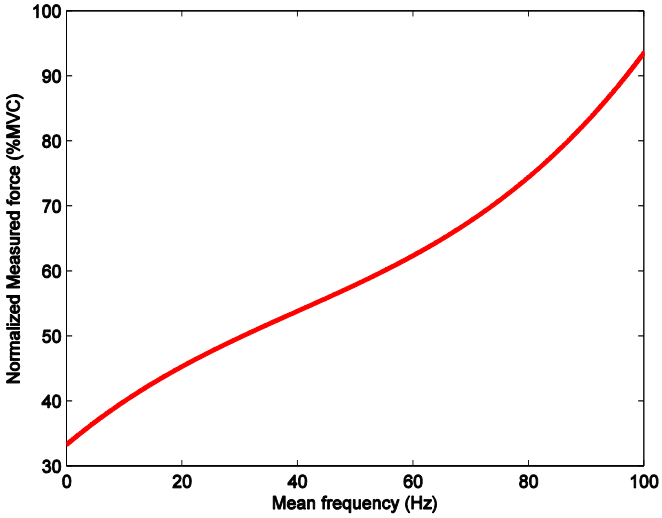

(c)

Figure 3.14 sEMG *MF*-force relationship. (a) L_1; (b) L_2; (c) L_3.

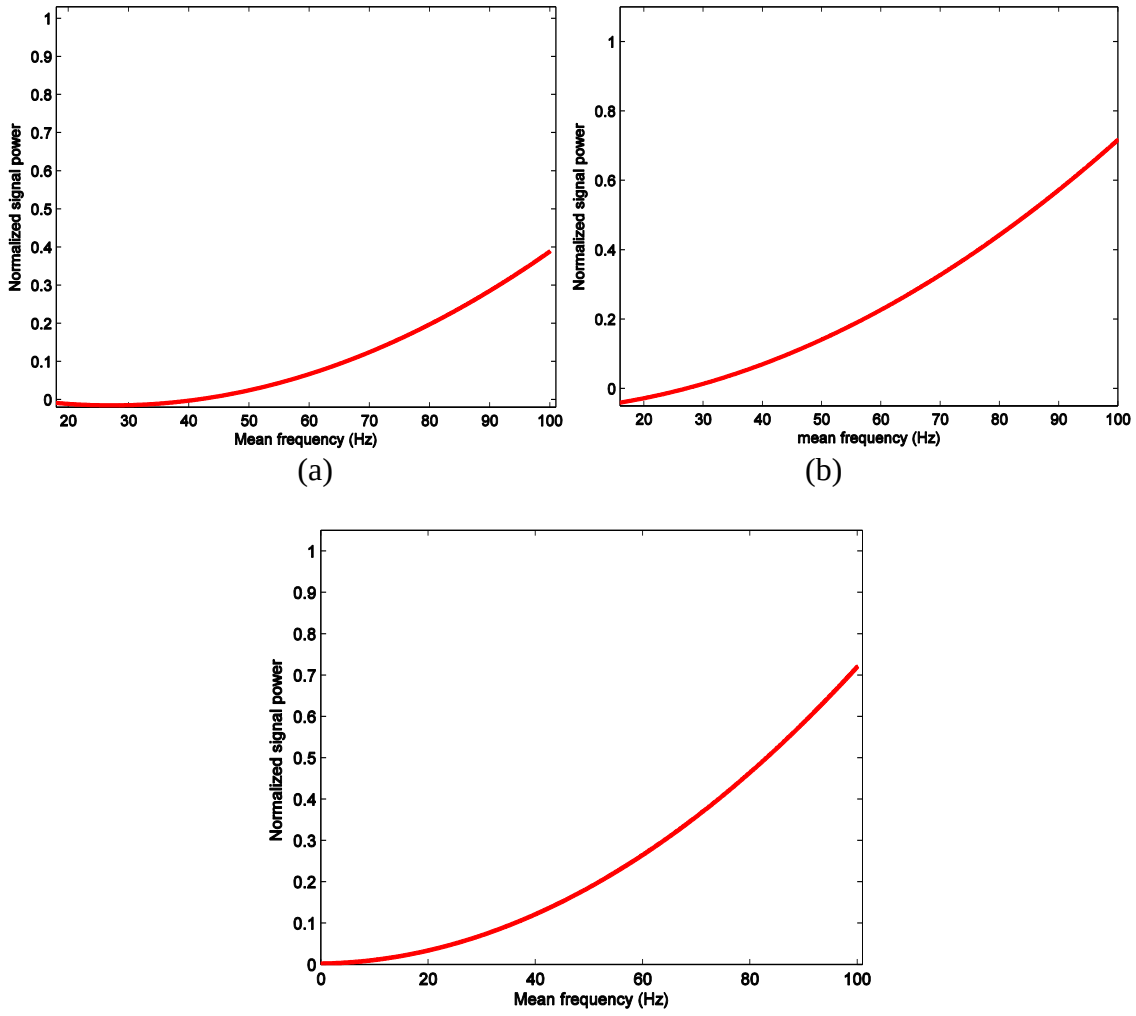

Figure 3.15 sEMG *MF-P* relationship. (a) L_1; (b) L_2; (c) L_3.

For each electrode location, the average R^2 value and standard deviation (SD) were calculated among all participants, which are depicted in Figure 3.16, Figure 3.17 and Figure 3.18 for amplitude-force relationship, *MF*-force relationship and *MF-P* relationship, respectively.

Among the three different electrode locations, the sEMG amplitude-force relationship shows very high R^2 value which indicates the windowed RMS correlates the muscle force well. More specifically, L_1 indicates the highest R^2 value (R^2=0.9265) on average than L_2 and L_3 with the average R^2 values are 0.9245 and 0.9188 respectively for all subjects.

For the relationship between *MF* and muscle force, the regression performance of L_2 with R^2=0.8584 outperforms the others among the subjects. However, the average R^2 values obtained from all the electrode locations are not very high.

As shown in Figure 3.18, it is evident that L_2 gives the highest R^2 values (R^2=0.9404) and L_3 gives the lowest R^2 values (R^2=0.7213) on average for the *MF-P* relationship.

A single factor ANOVA performed on the amplitude-force relationship regression indicates a significant difference between the three electrode locations (ANOVA, p=0.8510). In addition, for *MF*-force relationship, the differences between the electrode positions are statistically significant (ANOVA, p=0.1958). However, no statistically significant differences are noted between electrode locations for *MF-P* relationship (ANOVA, p=0.043).

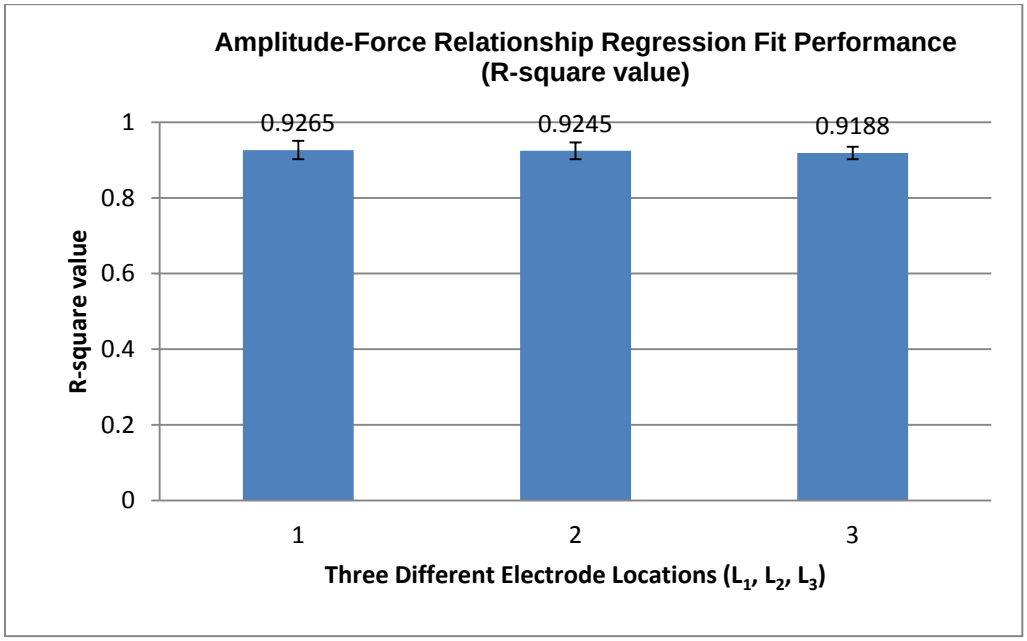

Figure 3.16 sEMG amplitude-force relationship regression fit performance with three electrode locations (Averaged R^2 value and SD).

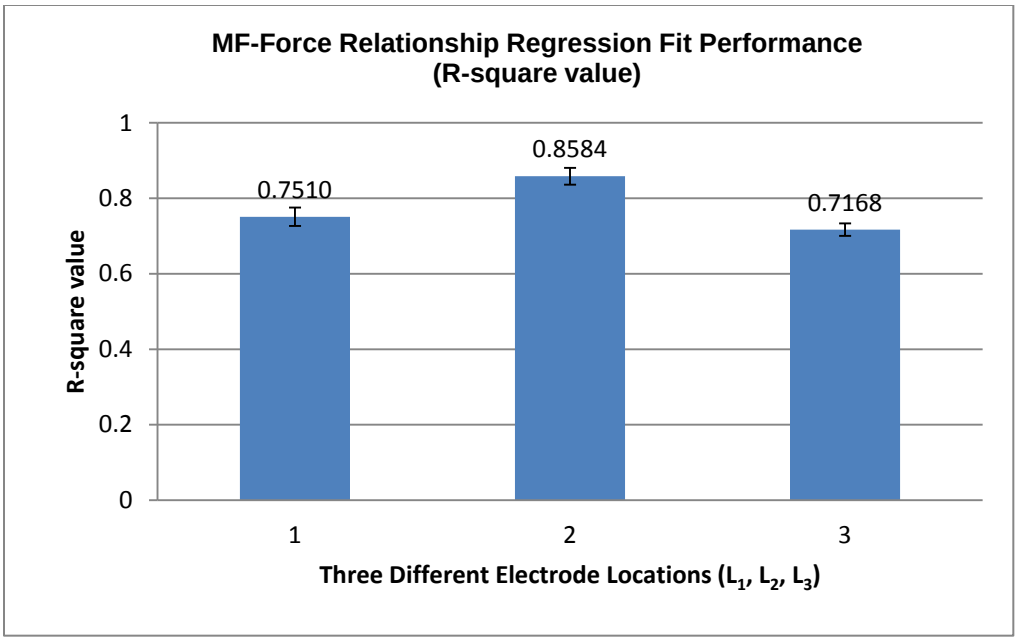

Figure 3.17 sEMG *MF*-Force relationship regression fit performance with three electrode locations (Averaged R^2 value and SD).

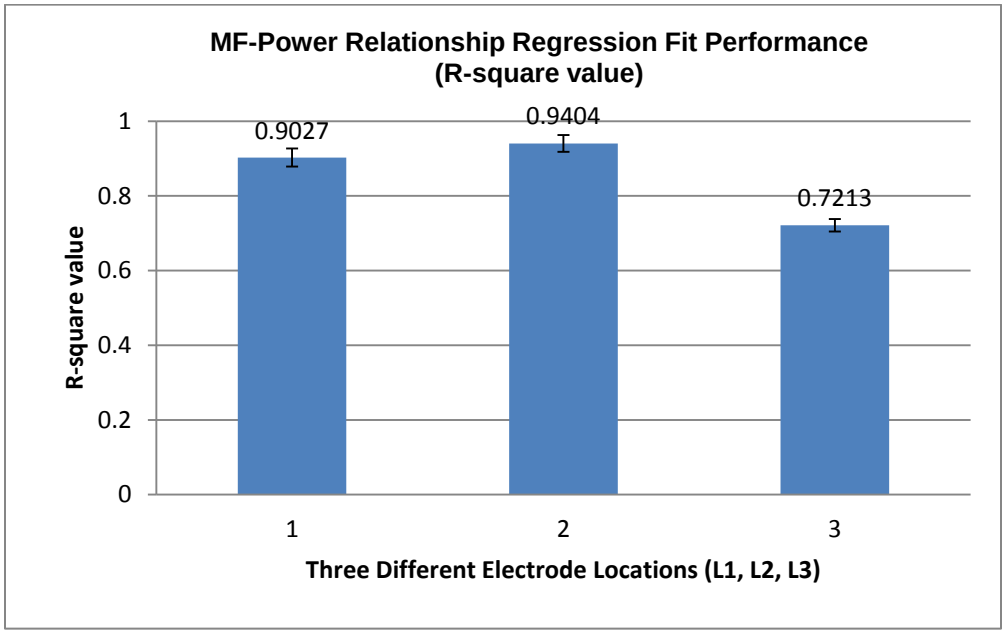

Figure 3.18 sEMG *MF-P* relationship regression fit performance with three electrode locations (Averaged R^2 value and SD).

These electrode locations comparison results may vary from subject to subject since the exact electrode locations changes slightly between the subjects, but they cover a position approximate 2cm range along the biceps brachii muscles based on the experiment measurements. Moreover, sEMG is unlikely to measure every precise position for each subject since the muscle lengths varies with subjects, which is another factor influencing the relationship results. Although the maximum displacement for each set of the electrodes was 10 mm, the new *MF*-force relationships and *MF-P* relationships, showed higher R^2 values as the second electrode location was in the innervation zone.

From the results, L_2 has a better performance for *MF*-force and *MF-P* relationships. The relationships results indicate that a large and well-designed region to attach the electrodes to biceps brachii will give the most representative sEMG signals to achieve better regression fitting for establishing these relationships. In addition, the R^2 values comparison between different electrode locations provides important information on selecting suitable electrode location in following experiments.

3.7 Summary

In this chapter, three relationships, sEMG amplitude-force relationship, *MF*-force relationship and *MF-Power* relationship are established based on the time-domain analysis and time-frequency analysis. The spectral parameters of sEMG signal, *MF* and signal power *P*, are extracted using CWT. The regression fitting results show that not only the signal amplitude (windowed RMS) increases non-linearly with the increasing exerted force, but the spectral parameter *MF* rising trends are in line with the force non-linearly. These two relationships will be employed in next chapter for estimating muscle force. In addition, non-linear relationship is also observed from the relationship between *MF* and signal power *P*. The *MF-P* relationship will contribute to the novel muscle fatigue detection method in Chapter 5.

Furthermore, based on the relationship establishment algorithms, the influence of electrode locations on these three relationships is also investigated in this chapter. As

shown from the relationships regression fitting figures, no much difference is found for each relationship obtained under different electrode positions. However, for the amplitude-force relationship, the statistical analysis results show that L_1 outperforms the others with highest R^2 value on average for all subjects. L_2 has a better performance for *MF*-force and *MF-P* relationships. The relationships results indicate that a large and well-designed region to attach the electrodes to biceps brachii will give the most representative sEMG signals to achieve better regression fitting for establishing these relationships.

CHAPTER 4

MUSCLE FORCE ESTIMATION

4.1 Introduction

This chapter presents the algorithms to estimate muscle force based on the previous established amplitude-force relationship and *MF*-force relationship, respectively. Since there is an electromechanical delay between the onset of electrical activity in muscles and the onset of force generation by muscles contraction, proper signal processing methods enable us to predict the force exerted by muscles before the actual force is applied by a few milliseconds. T_f describes the average time difference between the estimated force and the measured force from force sensor. The predictive capabilities of the two methods will be compared by correlation coefficient (CC) values, RMSE and T_f values between the estimated force and measured force.

Knowledge of internal forces and moments of muscles during movement is important for developing better active and intuitive rehabilitation robotics for stroke patients. The ability to predict the muscle forces in patients following stroke benefits the treatment planning and evaluation of therapies geared at improving patient function. Moreover, rehabilitation devices can use the predicted muscle force value as an effective control signal. Therefore, to estimate muscle force for stroke patients, the proposed force estimation algorithms are applied to sEMG signal recorded from the post-stroke patients.

Since sEMG signals recorded from the affected side of stroke patients are likely to be abnormal, relationships between sEMG signal and force cannot be developed accurately. These relationships may not be just a non-linear function of the selected sEMG features. Therefore, instead of establishing the non-linear sEMG-force relationships, artificial neural networks (ANN) is used to approximate the complex nonlinear mappings directly from the input sEMG signal features. The rest of this chapter presents the CWT-ANN based muscle force estimation algorithm for both healthy subjects and stroke patient subjects.

4.2 Experimental Protocol

In this section, the experimental protocol is presented. First, the information about the subjects is described. In Subsection 4.2.2, the experiment setup and the data collection instruments are shown. Lastly, we highlight the experiment methods for collecting sEMG signals.

4.2.1 Subjects

The healthy subjects for the experiment presented in this chapter were the same ones recruited for the experiments in Chapter 3. To study stroke patients' sEMG signals, five post-stroke subjects (1 female and 4 male) were participated in this experiment. They were recruited from the National University Hospital (NUH). All the patients gave written informed consent prior to participating in this study. The experiments were approved by the NUH institutional review board. The post-stroke patients are aged from 56 to 68 with the mean $\pm$ SD of 61.2 $\pm$ 4.38 years. The inclusion criteria and exclusion criteria of stroke patients involved in the experiments are as follows:

- Inclusion criteria: (1) Hemiparesis or hemiplegia confined to one side of the body; (2) At least 6 months post-stroke with a stable medical condition and at least 6 months of rehabilitation therapy with neuromuscular facilitation techniques; (3)

Have the ability to produce more than a predetermined minimal force at the knee joint and is able to walk.

- Exclusion criteria: (1) peripheral neuropathies; (2) other diseases of the central nervous system; (3) peripheral arterial disease; (4) chronic heart failure; and (5) orthopedic diseases; (6) severe cognitive or affective dysfunction; (7) brainstem lesion; (8) tremor and contracture.

Among the stroke subjects, four patients suffered from left sided hemiparesis and the other one from right sided hemiparesis. The clinical characteristics of the patients are listed in Table 4.1.

Table 4.1. An Overview of Clinical Information Regarding the Five Stroke Patients.

Subject	Gender	Age (years)	Time Since Event (Months)	Hemiplegic Side	Diagnosis Cause
1	Male	56	NA	Left	NA
2	Male	68	54	Left	Right corona radiate infarct
3	Male	60	65	Left	Right basal ganglia bleed
4	Female	62	64	Left	Parietotemporal bleed
5	Male	60	25	Right	Right hemiparesis

NA: Clinical information was not obtained from the therapist at the time of data collection for the first subject.

4.2.2 sEMG and Force Measurements

For the healthy subjects, the sEMG signals were recorded from the biceps brachii, triceps brachii, rectus femoris and biceps femoris muscles of the dominant side separately. The same skin preparation as described in the previous chapter was performed. In addition, the sEMG and force signals were collected using the same setup as mentioned in Chapter 3 (Subsection 3.2.2).

In order to make the proposed force estimation algorithms beneficial to the lower limb motion recovery for stroke patients, and implement the algorithms to the lower limb rehabilitation device, the sEMG signals were recorded from rectus femoris and biceps femoris from the affected side of stroke patients. However, muscular atrophy due to stroke reduces the amplitude of sEMG signals measured from the stroke patients. For example, the sEMG signals amplitude from the fourth stroke subject's biceps femoris and the first subject's rectus femoris are very small and cannot be separated from the baseline noise level.

The sEMG electrode locations on the target muscle skin surface were found with the assistance from hospital therapists. Figure 4.1 shows the sEMG and force measurement setup designed for stroke patients. The setup is almost same as the one described in Chapter 3 (Subsection 3.2.2), but it is designed for lower extremities experiments usage only.

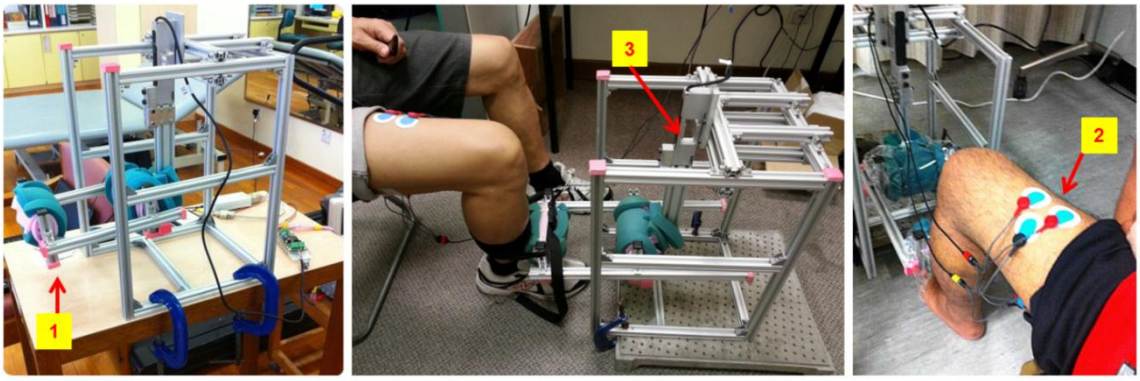

Figure 4.1 Illustrations showing the force measurement designed for stroke patient's lower extremities data collection. 1: Handle for legs experiments; 2: sEMG electrodes; 3: force sensor.

4.2.3 Experiment Methods

During healthy subject's experiments, the subjects were seated comfortably on a chair. The basic muscle contraction details and the preparation are same as Chapter 3 (Subsection 3.2.3), but to perform different muscle contraction trials. In this experiment, two different contraction trials were performed by each subject using per muscle. Each trial was conducted on different days to avoid the influence from muscle fatigue.

- ***Trial 1: MVCs measurements***

  The subjects were asked to contract muscles to MVC while pulling or pushing the handle of the force measurement setup with the joint angle at 90 degrees. Each MVC value was held for at least 3-5 seconds. After a two minutes rest, same contractions were repeated at least two more times to ensure the recorded signals represented the maximum force of each subject. The subjects were encouraged verbally to exceed previous force level. These measured MVCs will be used in the following trials to determine the general force target of each submaximal contraction.

- ***Trial 2: Force-Varying contractions***

  During this trial, a target trajectory of force amplitude in the shape of a force-varying half-sinusoidal was displayed. The subjects exerted the muscle contraction force in accordance to the trajectory with the peak target force up to 40% MVC by performing joint flexion or extension. Precise tracking performance was not required for a successful experiment. Actually, the purpose of the target tracking was to ensure that subjects exerted the contraction forces at a roughly constant frequency. Subjects took a few minutes (followed by a 5 minutes rest) to become familiar with the tracking task as none had any prior experience. Five or six flexion/extension contractions were conducted per trial. The contraction period of every repeated cycle contraction was limited approximately to be two seconds.

The same trials were performed by healthy subject's each muscle separately. The forces were measured by pushing the setup handle for triceps brachii and rectus femoris, namely, elbow or knee joint extension. The measured MVCs will be used to normalize the signals. A sample of the raw sEMG signal (from biceps femoris) and the measured force recorded during the knee flexion is shown in Figure 4.2.

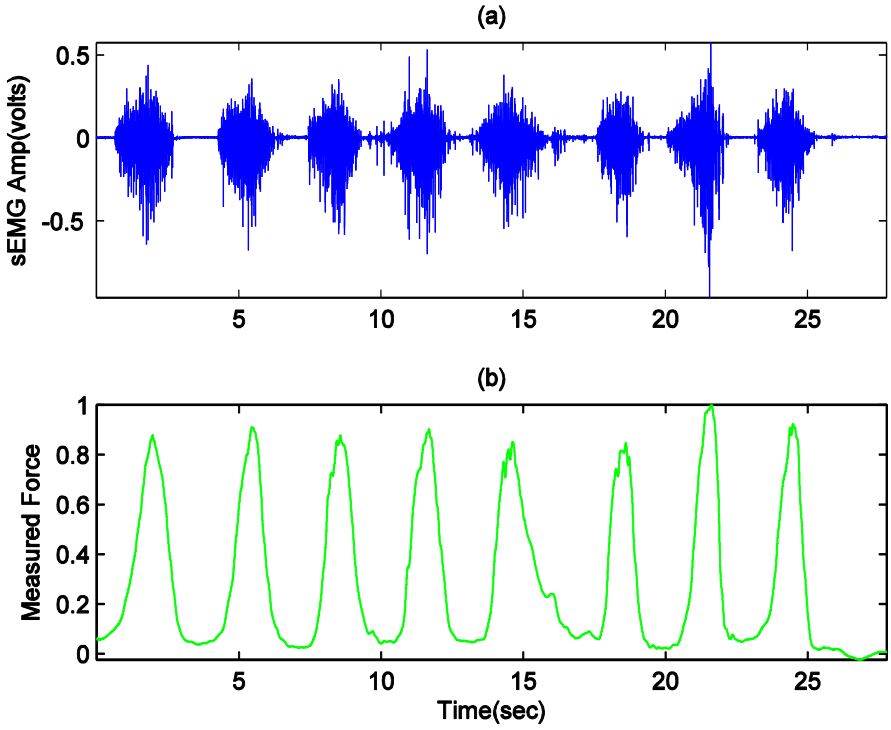

Figure 4.2 A sample of sEMG signal and force measured during knee joint flexion from healthy subject. (a) sEMG signal; (b) normalized measured force (force signal is normalized to the maximum value).

During data collection from stroke patients' muscles, the above-mentioned two trials were performed separately. Even though all the trials were completed in one day for each subject, at least 30 minutes rest time was given to the patients between each trial to reduce the influence of muscle fatigue.

4.3 Force Estimation based on the Established Relationships

As presented in Section 2.2, the additional MUs recruitments and the increase of firing rate of the already active MUs lead to the generation of muscle force. The phenomenon results in the changes in sEMG amplitude and *MF* with the varying muscle force. Since non-linear relationships have been found between sEMG features and force, it is feasible to predict force exerted by muscle based on these relationships in time-domain and the time-frequency analysis. Here, two methods, the time-domain analysis and the time-

frequency analysis methods, are proposed and compared by calculating the T_f, CC and RMSE between measured force and estimated force.

4.3.1 Electromechanical Delay

It is well known that there is a time lag between sEMG signal and the generated force. Generally, this delay is defined as electromechanical delay (EMD) [125] which presents the delay between the onset of electrical activity and the onset of measurable force generated by muscle contraction. The EMD is investigated as the difference between these two distinct onset time [126]. When AP in muscles initiates contractile phenomenon, the elements in the sarcomeres begin to contract but this contraction does not generate simultaneous movement on the joint. The existence of serial and parallel elastic components within the muscle is the main reason for this delay [127].

The EMD can be easily observed if both sEMG and the output force are measured simultaneously. Figure 4.3 depicts the sEMG signal and the measured force (this force value is normalized to the maximum value of the sEMG signal amplitude to simplify the comparison) generated at the same time. In this figure, T_{s_sEMG} is the general starting point of the sEMG signal of this single contraction, T_{s_Force} is the start of the measured force. As shown in Figure 4.3, it is apparent that there is a delay from the beginning of sEMG and the onset of the muscle force.

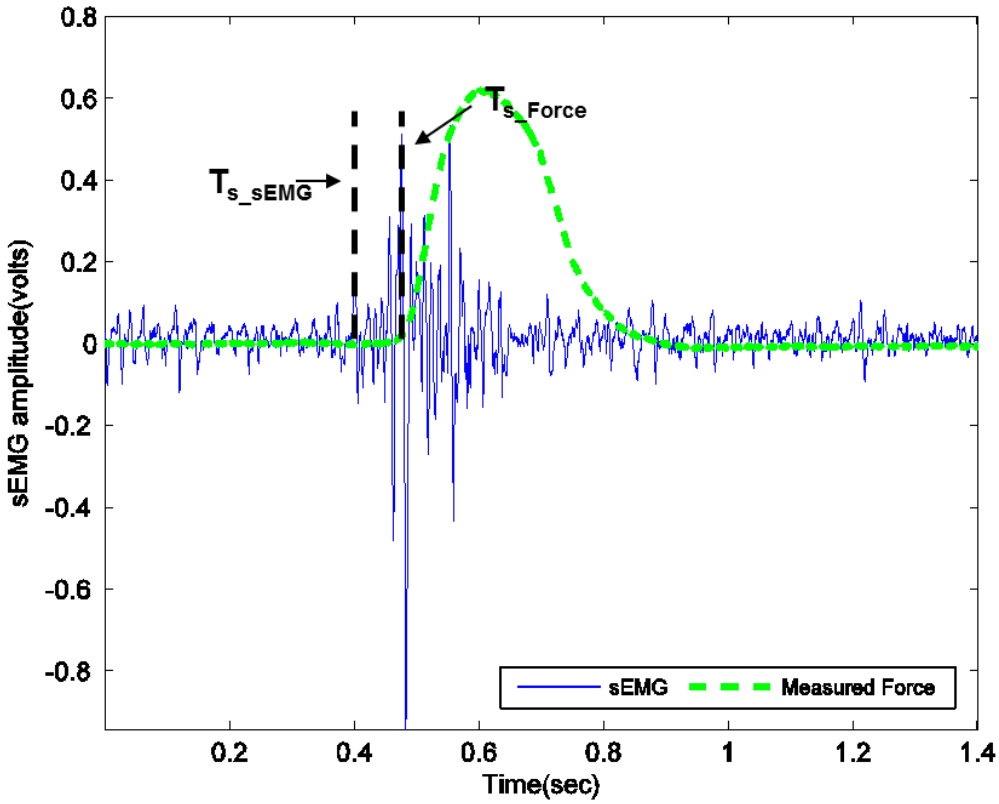

Figure 4.3 sEMG signal and normalized measured force from one single contraction.

Some studies have been done to observe the EMD between the onset of sEMG and muscle force. Imman et. al. [28] reported a delay of 80±20 ms between the peak muscle force and the peak in a rectified and smoothed sEMG from three muscles under isometric contractions. The EMD was also reported by Corser [125]. In his study, sEMG signals were recorded from forearm muscles during various forearm movements, and approximate 25 to 75 ms delays were found between the onset of sEMG and the onset of movements. However, the time delay values may vary in a wide range due to the differences in methodologies used.

Figure 4.3 also shows that the sEMG signal reaches to the peak much earlier than the exerted force, which notably implies that proper signal processing methods with suitable filters have the potential to predict the force exerted by muscle before the force measured by force sensor. However, few studies considered the EMD when estimating muscle force/torque using sEMG signals [9]. Lubecki et al [3] employed filters and RMS to develop a muscle force estimator. Results demonstrated that the signal processing was

done with a small time delay of less than 60 ms which is an enough period to predict the force/torque generated by muscles. Therefore, using a proper signal processing approach enables us to predict the muscle force before the actual force is applied by a few milliseconds. In this thesis, the actual applied force that we refer to, is taken from the force recorded with the data acquisition system. Even though the force sensor induces time delay to the force measurement system, we appropriately designed the circuit to reduce the time delay given by the force measurement system to the minimum.

4.3.2 Force Estimation Methods

Two different methods, CWT-based method and windowed RMS method for force/torque estimation are presented in Figure 4.4.

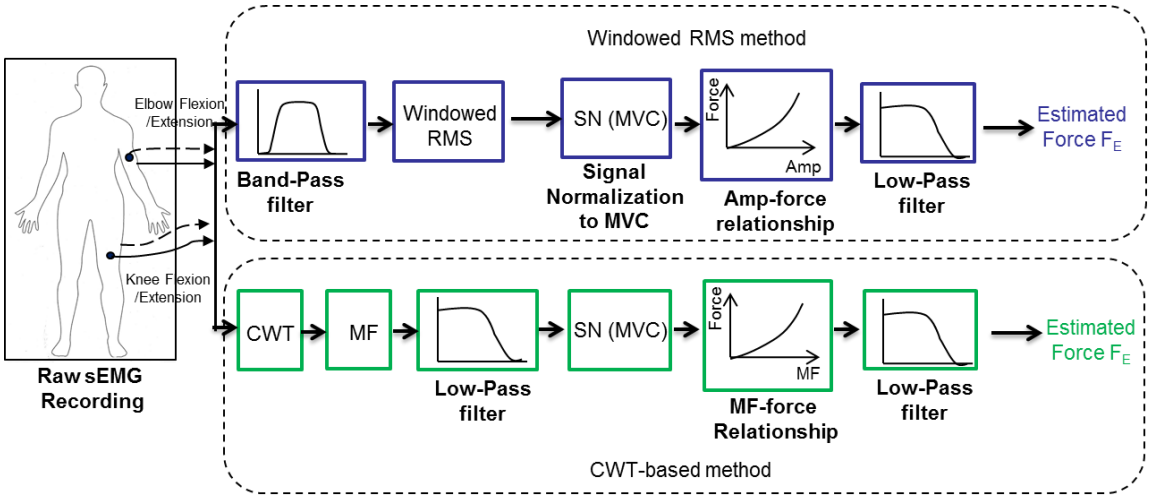

Figure 4.4 Signal flow diagram for two muscle force estimation methods.

The upper path shows the windowed-RMS based method. This method is based on the sEMG amplitude-force relationship. The recorded signal was first band-pass filtered. The cut-off frequencies for this filter were selected to remove the movement artifacts and high frequency signals which are not related to the muscle activations. Accordingly, a 4^{th} order Bessel band-pass filter with f_1=35 Hz and f_2=650 Hz cut-off frequencies was employed.

Then a windowed RMS was applied on the filtered signal. The windowed RMS parameter, such as the window length, was same as the one used in sEMG amplitude-force relationship establishment (Section 3.3). In addition, as mentioned in Section 3.3, it is necessary to normalize the signal to MVC to compensate for the variability due to the affecting factors.

The proposed time-frequency analysis method is depicted in another path of Figure 4.4. This method is based on the *MF*-force relationship. *MF* was first calculated from CWT scalogram. Figure 4.5 shows a single force-varying contraction and the corresponding contour scalogram. Most dominant energy is distributed at the large signal amplitude part. Meanwhile, it also can be observed that high percentage of the energy is located above approximate scale 40 which corresponds to 20.31 Hz. In this figure, the arrow illustrates the direction of frequency increasing, which corresponds to the scale decreasing direction.

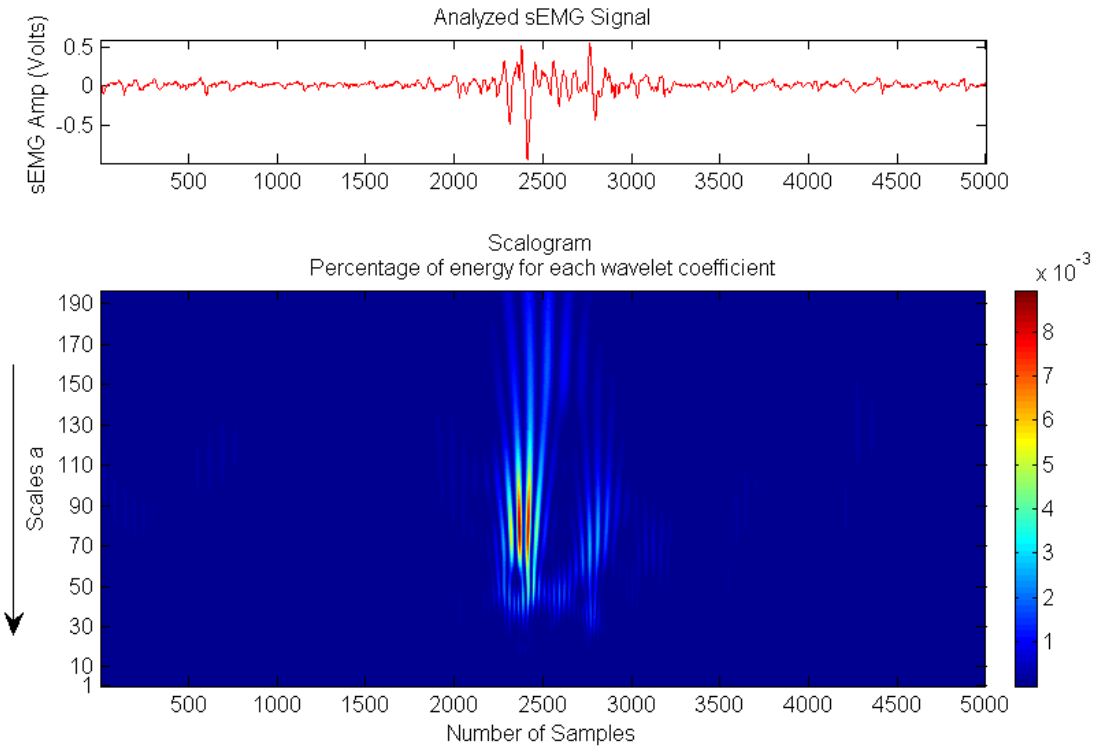

Figure 4.5 sEMG signal from one single contraction and the corresponding scalogram contour plot.

To smoothen *MF* by removing the spurious peaks, a low-pass filter was first applied. Appropriate cut-off frequency selection is crucial for the force estimation performance. T_m describes the average time difference between the filtered *MF* and the measured force from force sensor. Suitable low-pass filter ensures longer T_f, high correlation coefficients and low RMSE between the estimated force and measured force. To present the method for selecting the most suitable low-pass filter type and cut-off frequency, sEMG of a single contraction from one biceps brachii varying force trial is employed as an example.

Three types of filters, Bessel filter, Butterworth filter and Chebyshev filter, are considered and compared during the filter selection. Butterworth filter is the maximally flat amplitude filter and provides a near zero attenuation until near the cut-off frequency, and then descends into the attenuation smoothly. However, this filter induces some overshoot and ringing on the sharp rising waveforms, and gets even worse with higher orders. The Chebyshev filter has a better rate of attenuation beyond the pass-band than Butterworth, but it has considerably more ringing in step response than Butterworth. Compare with Butterworth filter and Chebyshev filter, Bessel filter outperforms by achieving flat group delay and linear phase response with very little overshoot or ringing [128]. In addition, Bessel filter can be easily implemented in the real-time system. Therefore, Bessel filter is selected as the low-pass filter in this force estimation method.

It should be noted that filters often induce time delay between the sEMG *MF* and the measured force, which definitely influences the T_f value. Filters with very low cut-off frequencies make the output signal quite smooth, but induce very long time delay, which renders the muscle force prediction is meaningless since we are predicting the muscle force in advance to the force exerted. Whereas, without filters or filtering with a high cut-off frequency leads to a noisy output signal with high frequency spikes, even though the T_m value is larger. Therefore, the most suitable cut-off frequency represents a compromise between the optimal estimated force shape and larger T_m value.

Five cut-off frequencies, namely, 12.5 Hz, 10 Hz, 7.5 Hz, 5Hz and 2.5 Hz, were compared. Figure 4.6 illustrates the measured force and filtered *MF* with different cut-off

frequencies. In order to simplify the comparison procedure, the filtered *MF* and measured force are normalized to 1 to be plotted in one figure.

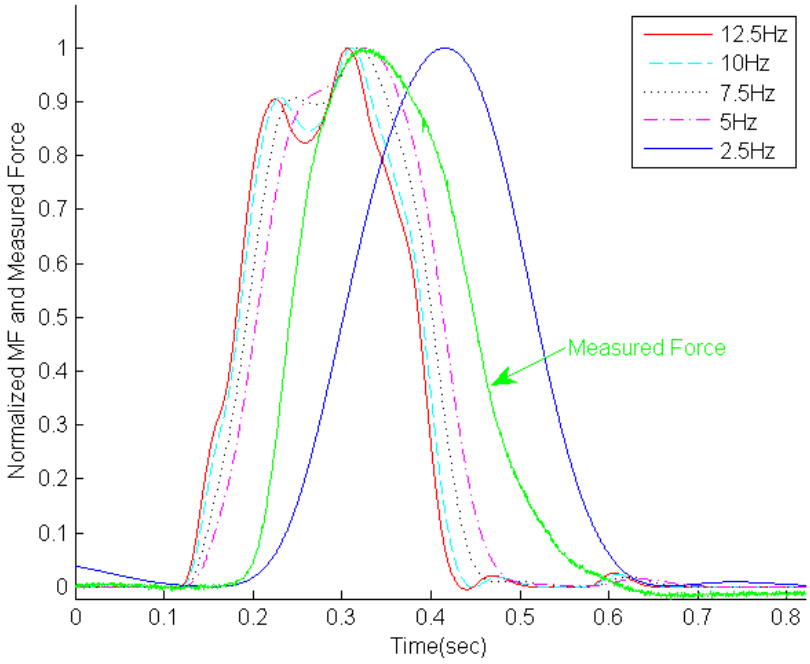

Figure 4.6 Measured force and filtered *MF* with different cut-off frequencies: 12.5 Hz, 10 Hz, 7.5 Hz, 5 Hz and 2.5 Hz. The arrow points to the measured force. All values are normalized to 1 for comparison.

As illustrated in Figure 4.6, among the compared five cut-off frequencies, the highest cut-off frequency at 12.5 Hz shows the least smooth shape. Whereas, the lowest cut-off frequency at 2.5 Hz yields almost same signal shape as the measured force, but a very long time delay can be observed when comparing with others cut-off frequencies. Table 4.2 tabulates the comparison of these cut-off frequencies by calculating the T_m and correlation coefficients between filtered *MF* and measured force. The cut-off frequency at 5 Hz demonstrates the highest correlation coefficients between filtered *MF* and measured force, yet the T_m value is acceptable. In order to compromise between the closest shape to measured force and proper temporal delay, a 4^{th} order Bessel filter with 5 Hz cut-off frequency is chosen to smoothen the *MF* signal.

Table 4.2 Cut-off Frequency Selections for Low-pass Filtering *MF*.

Cut-off frequencies	$T_m(ms)$	Correlation Coefficients
12.5 Hz	67.4	0.9849
10 Hz	62.2	0.9865
7.5 Hz	50.6	0.9891
5 Hz	38	0.9908
2.5 Hz	-63	0.9895

*T_m value: Negative value indicates that the measured force leads the filtered *MF*, while the positive T_m value demonstrates that the filtered *MF* leads the measured force.

Subsequently, the filtered *MF* signal was normalized to the maximum value of the muscle contraction trial. The estimated force was obtained by feeding the normalized signal to the *MF*-force relationship polynomial. Based on the analysis of the last chapter (Subsection 3.4.3), the relationship polynomial estimators for all the measured four muscles are non-linear and shown in Table 4.3. In this table, for the amplitude-force relationship, x is the windowed RMS, whereas for the *MF*-force relationship, x is the filtered *MF* signal. The output Y of the polynomial is the estimated force.

Table 4.3 sEMG Signal Amplitude-Force Relationship and *MF*-Force Relationship Polynomials for the Measured Four Muscles.

Muscle groups	Windowed RMS Method Amplitude-Force Relationship	CWT-based Method MF-Force Relationship
Biceps brachii	$Y=93x^3-1211x^2+5703x-0.5$	$Y=-2.171x^3+1050x^2+67390x+118100$
Triceps brachii	$Y=38870x^3-3850x^2+204.3x-0.9529$	$Y=0.0001388x^2-0.01426x+0.3615$
Rectus femoris	$Y=396000x^3-25300x^2+533.3x-1.238$	$Y=1.607x^3-503.8x^2+65620x$
Biceps femoris	$Y=143.3x^3-335.9x^2+309.4x$	$Y=7.174x^3-1195x^2+71350$

At this stage, sometimes, the estimated force is not very smooth for both methods. To achieve higher force estimation accuracy and to smoothen the output signal, a low-pass filter can be used for post-processing, even though it induces some more time delays. For both of the time-domain method and the CWT-based method, the estimated force was filtered using a 4th order Bessel low-pass filter with 9Hz cut-off frequency. However, some estimated forces are appropriately smooth (the CC value between the estimated force and measured force is higher than 0.95) and there is no need to be further filtered. Thus, the low-pass filter is optional and depends on the performance of estimated force.

The long positive T_f value can be observed since the estimated force leads the measured force generally. This T_f value is calculated by cross-correlation analysis of the estimated force and the measured force. The analysis determines the T_f that maximizes the cross-correlation coefficient between the predicted force and measured force. To validate the proposed methods, each force estimation result was evaluated against the corresponding measured force with another two criteria, cross-correlation coefficients (CC) and RMSE, which are calculated using the following expressions,

$$RMSE = \frac{\sum_i (y_i - \hat{y}_i)^2}{\sqrt{\sum_i y_i^2}\sqrt{\sum_i \hat{y}_i^2}} \tag{4.1}$$

$$CC = \frac{\sum_i y_i * \hat{y}_i}{\sqrt{\sum_i y_i^2}\sqrt{\sum_i \hat{y}_i^2}} \tag{4.2}$$

where y_i is the measured force and $\hat{y}_i$ is the estimated force. Cross-correlation is a measure of similarity of the y_i and $\hat{y}_i$ regardless of scaling. The closer the value is to 1, the higher the level of similarity is between the two signals. The two validation parameters were computed after adjusting for T_f between the estimated and measured forces. Between the two proposed methods, a one-way ANOVA was performed to determine if there is any significant difference, and the level of significance value alpha was set at $p \leq 0.05$.

4.3.3 Results and Statistical Comparison

Figure 4.7 shows the force estimation results from the two proposed methods comparing with the measured force from biceps brachii during one single contraction (Subject 12). The solid line indicates the measured force. The red dashed line depicts the force estimated by the proposed windowed RMS method, while the blue dash-dot line shows the predicted force by the CWT-based method. The force amplitude was normalized to the maximum force value to avoid the variability induced from different subjects and different muscles during muscle contractions. Apparently, the estimated force is leading the measured force and the shape of the predicted force is consistent with the measured one. In addition, the force predicted by CWT-based method is in advance to the force estimated by windowed RMS method.

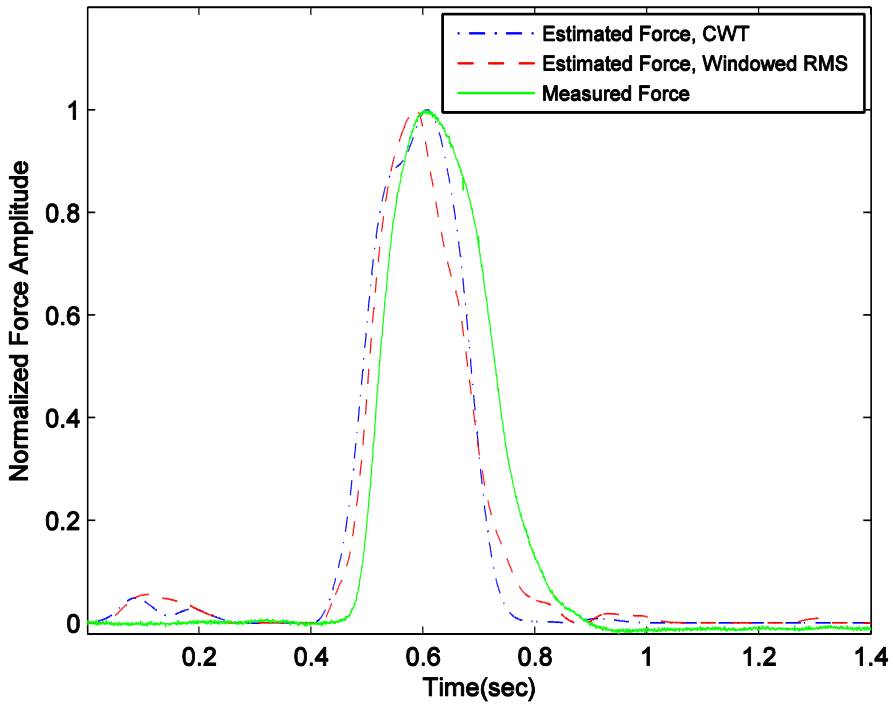

Figure 4.7 Force estimation results using the two proposed methods (subject 12). The green solid line indicates the measured force, while the red dashed lines depicts the force estimated by the proposed windowed RMS method and the blue dash-dot line shows the predicted force by the CWT-based method. (Force amplitude is normalized to 1).

Figure 4.8 illustrates the estimated force and measured force from four different muscles under flexion/extension performed by Subject 8. As illustrated in this figure, the muscle force generated by the four muscle groups can be estimated by both methods in similar shape.

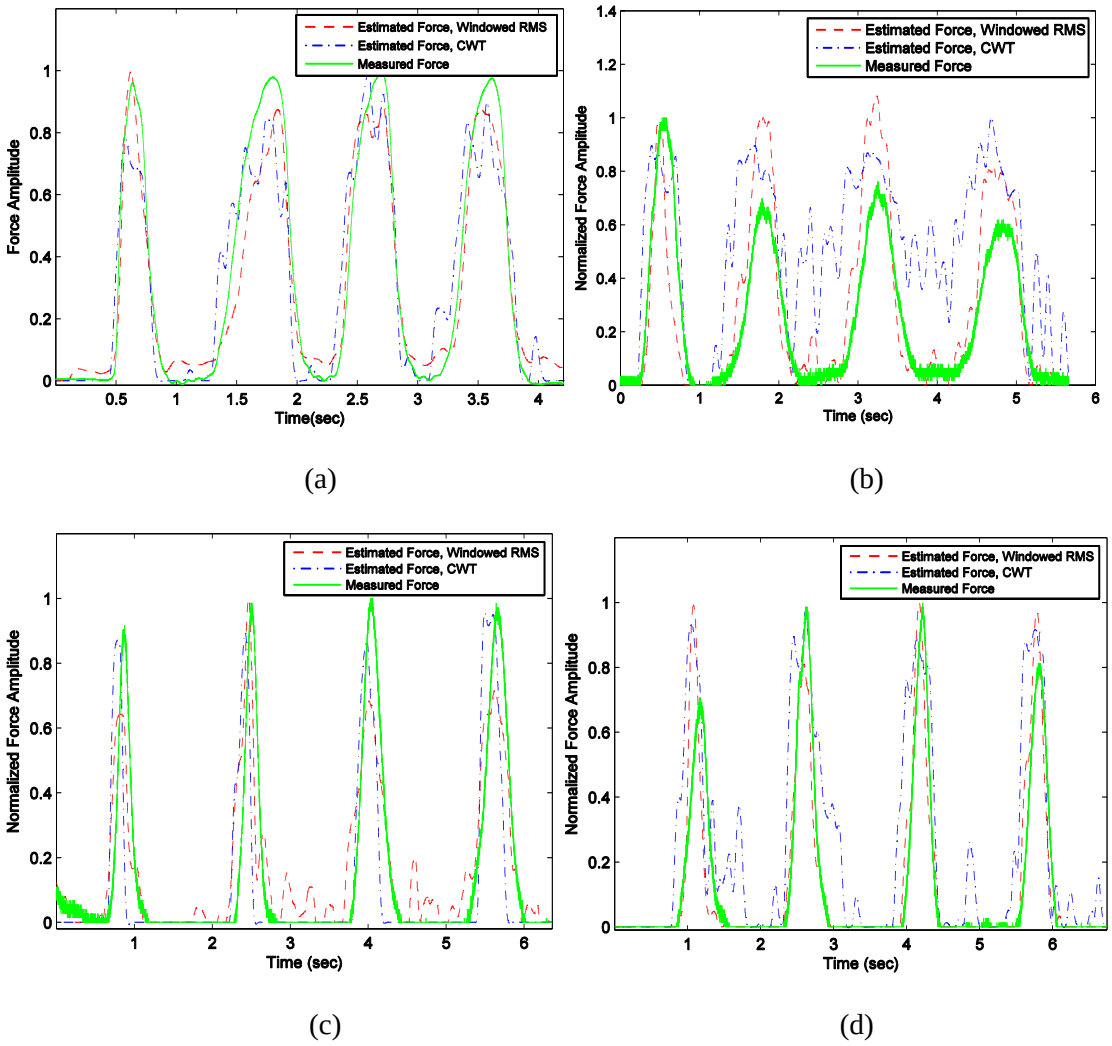

Figure 4.8 Force estimation results using the two proposed methods (Subject 8). The green solid line indicates the measured force, while the red dashed line depicts the force estimated by the proposed windowed RMS method and the blue dash-dot line shows the predicted force by the CWT-based method. (a) Biceps brachii (elbow flexion), (b) Triceps brachii (elbow extension), (c) Rectus femoris (knee extension), (d) Biceps femoris (knee flexion).

The T_f values calculated based on the correlation analysis of the estimated force and measured force are tabulated in Table 4.4. The T_f values obtained from CWT-based method have the average value range between 35.9±9.7 ms and 75.4±23.7 ms for different muscles among all the participants. While for the windowed RMS method, T_f ranges from 10.4±9.2 ms to 43.5±17.7 ms in average for all measured muscles. A one-way ANOVA reveals that significant differences are noted in T_f for every single muscle between the CWT-based method and windowed RMS method (p<0.05).

Table 4.4 CWT-based method vs. Windowed RMS method (T_f for each muscle group in milliseconds).

Subjects	4 Muscle groups							
	Biceps Brachi		Triceps Brachi		Rectus Femoris		Biceps Femoris	
	CWT	Windowed RMS	CWT	Windowed RMS	CWT	Windowed RMS	CWT	Windowed RMS
s1	36.8	31.6	34.2	7.6	90.8	54.8	96.4	74.8
s2	40.4	7.2	58.4	39.2	99.4	59.2	25.8	26.8
s3	44.4	0.4	76.2	49.6	63.8	46.4	42.4	32.4
s4	44.2	6	55.6	46	90.4	49.2	74.4	40.8
s5	51.8	5.6	100	72.8	104.6	53.6	51.6	46.8
s6	39.6	7.6	41.6	38	18.6	61.2	51.8	23.2
s7	20.4	2	68.2	44	107.6	64.8	68.8	60.4
s8	50.2	12	46.6	42	88	55.2	66	43.6
s9	29.4	15.2	60.2	43.6	67.2	48.8	69	49.6
s10	25.4	5.6	49.4	49.4	75.8	42	70.4	30.8
s11	23.8	11.2	34.2	33.2	61.4	14.8	107.8	81.2
s12	34.6	4.8	58.4	39.6	55.2	27.2	92.8	23.6
s13	33.6	28.8	76.2	51.6	69	16.4	57	27.2
s14	28.4	8.8	55.6	30.4	64.2	15.2	49.2	35.6
Average±svd	35.9±9.7	10.4±9.2	58.2±17.9	41.9±14.1	75.4±23.7	43.5±17.7	65.9±22.3	42.6±18.5

Figure 4.9 shows the two methods comparison in the average T_f between the estimated force and the measured force. The average T_f of the 14 subjects obtained from CWT-based method is longer than windowed RMS method in all measured muscles. At least 15.3 ms difference of T_f is observed between the two methods throughout all the measured muscles.

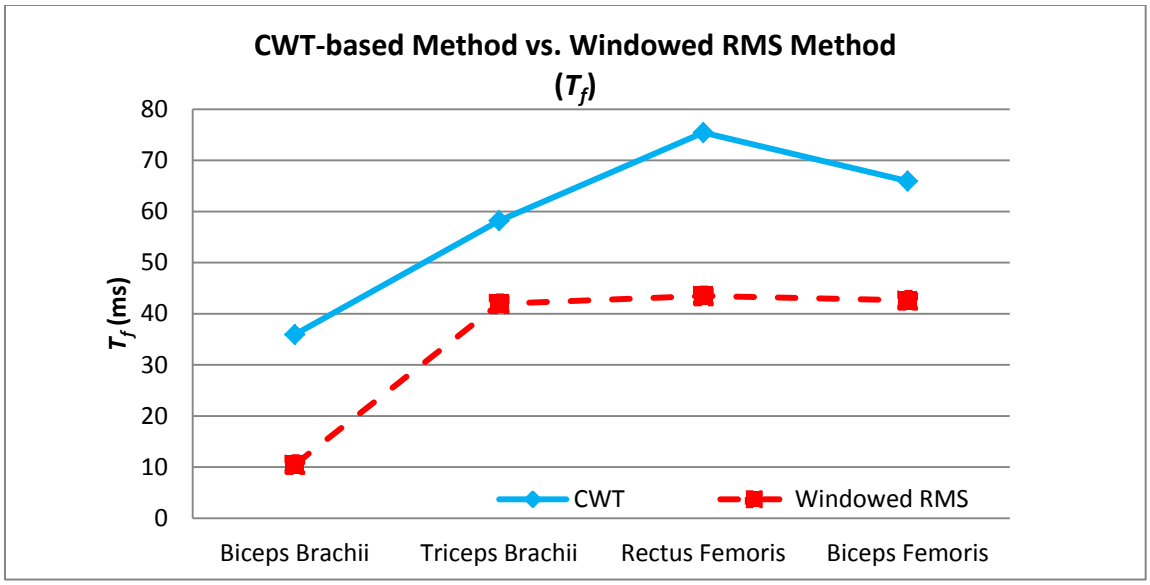

Figure 4.9 T_f comparison between CWT-based method and windowed RMS method of 14 subjects.

Figure 4.10 depicts the average RMSE and CC values of the four measured muscles. Generally, the CC values for all the subjects are high and the RMSEs are low, which indicates both methods have a good performance in following the shape of the measured force. Good agreement in shape, similarity in magnitude and time to peak are observed, when comparing the estimated force with the experimentally measured force.

More specifically, for the results from CWT-based method, the average RMSE is lower with 0.1524 ± 0.016 in triceps brachii and 0.2152 ± 0.040 rectus femoris when it is compared with the windowed RMS method. On the contrary, lower RMSEs are yielded from windowed RMS method in biceps brachii and biceps femoris with 0.1312 ± 0.062 and 0.1929 ± 0.042 respectively.

High CC values are observed between estimated force and measured force for both methods. *P*-value which is used for testing the hypothesis of no correlation are all less than 0.05, indicating significant correlations between the estimated force and measured force. However, the windowed RMS method outperforms CWT-based method with slightly greater values of average CC>0.9527, while the average CC for the CWT-based method is larger than 0.8693 for all measured muscles.

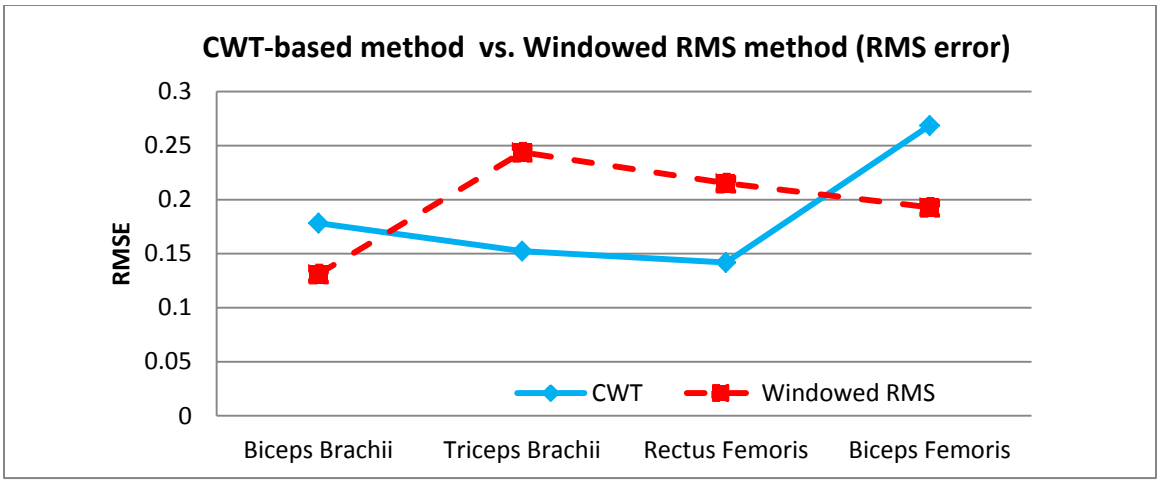

(a)

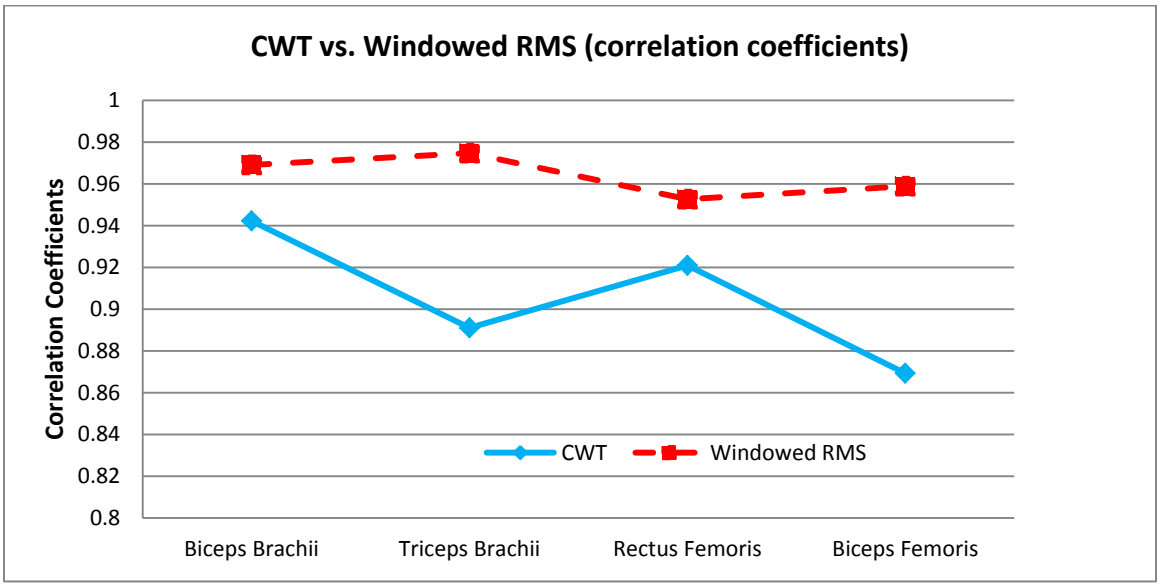

(b)

Figure 4.10 Average RMSE and correlation coefficients comparison between CWT and windowed RMS with the four different muscle groups of the 14 subjects. (a) RMSE. (b) Correlation Coefficients.

Other than validating the proposed methods with sEMG signals from healthy subjects, stroke patients' sEMG signals are also used to validate the feasibility of the algorithms. The selected polynomials describing the sEMG amplitude-force relationship and *MF*-force relationship for rectus femoris and biceps femoris of stroke patients are all third order polynomials (Table 4.5). Based on these relationships, the estimated force and measured force for both methods are illustrated in Figure 4.11 (Stroke subject 3).

Table 4.5 sEMG Signal Amplitude-Force Relationship and *MF*-Force Relationship Polynomials Established from Stroke Patients sEMG signal.

Muscle groups	Windowed RMS Method Amplitude-Force Relationship	CWT-based Method MF-Force Relationship
Rectus femoris	$Y=27.29x^3-162.9x^2+245.2x-12.06$	$Y=1.645\times10^{-4}x^3-0.01154x^2+0.5522x+3.408$
Biceps femoris	$Y=-50.1x^3+50.59x^2+61.45x$	$Y=3.417\times10^{-5}x^3-0.005956x^2+0.8159x+46.46$

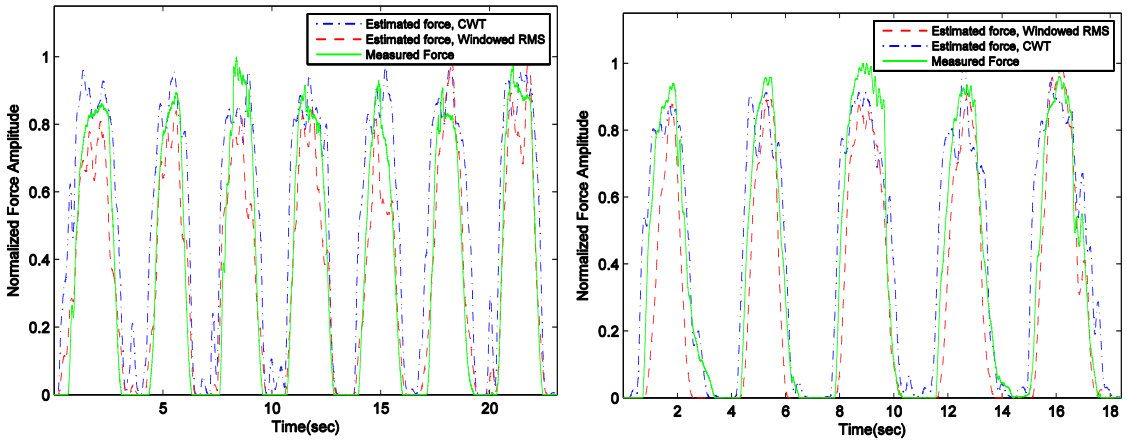

(a) (b)

Figure 4.11 Force estimation results using the two proposed methods (Stroke subject 3). The green solid line indicates the measured force, while the red dashed lines depict the force estimated by the windowed RMS method and the blue dash-dot line shows the predicted force by the CWT-based method. (a) Rectus femoris (knee extension), (b) Biceps femoris (knee flexion).

As illustrated in Figure 4.11, good force estimation can be accomplished with similar shape to measured force using stroke patients' sEMG signals. For the windowed RMS method, the CCs between the estimated force and measured force are high with 0.968 ± 0.014 and 0.9401 ± 0.1859 for rectus femoris and biceps femoris respectively. While high CCs obtained from the CWT-based method are 0.9594 ± 0.0212 and 0.9497 ± 0.0231 for both muscles on average. No significant difference is found between the two methods when the CCs were measured using ANOVA ($p<0.05$). In addition, for the measured two muscles, the RMSE are small with 0.1101 ± 0.0199 and 0.1279 ± 0.0327

on average for time-domain method, 0.1182 ± 0.027 and 0.1416 ± 0.0348 for time-frequency analysis method, respectively.

Figure 4.12 shows the statistical analysis results of T_f from stroke patients' sEMG signals using the two methods. The negative time values in this figure demonstrate that the estimated force lags the measured force. For the windowed RMS method, the mean values of the T_f value indicate that the estimated force does not lead the measured force. Whereas, for the CWT-based method, the average T_f shows the estimated force leading the measured force with 51.93 ms and 59.09 ms for rectus femoris and biceps femoris, respectively. The results also demonstrate that the CWT-based force estimation method outperforms the windowed RMS method since T_f calculated from CWT-based method is much longer not only for healthy subject but for stroke patients.

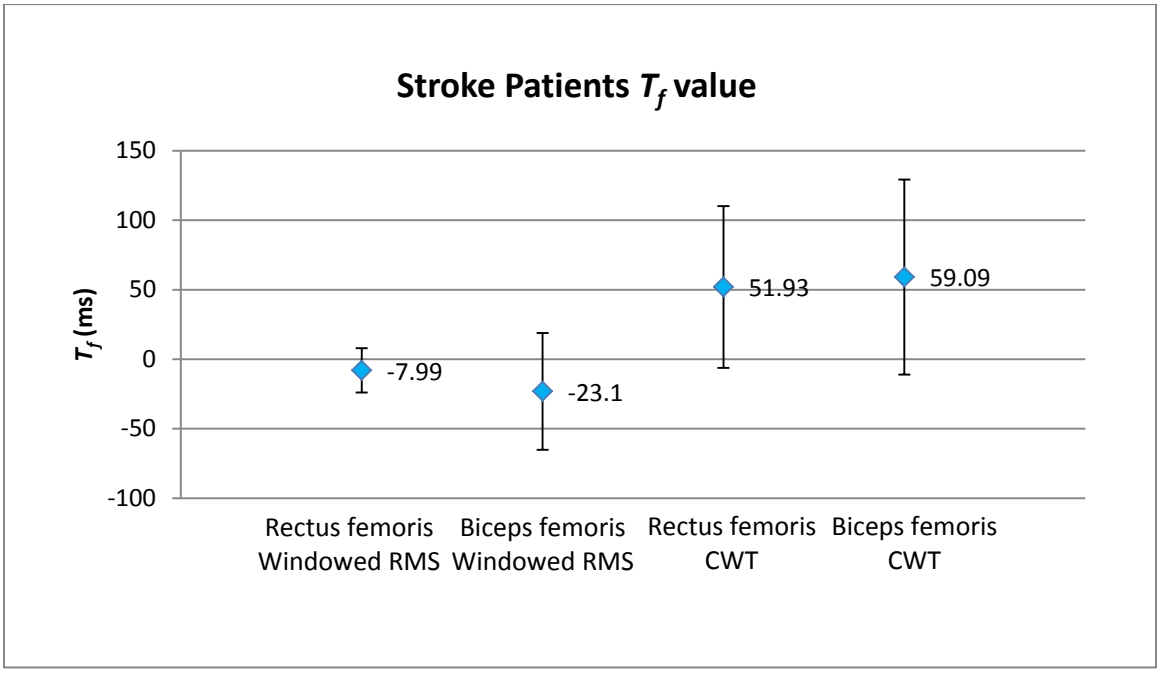

Figure 4.12 T_f between estimated force and measured force for stroke patients. The first two are obtained from windowed RMS method, while the other two are the results from CWT-based method. (Negative values: the estimated force lags the measured force).

4.4 Neural Networks based Force Estimation

In the previous section, the muscle force estimation methods are based on the sEMG amplitude-force relationships and *MF*-force relationships. Good similarity in the estimated signal shape and long T_f are achieved for healthy subjects. However, for post-stroke patients, the hemiparetic muscles have been shown to have altered fiber type proportions and fiber atrophy. These changes in muscle architecture influence the muscle force-activation relationship of patients. Although high average CC values and long T_f are yielded, not every trial achieves good force estimation performance using the two methods, since the established relationships may not be suitable for each patient. Meanwhile, not all patients' data can establish the relationships successfully. The *MF*-force relationship using second order or third order polynomial may not be sufficient. Among the five stroke patients, only stroke subject 3 and subject 5 generate the relationships with high correlation coefficients, while others relationships demonstrate very low coefficients and cannot be described with polynomials accurately.

In some literatures, ANN has been used to derive complex relationships without involving detailed information, such as mathematical expressions describing relationships [57, 60, 61, 129]. ANN is a computational system inspired by the learning characteristics and the structure of biological neural networks. One of the most widely used ANN is the multilayer perceptron (MLP). MLP is characterized by a set of input units, a layer of output units, and a number of hidden layers. Each input node is connected to each unit in the hidden layer. The connections between units have an associated weight *W*. Each unit of the hidden layer is connected to the neurons in the following layer, the hidden or output, in a similar way.

To predict force exerted by muscles without establishing complicated relationships for stroke patients, a novel approach based on CWT and ANN is presented in this section. sEMG signals collected from healthy subjects and stroke patients will be used to validate the feasibility of this new approach.

4.4.1 ANN Training

ANN is a mathematical model inspired by biological neural networks. It consists of interconnection of multiple layers of artificial neurons. The processing unit is called "neurons" which are interconnected and distributed in layer. The neurons are sorted in a number of layers and neuron outputs. In each layer, they are interconnected to the other layer neuron inputs. The ANNs are distinguished by their learning and recall mechanisms, the activation functions, the number of layers and neurons, and the distribution of the connections.

Figure 4.13 depicts the general architectural graph of a multilayer network. As illustrated in this figure, the blue circles are the neurons, and each neuron unit receives input from some other units or from an external source. The outputs of the neurons in each layer are interconnected to the other layer neuron inputs. Since a multilayer perceptron with a single hidden layer is sufficient to approximate any bounded continuous function, only one hidden layer is used for the ANN in this study.

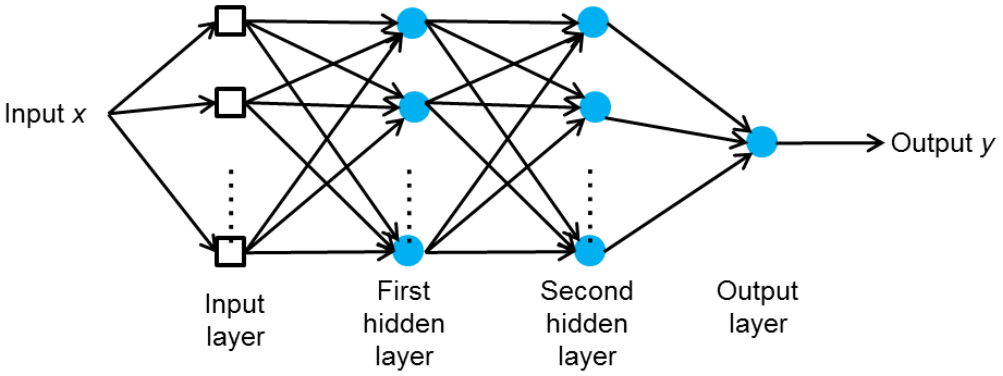

Figure 4.13 Architectural graph of a multilayer network.

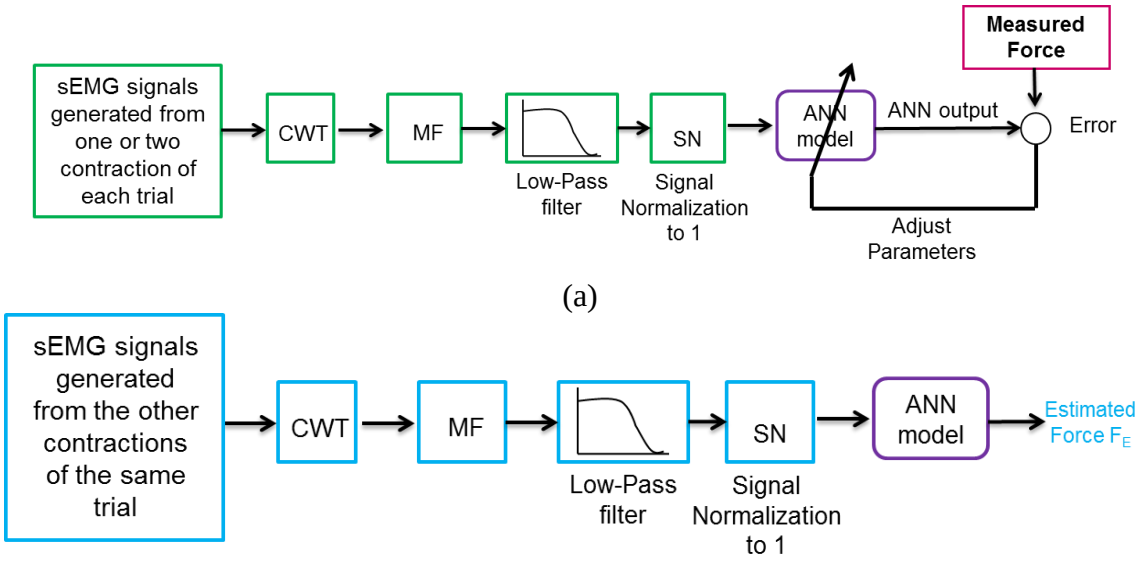

Figure 4.14 Signal flow diagrams for muscle force estimation. (a) ANN parameters training; (b) Muscle force estimation method.

Figure 4.14 illustrates the signal flow for the new muscle force estimation method based on CWT and ANN. During the ANN training, sEMG signals generated from one or two contraction of each trial were randomly selected as the subset to calculate the *MF* of signal power spectral. A 4^{th} order Bessel low-pass filter was applied to smoothen the *MF* signal by removing the high frequency spurious peaks. Then the filtered *MF* signal was normalized to the maximum values. The training desired output was the corresponding normalized measured force. During the network training, batch training is employed. The weights and biases are updated in batch training after all the inputs and targets are presented. In this kind of training, the weight updating is done at the end of a training epoch.

In MATLAB implementation, the weights in the ANN models were adjusted using the conjugate gradient back propagation (BP) algorithm that is a common employed method for training ANN models. It has a feed-forward stage and a learning stage. The two steps are repeated until the difference between the training output and the target signal is below a specified value.

Parameters selection of the ANN model is important for the performance of proposed method. Before training the network, the network input and the desired output data in

each training set were normalized to [minimum, maximum], which corresponds to -1 to 1. The networks were trained for 2000 epochs with a very small training performance goal (1e-15).

Different number of layers and hidden neurons were examined for the networks. In this study, only two layers with one single hidden layer are sufficient to approximate the bounded continuous function, since the training data were not very large and complicated.

The optimal number of hidden neurons that produce the small test error and high correlation coefficients (CC) value, guarantees good performance in the force estimation results. To choose a suitable number of hidden neurons, two criteria, the RMSE and the CC values were examined. Figure 4.15 shows the training and testing RMSE and CC results for selecting optimal number of hidden neurons. The training error keeps decreasing consistently with the increasing number of hidden neurons, while the CC is increasing. However, the CC value and the RMSE reach to roughly steady state from 6 hidden neurons onwards. ANN with the lowest training error is over-fitted to the training data, as shown by the fact that the test error increased. Therefore, an ANN with 6 neurons for the hidden layer was selected. Nevertheless, for different trials of healthy subjects and stroke patients, the optimal number of hidden neurons is different and the selection has to be repeated for each trial.

After the ANN model training, the sEMG signal generated from the other contractions of the same trial is used to calculate the *MF*. This filtered and normalized *MF* is the input to the ANN model. The output of this ANN model is the estimated force. This muscle force estimation method is shown in Figure 4.14 (b).

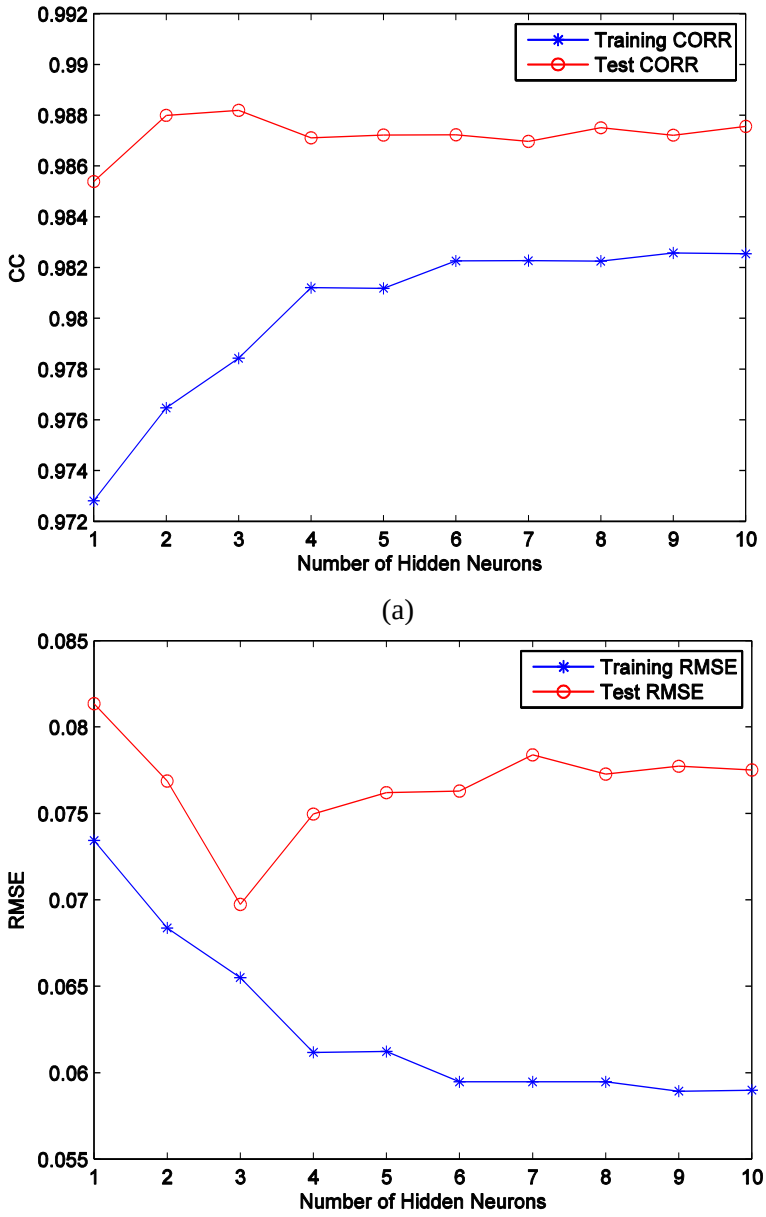

Figure 4.15 The ANN training and testing results to determine the optimal number of hidden neurons. (a) CC; (b) RMSE (sEMG signal from biceps femoris of stroke patient 3).

Since the position of sEMG electrodes relative to the motor units, muscle fiber types, muscle length, muscle volume, skin impedance are different from subject to subject, the network generated from one subject may not be applicable for other subjects. Therefore, the network was trained for each individual to avoid the influence of these variable factors.

4.4.2 Force Estimation Results

Figure 4.16 shows the example of training errors progress, in terms of mean squared errors, up to 56 epochs of training sets when training was stopped. Even though the best training performance is 0.0010188 which is larger than the training performance goal (1e-15), good performance still can be found from the validation results.

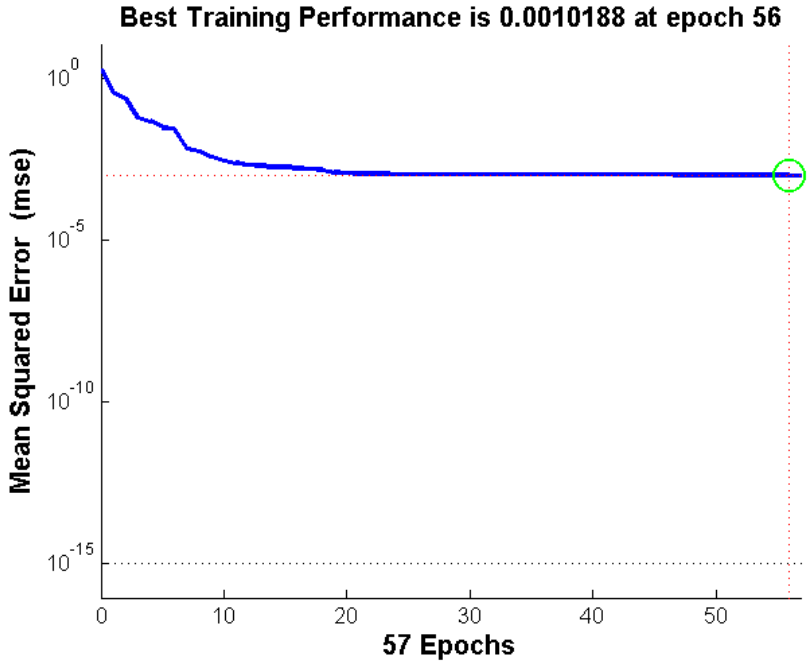

Figure 4.16 Progress of training errors (Performed by the sEMG signal recorded from stroke patient 5 biceps femoris during knee flexion).

The linear regression of the training target relative to the training outputs is illustrated in Figure 4.17. In this figure, Y is the training output and T is the training target. As shown in this figure, the Y=T curve almost overlaps the regression fitting line and the linear regression curve indicates good performance of this network with a very high R-value (R=0.9957).

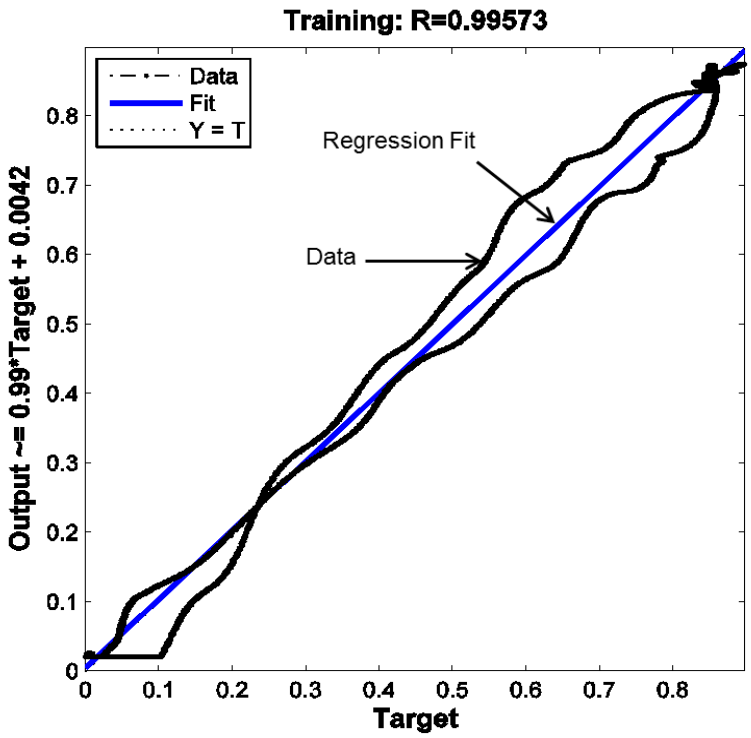

Figure 4.17 ANN training regression. T is the training target and Y is the training output. (Performed by the sEMG signal recorded from stroke patient 5 biceps femoris during knee flexion)

Figure 4.18 (a) (b) (c) (d) illustrate the results given by the CWT-ANN based force estimation method from four different muscles of healthy subject 12, 4, 14, 8, respectively. The results were quantitatively evaluated against the measured force using the RMSE and CCs for each single contraction of each healthy subject. For all the healthy subjects, the RMSE are averaged across all the participants and the measured muscles. The RMSE values are low with 0.1701 ± 0.047. Meanwhile, high CCs are obtained with 0.9398 ± 0.0230 on average for all measured muscles.

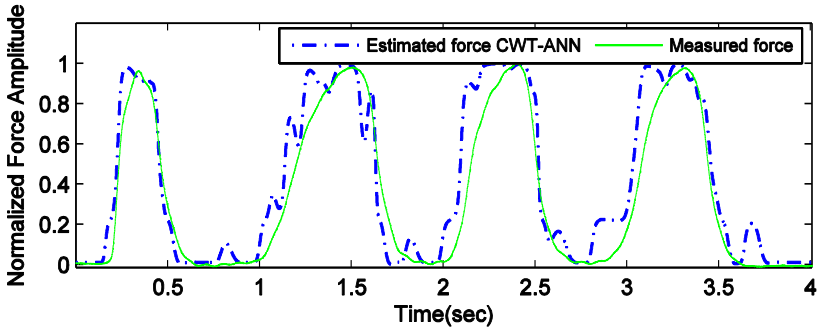

(a)

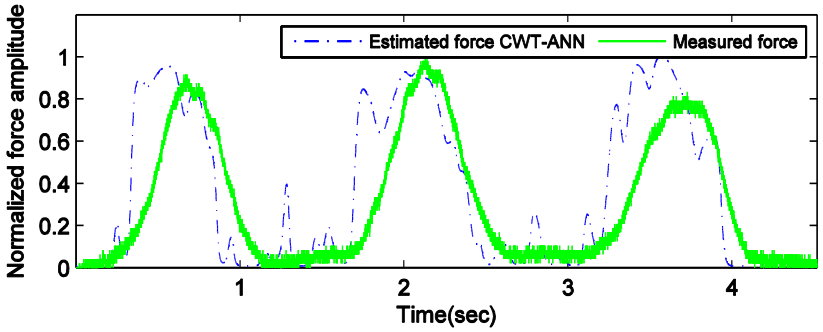

(b)

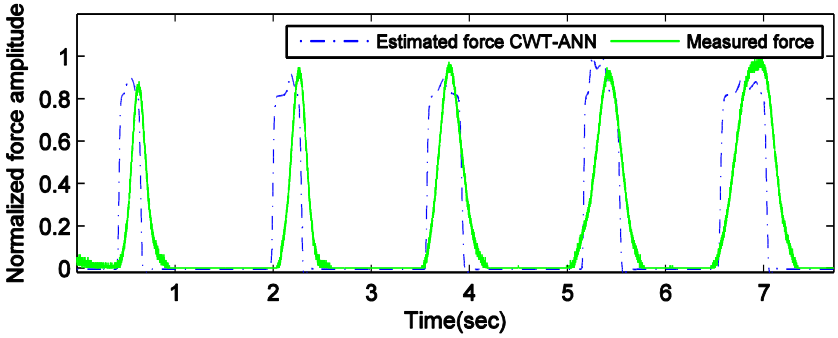

(c)

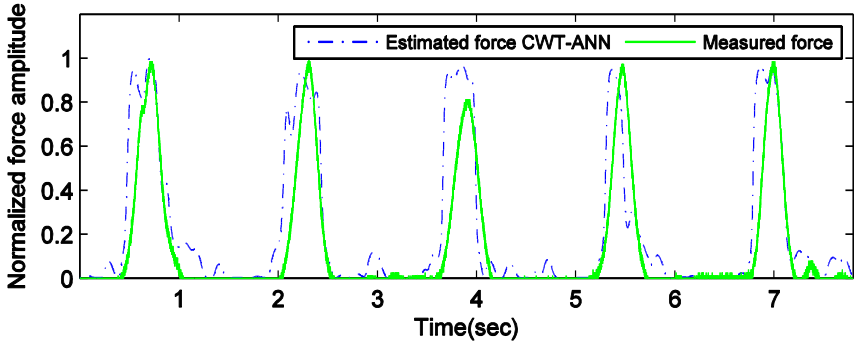

(d)

Figure 4.18 Force estimation results using the proposed CWT-ANN based approach. The green solid line indicates the measured force, while the blue dash-dot line shows the predicted force by the proposed method. (a) Subject 12, biceps brachii, elbow flexion; (b) Subject 4, triceps brachii, elbow extension; (c) Subject 14, rectus femoris, knee extension; (d) Subject 8, biceps femoris, knee flexion;

Figure 4.19 illustrates the sample of muscle force estimation results from two different muscles of stroke patient 2 and 3, respectively. The muscle force estimation results are quantitatively evaluated against the measured force using the RMSE and CC for each single contraction.

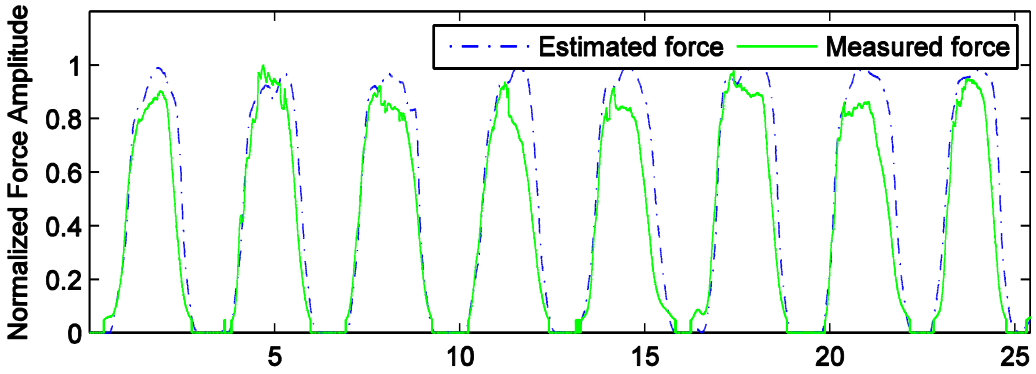

(a)

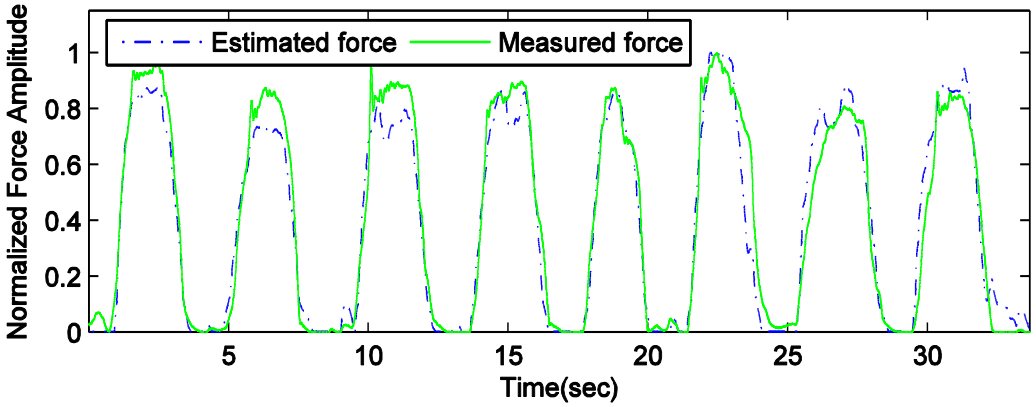

(b)

Figure 4.19 Force estimation results using CWT-ANN method. The green solid line indicates the measured force, while the blue dash-dot line shows the predicted force by the proposed method. (a) Stroke subject 3, Rectus femoris (knee extension), (b) Stroke subject 2, Biceps femoris (knee flexion).

For each stroke patient, same method is used to evaluate the performance of the proposed method. The corresponding RMSE and CCs are tabulated in Table 4.6. The RMSEs are averaged across participants and the measured muscles. The RMSE values are low with 0.1645 ± 0.0691 and 0.1584 ± 0.1036 for rectus femoris and biceps femoris respectively. Meanwhile, high correlation coefficients are obtained with 0.8967 ± 0.0934 for rectus femoris and 0.9029 ± 0.1406 for another muscle on average.

Table 4.6 Muscle Force Estimation Results of the Five Stroke Patients.

Stroke Patient	**CC**		**RMSE**	
	Rectus Femoris	*Biceps Femoris*	*Rectus Femoris*	*Biceps Femoris*
Patient 1	0.9247 ±0.1058	0.9135 ±0.0613	0.1342 ±0.05936	0.1419 ±0.0765
Patient 2	0.8068 ±0.1145	0.8434 ±0.1020	0.2389 ±0.0688	0.2437 ±0.0990
Patient 3	0.9670 ±0.0164	0.9371 ±0.1884	0.1037 ±0.0199	0.0933 ±0.0292
Patient 4	0.9391 ±0.0263	NA	0.1411 ±0.0227	NA
Patient 5	0.8800 ±0.0628	0.9730 ±0.0284	0.1642 ±0.0350	0.0849 ±0.0373
Average	0.8967 ±0.0934	0.9029 ±0.1406	0.1645 ±0.0691	0.1584 ±0.1036

*NA: sEMG signals recorded from the biceps femoris of patient 4 have very small amplitude and difficult to be separated from baseline noise level.

For the T_f value, not every single contraction indicates that the estimated force leads the measured force for stroke patients. For those contractions where the estimated force leads the measured force, the average T_f is 93.04 ms for recuts femoris and 64.45 ms for biceps femoris.

Although the muscle activation patterns of stroke patients result in a great variability [130-132], due to the dysfunction caused by spasticity, reduced coordinative control, muscle weakness and impaired sensory-motor control, from the force estimation results, the CWT-ANN based method shows a good performance on estimating muscle force for stroke patients.

4.5 Summary

In this chapter, three approaches are proposed to estimate the force exerted by muscles. The first two methods are based on the sEMG amplitude-force relationship and the *MF*-force relationship. The force estimation results are compared between the windowed RMS method and CWT-based method. Generally, the CWT-based method indicates longer T_f than the time-domain analysis method. However, slight higher correlation coefficients can be observed from the results of windowed RMS method, which implies

good consistent in the shape of the estimated force with the measured force. Another approach is developed based on CWT and ANN. The method is investigated to overcome the difficulty to establish nonlinear sEMG-force relationships from stroke patients' sEMG signals. sEMG signal collected from healthy subjects and stroke patients are used to validate the CWT-ANN based method. The results show that the muscle force/torque can be estimated with high correlation coefficients and low RMSE. It also can be concluded that ANN is an effective way to map the relationship between sEMG signals time-frequency features and force.

From the results obtained from these methods, great application potential can be found in force estimation for multiple groups of muscles. The proposed CWT-based method will be chosen for further implementation in rehabilitation device, since the force can be predicted much longer before the actual force is applied. With respect to the applications, longer T_f ensures the prompt delivery of the estimated force to the motor. Meanwhile, more advance information also ensures that the assistive device or rehabilitation device deliver assistive force/torque concurrently or even be faster than muscles. The implementation details and the real-time experiments will be presented in Chapter 6.

CHAPTER 5

MUSCLE FATIGUE DETECTION

5. 1 Introduction

Muscle fatigue is the reduction in the ability of a muscle to generate force or to maintain a target level of force [4, 5]. The accumulation of long period of fatigued contractions leads to muscle pain and even an increased risk of injuries [6]. Sudden accidents and injuries can be avoided by continuously monitoring the muscle fatigue progression. To this end, the electrical activation, muscle contraction strength, muscle state and fatigue features extracted from sEMG signals, have been commonly used for fatigue detection.

As presented in Section 2.3, typical fatigue detection studies focus on the isometric contraction where the muscle is trying to maintain a constant force. Under such circumstance, the time-domain features, such as RMS, MAV increase when the muscle fatigue occurs. While, the *MF* and *MDF* of sEMG signals power spectrum shift to the lower frequencies with time-frequency analysis. These changing characteristics are reliable fatigue indictors. However, isometric muscle contractions are not commonly involved in human daily activities where the dynamic muscle contraction is mostly carried out. During dynamic muscle contractions, *MF* and signal power *P* of the power spectrum change with the forces exerted by muscles. These changing fatigue characteristics are function of the applied force. Hence, it is necessary to consider the force generated by muscles as one of the key factors influencing the fatigue evaluation

results. Moreover, most of current fatigue detection approaches for dynamic contraction focus on developing efficient algorithms to extract and select fatigue relevant features from sEMG signals [8] [95, 102]. Whereas, some other studies classified muscle states into non-fatigue, transition to fatigue and fatigue [107] or developed fatigue index [103-105].

In this chapter, a novel fatigue detection method will be presented. This approach is based on CWT, and the *MF* and signal power *P* are correlated for detecting muscle fatigue. Most of current fatigue research mainly focuses on the clinical aspects. Research on the real-time implementation of detecting fatigue in assistive device or rehabilitation device has been scarce. Thus, generalized muscle fatigue levels could be useful to track the muscle state of the users. In this study, discrete fatigue levels are estimated, which describe the fatigue state changes generally, but not assigned to any quantified force values. To make the fatigue levels describe the real physiological fatigue changes more accurately, the fatigue levels are quantified to the muscle maximal capacity based on linear regression and statistical analysis. The feasibility of this approach is evaluated using the sEMG signals recorded under fatigue contractions from 14 healthy subjects and 5 stroke patients.

5.2 Experimental Protocol

In this chapter, the healthy subjects and stroke patients were the same ones recruited for the experiments in Chapter 4. In addition, the sEMG and force signals were collected using the same setup as mentioned in Subsection 3.2.2.

During the experiments, the subjects were seated comfortably on a chair. For healthy subjects, the sEMG signals were recorded from biceps brachii, triceps brachii, rectus femoris, and biceps femoris. For the stroke patients, the data were only collected from the lower extremity muscles: rectus femoris and biceps femoris of the stroke-affected leg. In this study, the constant force contractions and force-varying muscle contractions were both involved. Due to the limitations of the force measurement setup, the dynamic

contraction can only be performed with a varying force but constant joint angles. Thus, all the muscle contractions were performed with the joint extension or flexion at a 90 degrees joint angle.

Warm-up exercises consisting of 5-6 submaximal contractions were first performed by each subject. The exercise includes slow extension and flexion until the subject feels familiar with the setup and the experimental tasks. After the warm-up exercise, the subjects were asked to perform contraction trials in sequence. Each muscle contraction trial consists of three steps: pre-fatigue MVCs measurements, constant force contractions or force-varying contractions and post-fatigue MVCs measurements.

During the varying force muscle contractions, it is obvious that the muscle lengths, the electrodes locations and the movement velocity have significant influences on the sEMG signals collection. In our fatigue exercise protocol, we assume that these factors are adequately constrained to be considered constant throughout each trial. For stroke patients' data collection experiments, due to their weak muscles and the muscular changes in the affected side, the measured force may not be highly consistent with the requested applied force. The detailed 3 steps of each trial is descried as follows:

- ***Pre-fatigue MVCs measurements***

  The experimental protocol began with the acquisition of the MVC by pulling or pushing the handle of the setup (Figure 3.2), and kept the contraction force for at least 3-5 seconds with joint flexion or extension. The subjects were encouraged verbally to exceed previous force level. For each subject, the MVCs were performed at least three times to make sure the recorded signals represent the maximum force of the subject. The average MVC value was considered as the pre-fatigue maximum voluntary force. This value was also used in the following steps as the reference to set the submaximal force level for each subject.

- ***Isometric muscle contraction***

  During constant contraction trials, the subjects were asked to maintain a constant force until they felt exhausted and cannot continue any further. This kind of contraction trial was repeated 4 times with increasing force target for each time. The targeted force values were 20% MVC, 40% MVC, 60% MVC and 80% MVC.

  To track the MVCs changes during isometric contractions, the subjects were asked to perform another isometric contraction, exerting one MVC every 10 seconds in constant force contraction.

- ***Force-Varying muscle contraction***

  Three generally varying force contraction trials were conducted. The first trial was performed by a cycle of a contraction. The contraction force varied from a relax state to a target force value before returning to the relax state. The subjects first performed joint flexion or extension at the peak target force up to be 60% MVC repeatedly until exhaustion.

  Another contraction was performed with the same varying-force contraction, but one maximum force was exerted after every 5th cycle of 60%MVC contractions.

  Lastly, the subjects performed 10 cycles of 60% MVC joint flexion and extension followed by a period of 40 seconds of 40 % MVC constant force contraction to induce more muscle fatigue. The subjects completed the rest of this trial with more repeated 60% MVC joint flexion and extension until they felt exhausted. The contraction period of each repeated cycle contraction was limited approximately to be 4-s.

- ***Post-fatigue MVCs measurements***

  Right after above mentioned each fatigue contraction step, subjects were asked to produce at least three MVCs in their joint extension or flexion with the same muscle contraction protocol used for pre-fatigue measurements. These MVCs

were averaged and the values were used to compare with the pre-fatigue values to confirm the occurrence of muscle fatigue.

If all the steps in each trial are performed continuously, the muscles of each subject must be over-fatigued and might be a source of injury to the subjects. In addition, the fatigue from the previous steps will influence the following ones. Therefore, to reduce the influence of muscle fatigue between steps and to avoid over-fatigue, each trial was conducted on different days to ensure that the muscles were fully recovered from the previous trial. Figure 5.1 illustrates some examples of the measured forces of the isometric contraction and the varying-force contraction, which represents different activities of trials performed by the subjects.

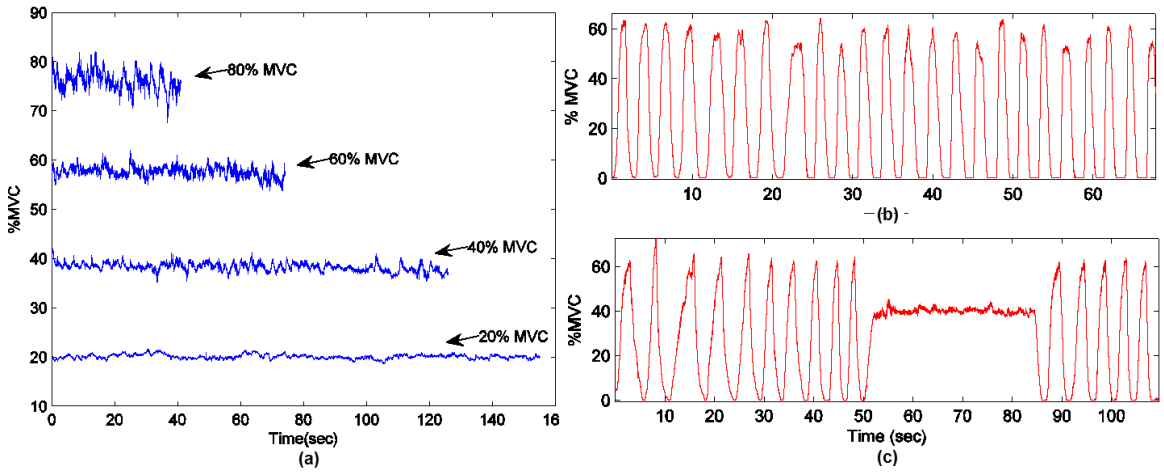

Figure 5.1 Example of measured force representing the contraction activities of the trials. (a) constant force muscle contractions, 4 target force levels, 20% MVC, 40% MVC, 60% MVC and 80% MVC; (b) varying force muscle contraction; (c) varying force contraction with around 40 s constant force contraction.

Since the pre-fatigue and post-fatigue MVCs were measured before and after fatigue contractions, the occurrence of muscle fatigue can be observed from the decreasing MVCs. Figure 5.2 shows one example of the MVC changes before muscle fatigue and after muscle fatigue. These MVCs were measured before and after the muscle contraction with a 60% MVC constant force from all healthy subjects. In order to compare the MVCs between subjects, the measured MVC forces before muscle fatigue are all expressed as

100% MVCs, and the post-fatigue MVCs are converted to a percentage of the pre-fatigue MVCs.

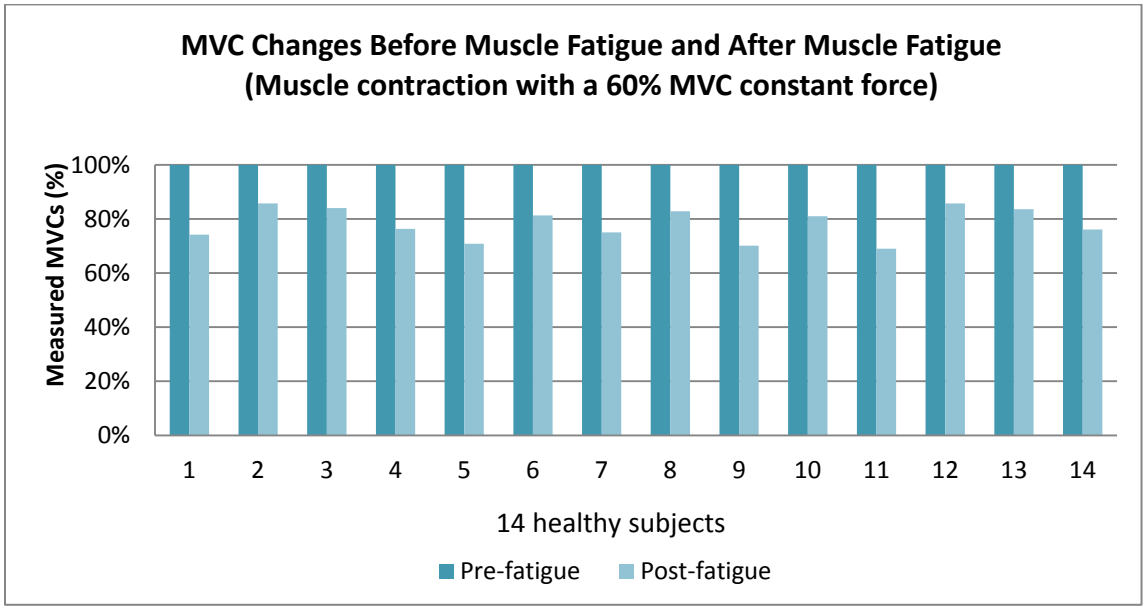

Figure 5.2 MVC changes before muscle fatigue and after muscle fatigue for the 14 healthy subjects. The example contraction trial is the 60% MVC constant force contraction.

Figure 5.3 depicts the averaged MVCs comparison between pre-fatigue and post-fatigue from all trials. The MVCs measured before fatigue contraction trials, is found to be significantly higher than the MVCs after fatigue, which indicates the capacity to maximally activate the muscles decreases due to fatigue contraction. Evidently, the MVC values decrease dramatically after the fatigue trials, which is a strong confirmation of fatigue occurrence. A single factor ANOVA was performed on pre-fatigue MVCs and post-fatigue MVCs. The ANOVA results indicate the difference between pre-fatigue MVCs and post-fatigue MVCs are significant since the *p*-value is larger than 0.05.

Based on this analysis, if any subjects' MVCs from pre-fatigue measurement and post-fatigue measurement do not show any decrease, they were asked to redo the experiments on different day.

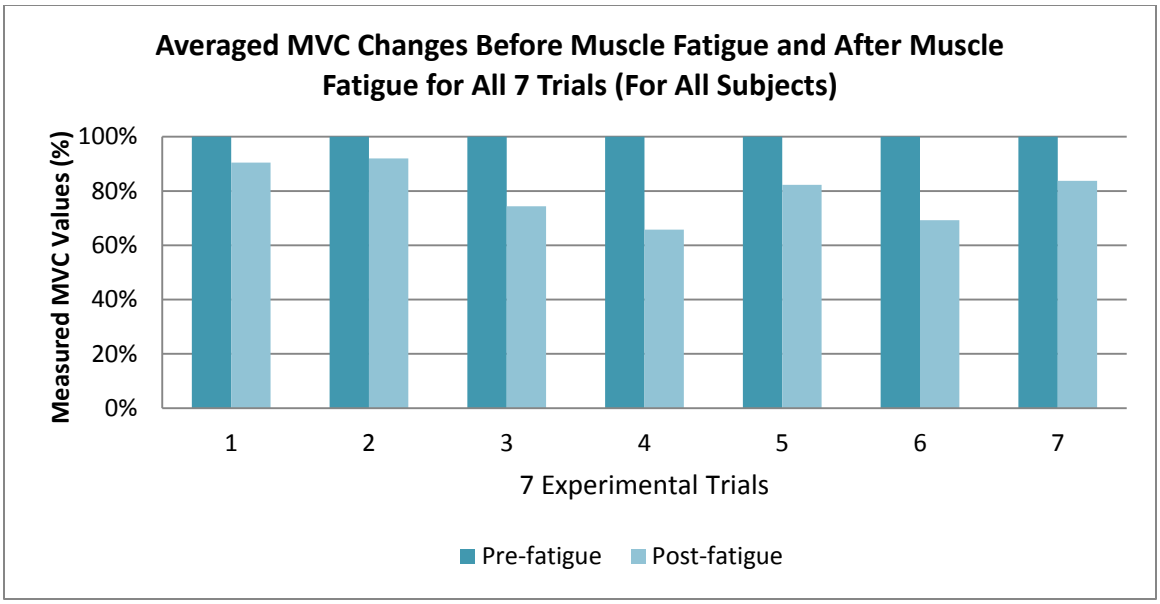

Figure 5.3 Averaged MVC changes before muscle fatigue and after muscle fatigue for the seven fatigue experimental trials. Trial 1 to 4 are the constant force contraction with 20% MVC, 40% MVC, 60% MVC and 80% MVC respectively, trial 5 to 7 are the varying force muscle contractions (Average value for all subjects).

5.3 Fatigue Detection

When muscles contract under a varying force, the sEMG signals cannot be assumed to be stationary, which implies that the traditional signal processing approaches, such as fast Fourier transform (FFT), may not be suitable to extract fatigue relevant features. Time-frequency analysis has proved to be feasible to extract fatigue features. *MF* and signal power *P* are the frequency domain characteristics, which change with the occurrence of muscle fatigue. However, these features change instantaneously as the exerted force, which implies that the fatigue assessment for varying force contraction should not only rely on tracking the changes of *MF* and signal power *P*. In this section, the approach for assessing muscle fatigue is proposed by correlating *MF* and signal power *P* based on CWT.

5.3.1 Time-frequency Analysis Method

In this method, frequency-domain characteristics of sEMG signals, *MF* and signal power *P* were extracted from CWT. The background theory of CWT and the procedures to calculate *MF* and *P* were mentioned in Chapter 3 (Subsection 3.4.1). The signals were first down sampled from 10 KHz to 1000 Hz. Figure 5.4 shows the contour scalograms which are calculated from the isometric muscle contraction with 40% MVC force target. These two scalograms compare the energy distribution for each wavelet coefficient of the first one-second and the last one-second of the completely constant contraction trial. Apparently, high percentage of the signal energy shifts to the lower frequency as the isometric contraction goes on, which is a significant sign of muscle fatigue for static contraction.

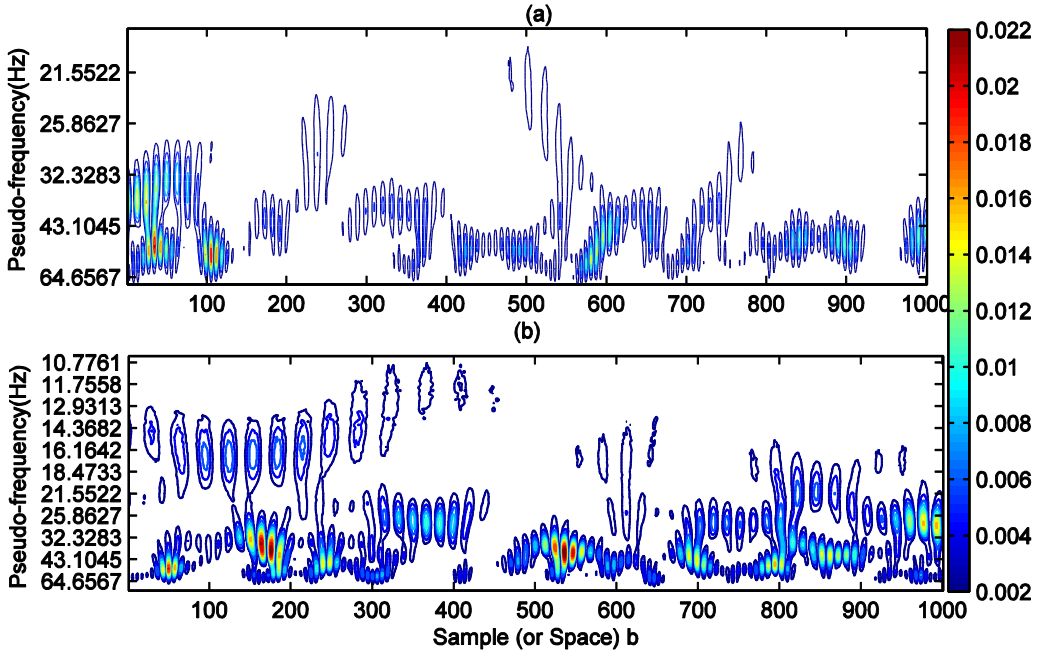

Figure 5.4 Contour scalograms of the 40% MVC isometric muscle contraction. The x-axis is the number of samples, and y-axis is the frequency which is converted from the scale. (a) Contour scalogram of the first one second; (b) Contour scalogram of the last one second.

Signal flow diagram describing the procedures to detect muscle fatigue is illustrated in Figure 5.5. The method presented in this figure is modified and improved based on the time-frequency analysis method described in [3]. The idea of this fatigue detection is to

yield the sEMG features relative changes by decoupling the muscle fatigue from the force exerted by muscles, since the sEMG features change with the force exerted by muscles during force-varying contractions. The following figure (Figure 5.5) states the step-by-step details of the signal flow of the proposed muscle fatigue detection method.

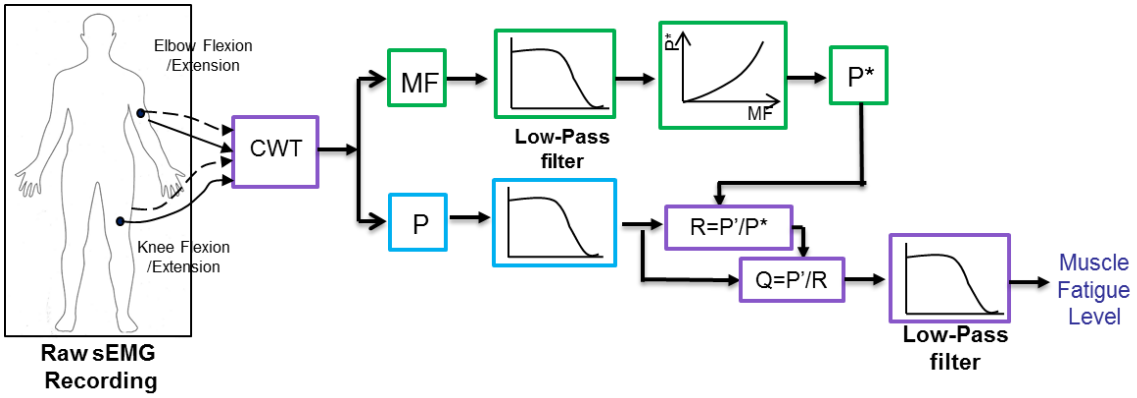

Figure 5.5 Signal flow diagram of muscle fatigue detection approach. MF is mean frequency, *P* is the signal power, *P'* is the filtered *P*, *P** is the estimated signal power.

First, *MF* and *P* were calculated using CWT from Equation 3.8 and 3.9. The signal power *P* and *MF* were further processed separately. To remove the high signal spikes and to reject the motion artifacts, the *MF* and *P* were first filtered with a 4^{th} order Bessel low-pass filter. To ensure the same signal bandwidth and group delay of the two paths, the low-pass filter cut-off frequency was selected to be 1.5 Hz for both *MF* and *P*, and the filtered *P* is represented as symbol *P'*.

The polynomial describing the relationship between filtered *MF* and signal power *P* (Subsection 3.4.3) for non-fatigue muscles was used to correlate the signal frequency changes with the signal energy changes. All available polynomial models were selected during curve fitting, such as linear, quadratic, cubic and higher order polynomial. For each muscle, a polynomial model was obtained from each subject. The polynomial estimator for per muscle group was selected by comparing which gives the highest R^2 value and lowest RMSE. The level of significance value alpha was set at $p \leq 0.05$. Even though there might be some other models like exponential, power, logarithmic etc. describing the relationships relatively accurate, considering the computational efficiency

when implementing in real-time system and to simplify the implementation process, only polynomials are employed in the thesis.

This relationship function covers the full range of force produced by muscle up to MVC under non-fatigue contraction. Based on the relationship study in Chapter 3, the relationship polynomials between *MF* and signal power *P* are tabulated in Table 5.1.

Table 5.1 sEMG Signal *MF-P* Relationship.

Muscle Groups	Polynomial Relationship
Biceps Brachii	$Y=6.371x^3-123x^2+16440x-4530$
Triceps Brachii	$Y=7.345x^2+50.01x-6700$
Rectus Femoris	$Y=4.553x^2+3.588x+6113$
Biceps Femoris	$Y=4.606x^2-0.4198x+169.7$

When the input *x* to the *MF-P* relationship is *MF*, the output of the polynomial *Y* is the estimated signal power *P**. Since *MF* is one of very important indicator of muscle fatigue, this *P** from the relationship not only depends on the *MF* of the signal power spectrum, but also a function of muscle exerted force and level of muscle fatigue. When muscle fatigue occurs under isometric muscle contractions, the *MF* shifts to lower frequency, which induces the *P** decreases slowly according to the regression polynomial. Figure 5.6 illustrates the *MF*, signal power *P* and estimated power *P** changes from two individual samples under isometric contraction. It is evident from the figures that the changing trend of *P** is decreasing, which follows the *MF* generally. In addition, as the contraction goes on, the signal power *P* shows a slowly increasing trend due to the growing muscle fiber firing rates.

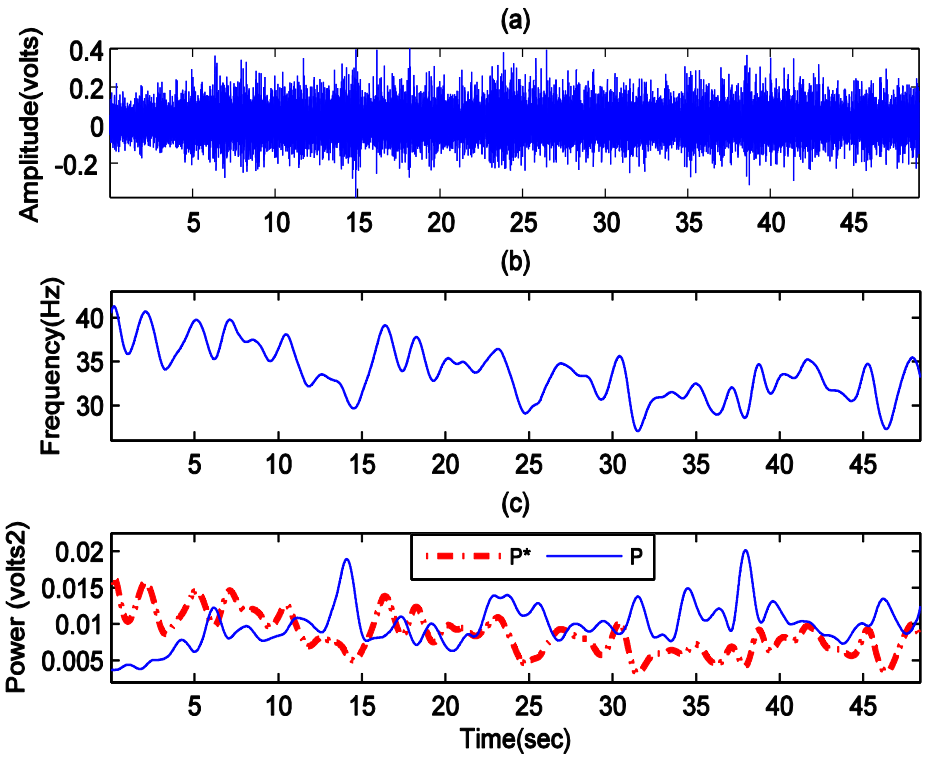

(A)

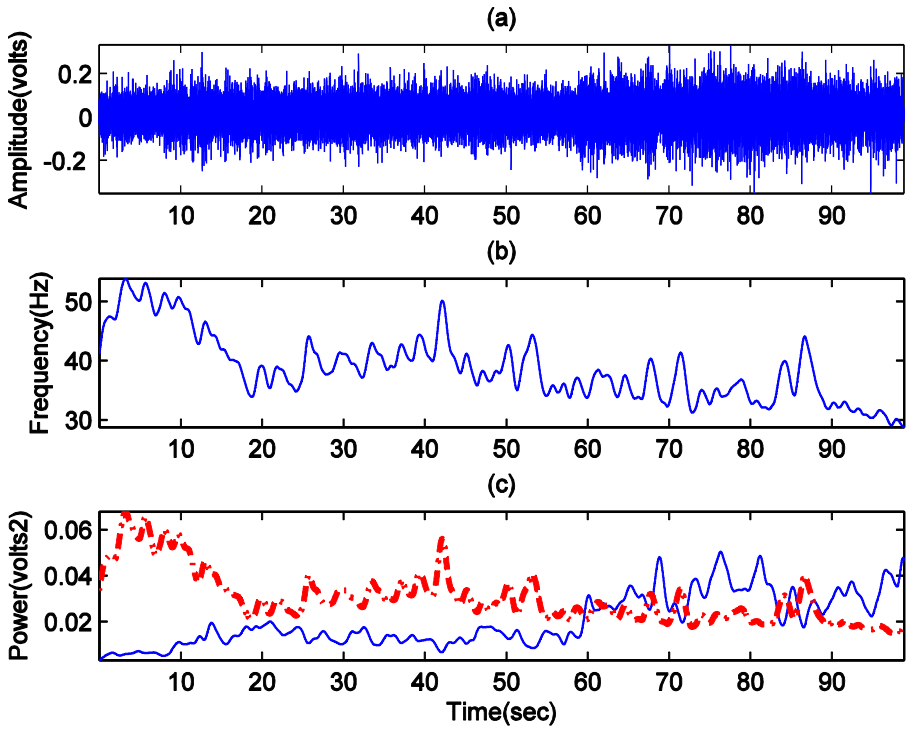

(B)

Figure 5.6 Two individual examples of the biceps brachii muscles during isometric muscle contractions. (a) Raw sEMG signal; (b) *MF*; (c) Signal power *P* and *P** changes. (A) Subject 7, 80% MVC. (B) Subject 2, 40% MVC.

Subsequently, to make the signal frequency contents independent from the force exerted by muscles, and to get the relative changes by comparing the two paths, *P* and *MF*, the ratio between *P* and *P** was computed as *R=P'/P**. This output value *R* had to be further filtered by a 4th order Bessel low-pass filter with 0.8 Hz cut-off frequency due to the signal variation over the time. To ensure the stability of the output, another ratio *Q=P/R* was calculated. This output signal *Q* is inversely proportional to fatigue and independent from the force exerted by muscles. A low-pass 4th order Bessel filter with 0.2 Hz cut-off filter was then implemented on *Q* to smoothen the signal and to remove the signal high frequency spikes.

The fatigue output was given as one of *n* levels with hysteresis and the values were normalized to a maximum value of 1.6. Signal threshold values for a given level of fatigue, which are 0.4, 0.8 and 1.2 respectively. The fatigue is defined and discretized into four levels (1 to 4), where level 4 means significant level of fatigue and level 1 corresponds to the non-fatiguing state. The second level and the third level are assumed to be light fatigue and intermediate fatigue, respectively [133]. Figure 5.7 shows the muscle fatigue detection results and discrete fatigue levels of Subject 13's muscle under 60% MVC isometric contraction calculated from the proposed fatigue assessment approach. The output fatigue level demonstrates that the muscle fatigue level increases to the third level in 23 seconds and stays at this level until the end of the experiment. This fatigue level is indicative information to show the general fatigue progress.

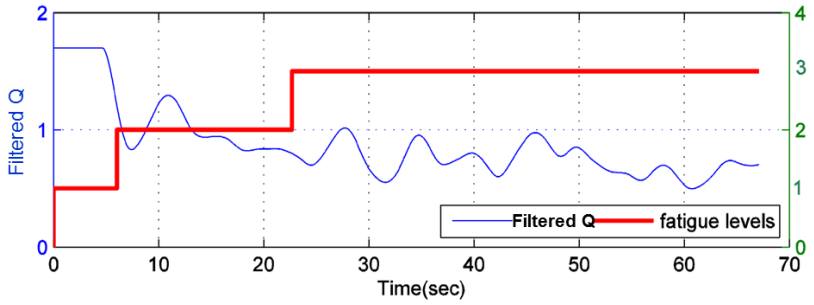

Figure 5.7 Filtered *Q* value (left Y-axis) and discrete fatigue level (right Y-axis). The result is obtained from 60% MVC isometric contraction (Subject 13).

It is apparent that the current approach works well for isometric muscle contraction, and the discrete fatigue levels are able to describe the general fatigue progress as well. However, when this approach was implemented on sEMG signals recorded from muscles under varying force contractions, some problems arise. Since the *MF* and *P* change with the varying force, *MF* and *P* might get very low values when the exerted force decreases to zero in one contraction cycle. For this reason, the $R=P'/P^*$ value usually goes to infinity. In addition, different individuals commonly result in wide frequency range of *MF* and signal power *P*. Therefore, it is necessary to normalize the *MF* and *P*.

To solve these problems, an improved approach with normalization and threshold setting has been developed, which is shown in Figure 5.8.

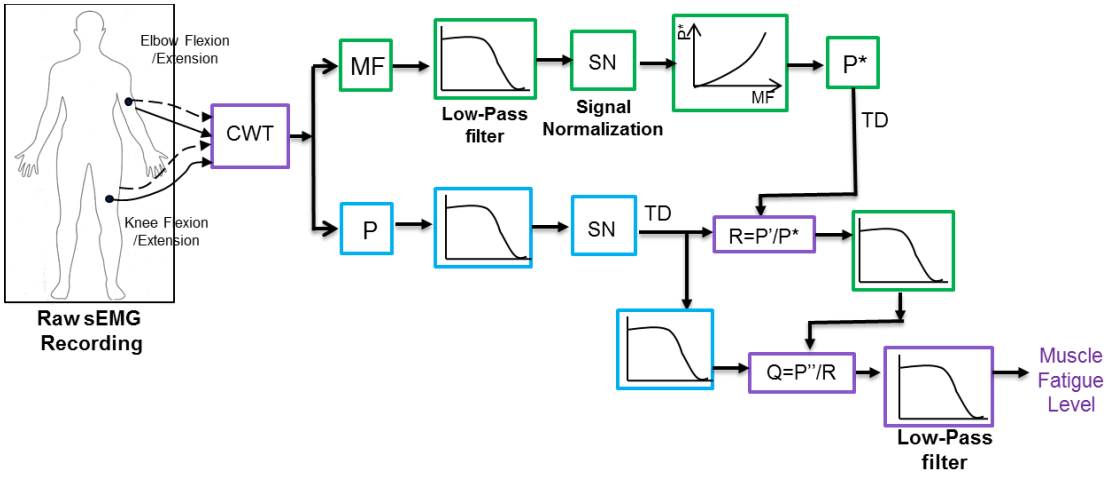

Figure 5.8 Signal flow diagram of improved muscle fatigue detection approach.

In this improved approach, signal normalization procedures were added to the filtered *MF* and *P*. This normalization aims at reducing variability between subject in sEMG amplitude and frequency range associated with, for example, differences in muscle length, force exerted by muscles varying force contractions. The filtered *MF* was normalized to a maximum frequency of 100 Hz and the filtered power *P'* was also normalized to 100. The normalized *MF* was then applied to get the estimated signal power *P** from the relationship polynomial. This *P** value was normalized to 100 as well to make the changes of *P** be consistent with the variation of *P'* for the same contraction trial.

When a muscle contracts under very small contraction forces, muscle fibers are activated randomly and not all the muscle fibers are involved. Therefore, to reduce the effects from signal power values introduced by very small muscle contraction forces and to attenuate the movement artifact noise, it is necessary to set thresholds on signal power *P'* and *P**. Meanwhile, the thresholds are a suitable way to avoid the problems induced by these infinity values when comparing *P* and *P**. The thresholds should be set as small as possible and the values are verified to impact significantly on the final fatigue results and the quantified fatigue levels. For each experimental trial, the threshold values have to be set individually.

As shown in Figure 5.8, other new added contents to this improved approach are the low-pass filters on *R* and *Q*. These filters were set with low cut-off frequencies. The low-pass filter on the *P'* value with threshold is to ensure the time delay is consistent with *P'/P**. In addition, the cut-off frequencies of the filters are different for each individual trial.

5.3.2 Signal Evaluation Results

To present the data validation results clearly, this section is divided into two parts, one is the results from isometric contractions and another is the evaluation results from force varying muscle contractions.

5.3.2.1 Isometric Contraction

When the improved fatigue detection algorithm is implemented to the sEMG signals generated during isometric contraction under 20% MVC, 40% MVC, 60% MVC and 80% MVC contraction forces, both *MF* and the estimated power *P** decease while the signal power *P* is slowly increasing (Figure 5.6).

One example of the *MF* and *P* calculated from the sEMG signal under isometric 80% MVC contraction of Subject 13's triceps brachii is shown in Figure 5.9. The dash-dot lines are the slopes of *MF* and *P* fitted using linear regression in MATLAB. The slope value for the decreasing *MF* is -0.87, and this slope value for the increasing signal power

is 2.3. Apparently, the *MF* decreases and *P* increases dramatically over the experiment period, which is a strong evident of muscle fatigue. The increasing signal power *P* is a frequency domain feature which reflects the signal energy change. This energy change is generally same as the signal amplitude variation obtained from windowed RMS. This increasing signal power with constant force contraction mainly reflects the recruitment of new motor units and increasing muscle firing rates under fatigue state.

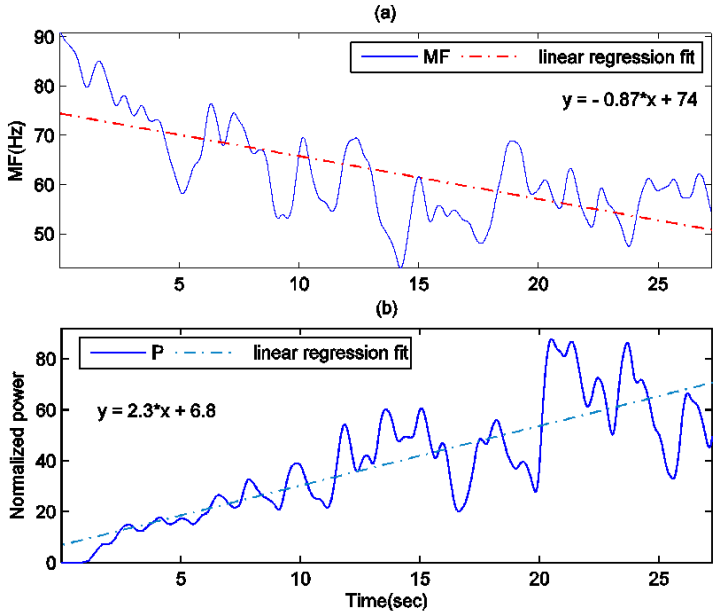

Figure 5.9 *MF* and signal power *P* from sEMG signal under isometric 80% MVC contraction of Subject 13's triceps brachii. The dash-dot lines are the slope of *MF* and *P* obtained using linear regression method.

The muscle fatigue detection results and discrete fatigue levels of Subject 7 under the four force levels contractions are shown in Figure 5.10. During the 4 trial sessions, a downward trend can be observed from the filtered *Q* value as the muscle fatigue levels increase. In this individual's example, the muscle fatigue levels increase to the 3rd level for all 4 exerted force values but at different shift time. It takes approximately 70 seconds for the subject to reach the 3rd level for 20% MVC force level. While for 40% MVC, it only takes 22 seconds for the fatigue level to rise to the 3rd level. For the 60% MVC and 80% MVC targeted forces, it takes just 17 seconds and 13 seconds to reach the 3rd discrete fatigue level, respectively. Evidently, the time duration for each isometric

contraction trial decreases as the targeted exerted force values increase due to the earlier occurrence of muscle fatigue.

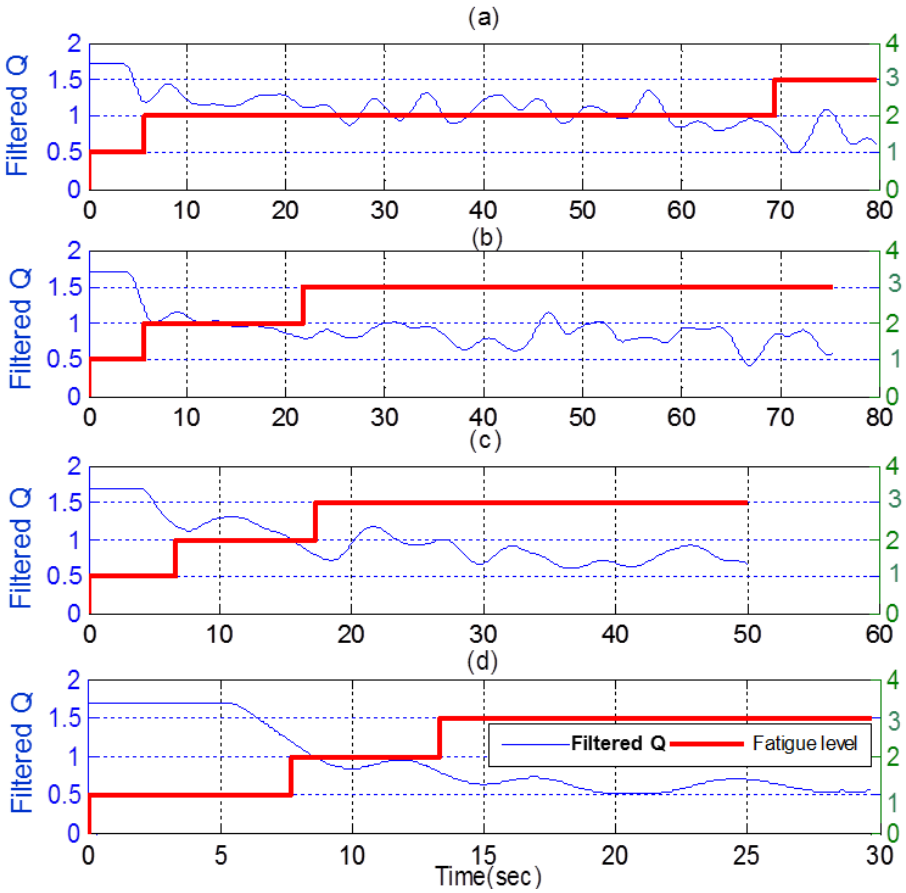

Figure 5.10 Subject 7's filtered *Q* values (Left *Y*-axis) and discrete fatigue levels (Right *Y*-axis) with isometric contraction from biceps brachii with force exerted by muscle at 4 force targets. (a) 20% MVC; (b) 40% MVC; (c) 60% MVC; (d) 80% MVC.

Figure 5.11 illustrates the average time duration for each fatigue level of all the participants. The time duration of each isometric contraction trial decreases remarkably, due to the increasing muscle fatigue. The increasing force targets have gradually shorten the period of each fatigue level and accelerated the shifting of the fatigue level to higher levels. In addition, for very high contraction force target, the fatigue level reaches to the 4^{th} level and the average time duration of each level is much smaller than other constant force levels.

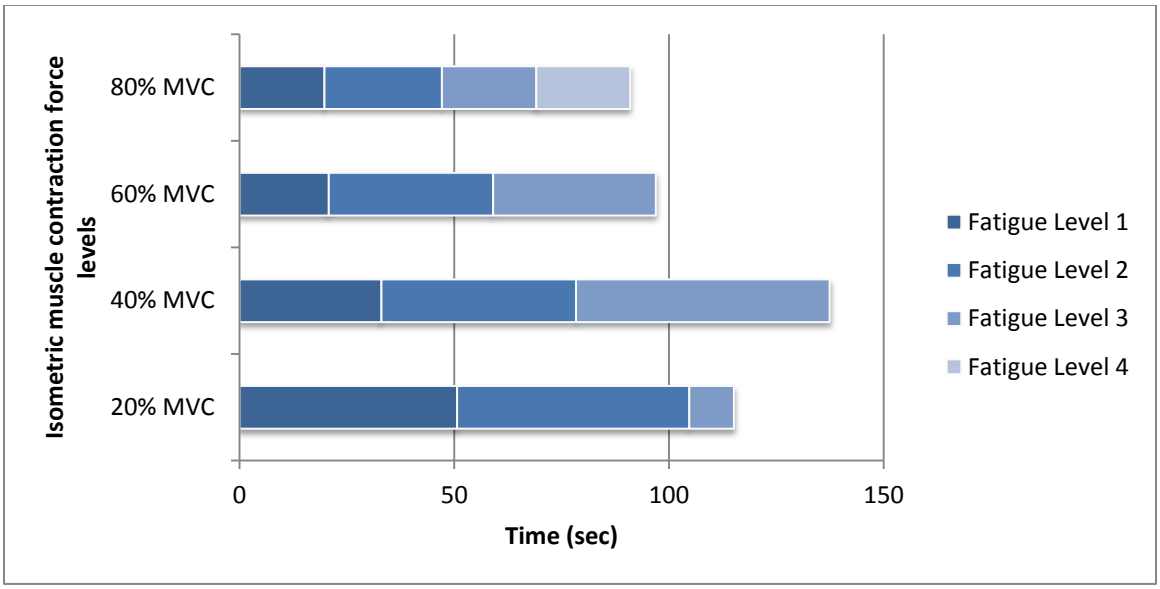

Figure 5.11 Time duration (average value) of each fatigue level under the four force targets. Fatigue level from 1 to 4 represents the increasing severity of muscle fatigue.

5.3.2.2 Force-varying Contraction

In the force-varying contraction trials, the changes in *MF* and signal power *P* of all subjects are in accordance with the change in force exerted by the muscles. Figure 5.12 to Figure 5.14 show the recorded raw sEMG signals, the force exerted by muscles, *MF*, *P* and the estimated power *P** when the subjects performed three different varying force contraction trials. Figure 5.12 is the results from the biceps femoris of Subject 1, Figure 5.13 shows the results from rectus femoris of Subject 5 and the Figure 5.14 is from biceps brachii of Subject 3. In these figures, the measured force values are normalized to have a maximum force of one, and the *P* and *P** values are normalized to 100 to simplify the comparison.

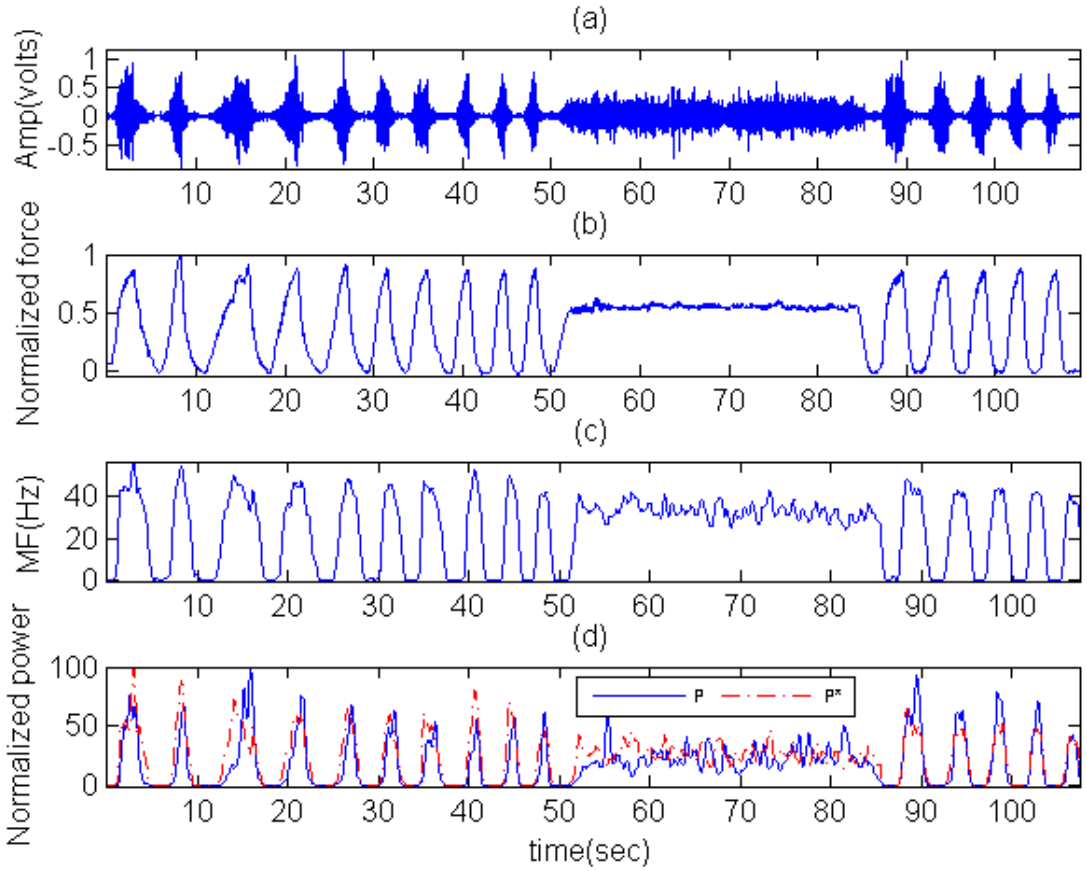

Figure 5.12 Biceps femoris muscle during varying repetitive elbow flexion and a period of constant force contraction of Subject 1. (a) Raw sEMG signal; (b) Measured force (normalized to 1); (c) *MF*; (d) Signal power *P* and the estimated signal power *P**.

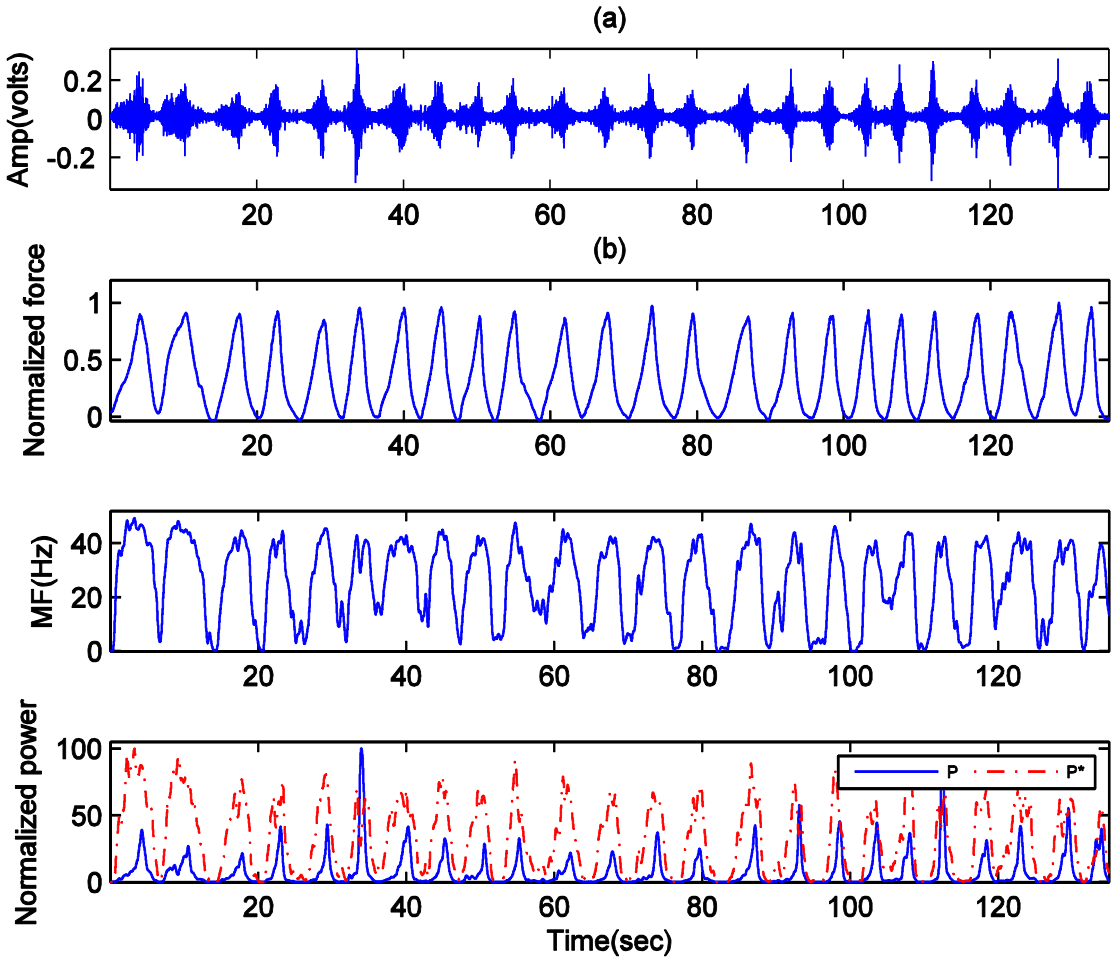

Figure 5.13 Rectus femoris muscle during varying repetitive knee extension of Subject 5. (a) Raw sEMG signal; (b) Measured force (normalized to 1); (c) *MF*; (d) Signal power *P* and the estimated signal power *P**.

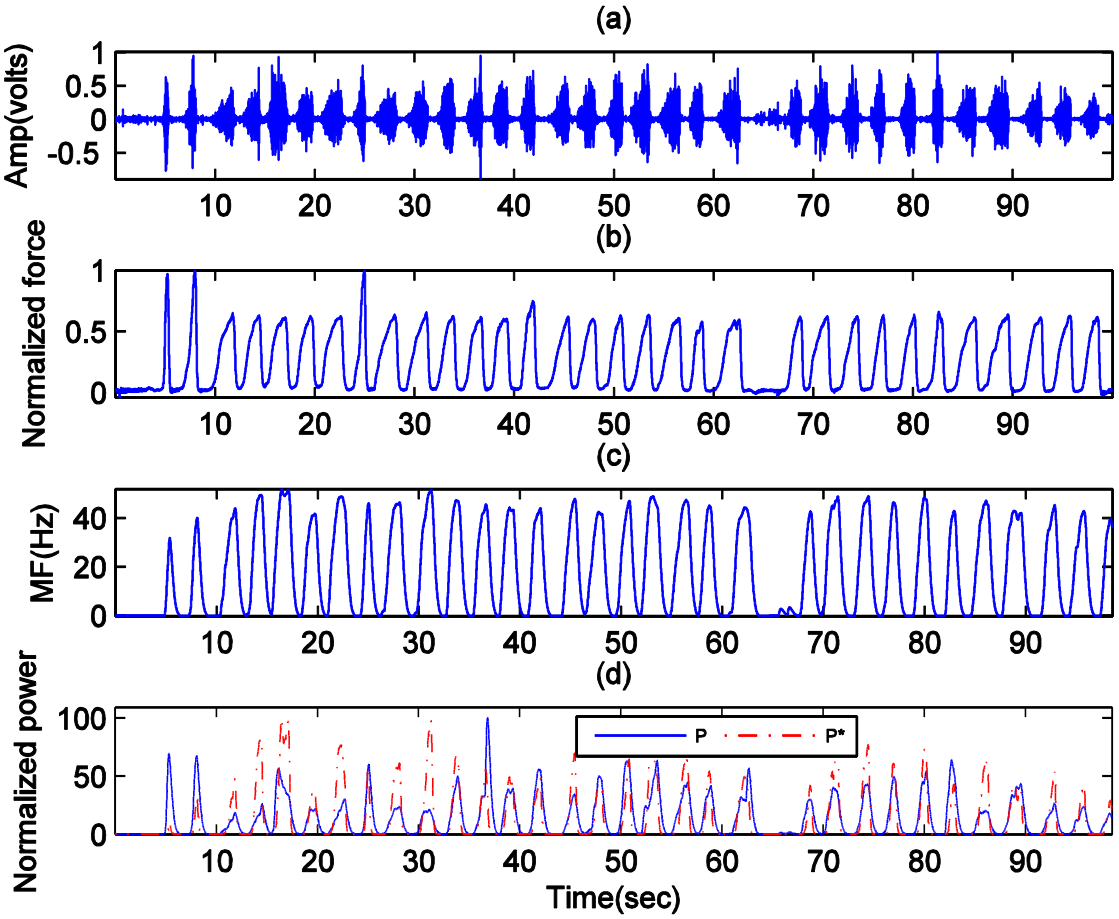

Figure 5.14 Biceps brachii muscle during varying repetitive elbow flexion of Subject 3. (a) Raw sEMG signal; (b) Measured force (normalized to 1); (c) *MF*; (d) Signal power *P* and the estimated signal power *P**.

From the above three figures, the peak values of *MF* for each submaximal contraction show a slight decrease over the whole contraction trial period, while the peak values of *P** also illustrate a downward trend. Meanwhile, the changes of these parameters depend highly on the force exerted by muscles.

Figure 5.15 depicts the individuals' fatigue detection outputs and the discrete fatigue levels, which correspond to the data illustrated in Figure 5.12, Figure 5.13 and Figure 5.14. The fatigue detection output filtered *Q* value decreases rapidly and smoothly over the experiment period which leads to the increasing fatigue levels. For the recorded data shown in Figure 5.12, the fatigue levels keep increasing and goes up to the 4^{th} level in 72

seconds, which implies that the 40 seconds static muscle contraction induced muscle fatigue significantly. During Subject 5's rectus femoris repetitive varying force contraction (Figure 5.13), the discrete fatigue level stabilizes on the 3rd level at 63 seconds. The results illustrated in Figure 5.15 (c) show a slight fluctuation. The fatigue level reaches to the 4th level at 58 second for a short while, then shifts back and stabilizes at the 3rd level.

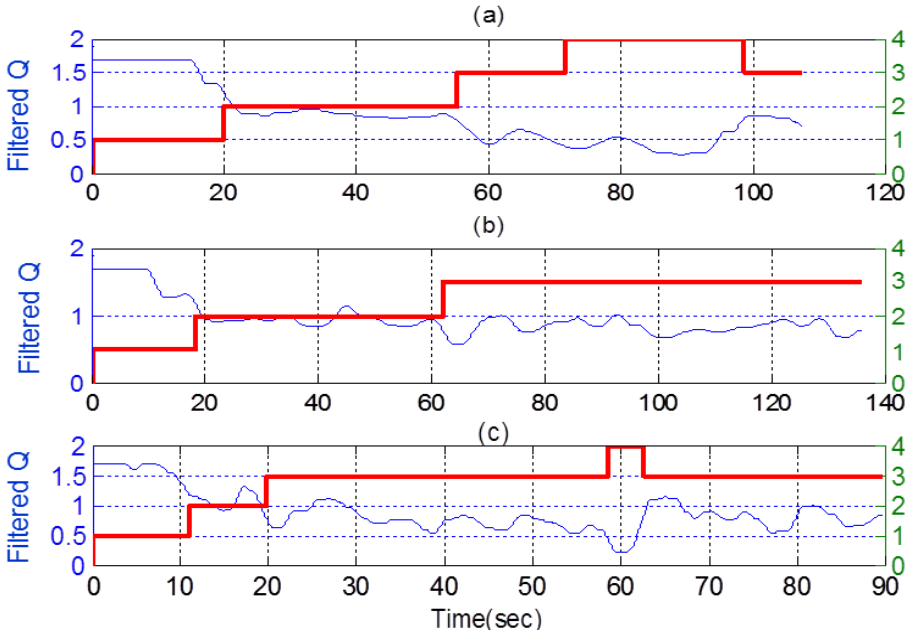

Figure 5.15 Three individual examples of varying force muscle contractions fatigue detection results and discrete fatigue levels. (a) Subject 1, biceps femoris; (b) Subject 5, rectus femoris; (c) Subject 3, biceps brachii.

The fluctuation in the fatigue output is the reason why there is a sudden shift in the fatigue levels, which sometimes appears in the fatigue detection results. The instability is probably induced by the fast velocity of varying force, signal artifact noises and the fatigue output filtered *Q* value. In addition, the varying force generated by the muscles, variations in the muscle length, motor unit synchronization and the changing contraction velocities may also contribute to this instability. Even though the instability in the comparison ratio *Q* can be eliminated using low-pass filters, very low cut-off frequency filters bring much more time delays. From the experimental aspects, since the contraction within individual trials follows a fixed and repetitive force trajectory, some of the

affecting factors are assumed to be similar, and their effects on the results can be cancelled out. Therefore, the slight fluctuation in these levels is ignored and assumed to stay at the origin level where the fatigue levels are fluctuated in a short period.

Since the occurrence of muscle fatigue is a gradual process, the influence of temporal delay given by low-pass filters are assumed small and can be roughly ignored, even though low-pass filters lead to the group delays in approximate 3.8 seconds. In this study, even though the proposed fatigue detection algorithm has a slow response, the fatigue levels are still viable to indicate the fatigue state as the muscle fatigue in human body is a slow progress.

5.3.3 Quantifying Fatigue Levels to MVCs

So far, the muscle fatigue progress can be described using the discrete fatigue levels. However, these fatigue levels indicate the stable response without visibly correlated to the force exerted by muscles. As one commonly accepted definition of muscle fatigue is the long lasting decrease of the ability to contract and exert force, or to maintain the required level of strength, the fatigue progress should be much more representative if it is described using the muscle maximum force capacity. Therefore, the reduction of the force can be a straightforward way to associate with the increasing fatigue levels. Accordingly, the fatigue levels should be quantified to make the fatigue estimation close to the real physiological fatigue changes of human body.

To correlate the fatigue levels with force exerted by muscles, the muscle force values from the contractions with MVC measured every 10 seconds were employed. This kind of contraction was performed by exerting a MVC every 10 seconds during constant force contraction and varying force contraction. These MVCs reflect the force capacity of the muscles during fatigue progress.

During one trial, the measured MVCs have a decreasing trend generally. These MVC values were normalized and expressed in percentage of the highest MVC. The filtered Q values were extracted at the time when MVC was applied. From the results shown in

previous section, the filtered *Q* values fluctuate slightly but decrease slowly during the fatigue period. Since the time duration of each trial contracted under different muscle force is different from others, the measured number of MVCs is varied from trial to trial.

Subsequently, the MVC values and the corresponding normalized *Q* values were correlated using curve fitting tool in MATLAB. Figure 5.16 illustrates examples of the regression fit between filtered *Q* value and the MVCs from a constant force contraction and a varying force contraction. As shown in this figure, a second order polynomial describes the relationship between *Q* and MVCs with high *R*-square value (R^2=0.9861) and another is correlated high with 0.9706 *R*-square value. Based on this regression method, linear or quadratic models are employed to correlate the *Q* values with MVCs for different fatigue contraction trials.

In this fatigue detection study, the fatigue levels are transited when the filtered *Q* is 1.2, 0.8 and 0.4, which corresponds to the 4 fatigue levels (1 to 4 level). Level 1 means non-fatiguing state, while level four corresponds to the significant level of fatigue. To quantify the fatigue levels, MVC values corresponding to the transition fatigue levels are calculated from the *Q* value and MVCs relationships.

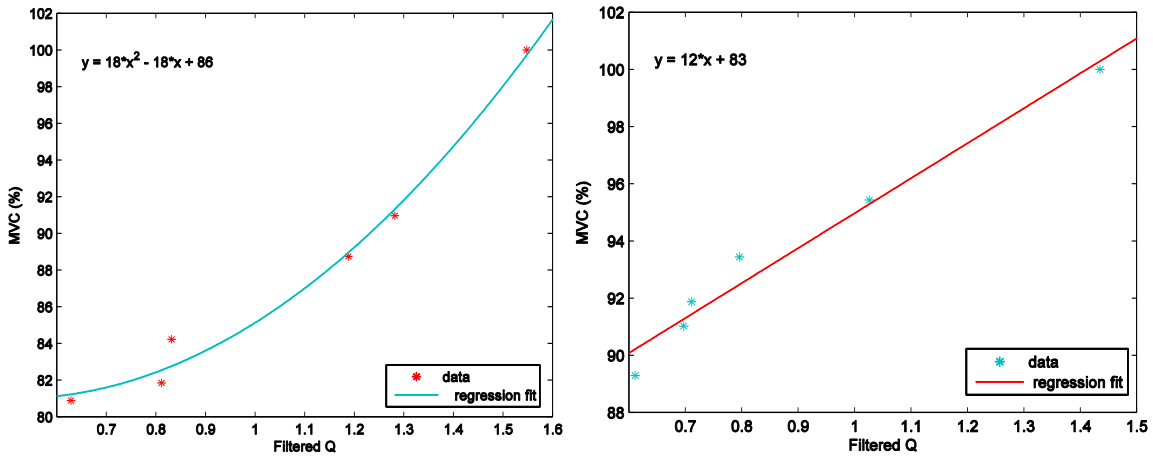

(a) (b)

Figure 5.16 Examples of regression fit between filtered *Q* and MVCs. (a) Triceps brachii, Subject 2, 40% MVC constant force contraction; (b) Bicep brachii, Subject 11, varying force contraction.

The average MVC values correlated to the fatigue levels are tabulated in Table 5.2. The first column is the *Q* value at the fatigue level transition points. The fatigue levels are quantified to the MVCs ranges in reference to MVC without fatigue.

Table 5.2 Fatigue Levels Quantification to Non-fatigue MVCs.

Filtered *Q* value range between the level transition points	**Fatigue level Range**	**MVCs range corresponds to the fatigue level (%)**
1.6 to 1.2	Level 1 to Level 2	85.81-100
1.2 to 0.8	Level 2 to Level 3	64.18-98.96
0.8 to 0.4	Level 3 to Level 4	41.44-91.57

5.3.4 Stroke Patients Fatigue Assessment

During stroke patients fatigue experiments, the experimental measurements are same as the healthy subjects. Two constant force contractions and one varying force contraction trials were performed by stroke patients. For the constant force contractions, the force targets were 60% MVC and 80% MVC. While during the varying force contraction trial, stroke patients exerted the muscle contraction force repeatedly in a cycle from a relax state to 60% MVC until exhaustion.

From the pre-fatigue and post-fatigue MVCs measured before and after fatigue contractions respectively, the occurrence of muscle fatigue can be observed since the MVCs are decreasing dramatically. Same as the healthy subjects, to simplify the MVCs comparison between subjects, the measured maximal forces before muscle fatigue are all expressed as 100% MVC, and the post-fatigue MVCs are converted to a percentage of 100% MVC. For each stroke patient, the MVCs are averaged throughout the fatigue trials and the measured muscles, which are shown in Figure 5.17. Between the pre-fatigue and post-fatigue MVCs, a one-way ANOVA was performed to determine if there is any significant difference. The level of significance value alpha was set at $p \leq 0.05$. Before

fatigue, the capacity of patients to activate maximally their rectus femoris and biceps femoris were found to be significantly higher than the MVCs after fatigue (p=0.00013).

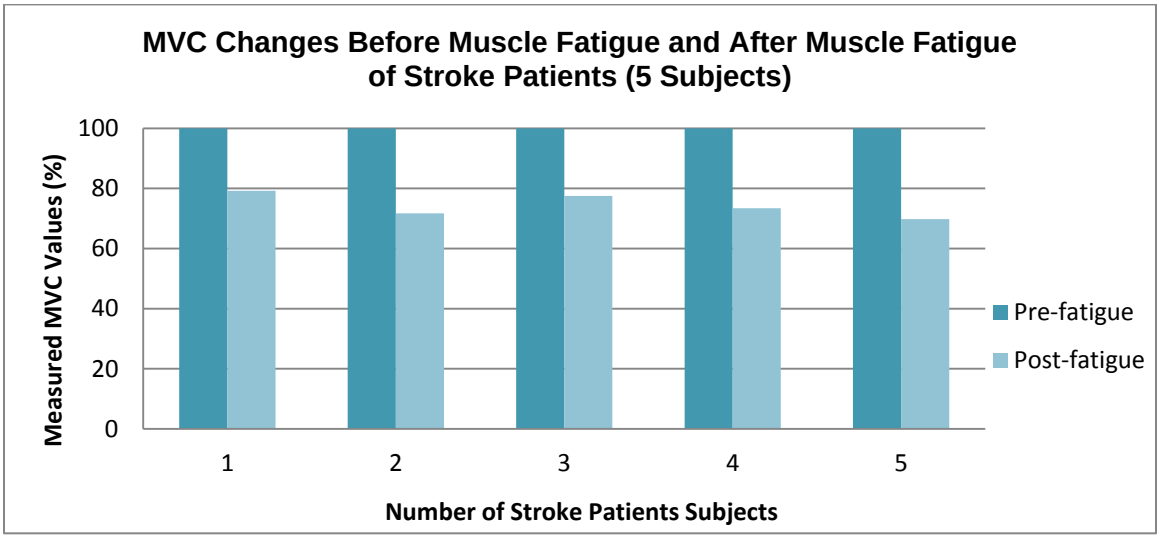

Figure 5.17 Averaged MVC changes before muscle fatigue and after muscle fatigue for the five stroke patients.

For each constant force contraction trial, *MF* of the first five-second and the last five-second of the complete contraction were calculated. The mean values of the *MF* from the measured muscles were obtained and illustrated in Figure 5.18. When the rectus femoris involved in constant force contraction, the average *MF* values decrease from 52.73±13.21 to 45.99±9.52. Decreasing trend is observed for biceps femoris with *MF* average values changing from 60.09±13.79 to 51.40±21.42 (p=0.04, p<0.05). These results are also a strong indication of muscle fatigue during the fatigue contraction period.

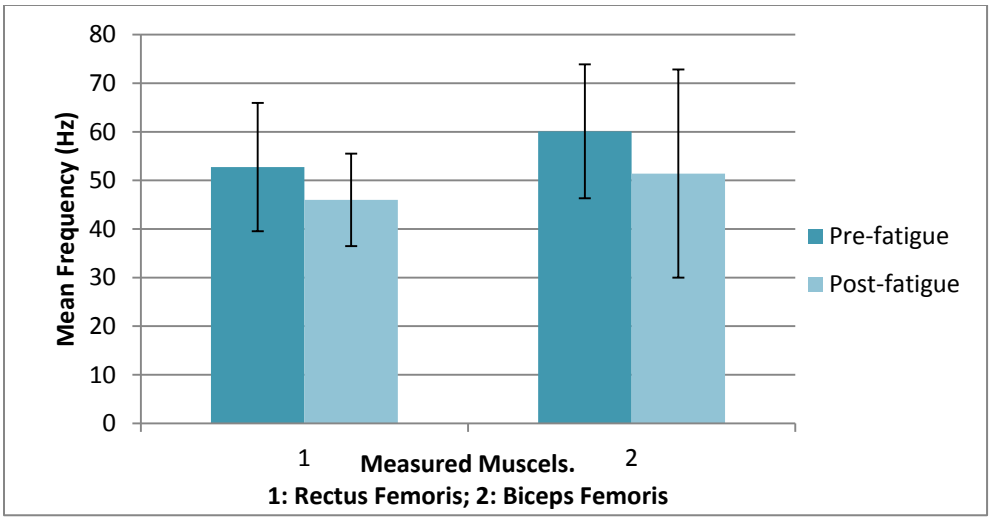

Figure 5.18 Averaged *MF* of the first five-second and the last five-second for stroke patients recuts femoris and biceps femoris muscles.

The time-frequency analysis method presented in Subsection 5.3.1 was applied to assess muscle fatigue of stroke patients affected muscles. The polynomials describing the relationship between filtered *MF* and signal power *P* for rectus femoris and biceps femoris of stroke patients were first established using the methods presented in Subsection 3.4.3. The relationship polynomials between *MF* and signal power *P* with regression fitting are tabulated in Table 5.3.

Table 5.3 sEMG Signal *MF-P* Relationship of stroke patients.

Muscle Groups	Polynomial Relationship
Rectus Femoris	$Y=4.644x^3+168.7x^2-466.9$
Biceps Femoris	$Y=3.258x^2+272.3x-1965$

To make the proposed fatigue detection method much more suitable to detect the stroke patients muscle fatigue, some filter parameters, such as the filter order, filter cut-off frequency, are modified according to the algorithm implementation performance step by step.

The muscle fatigue detection results and discrete fatigue levels of stroke patient 2 under 60% MVC isometric contraction are shown in Figure 5.19. As illustrated in this figure, a

downward trend can be observed from filtered *Q* as the muscle fatigue levels increase. In this stroke patient's example, the muscle fatigue levels increase to the 2nd level in 18 second, and the level shifts to the 3rd level in 52 seconds.

Figure 5.20 illustrates another results example from sEMG signal generated during varying force contraction performed by stroke patient 5. Apparently, in varying force contraction, the changes in *MF*, *P* and the estimated power *P** follow the exerted force. From the fatigue detection results, filtered *Q* value keeps decreasing leading to the shifts in fatigue levels. The fatigue level reaches to the 3rd level in 130 seconds, which is the indicative information representing the fatigue progress generally during the fatigue contraction period for stroke patients.

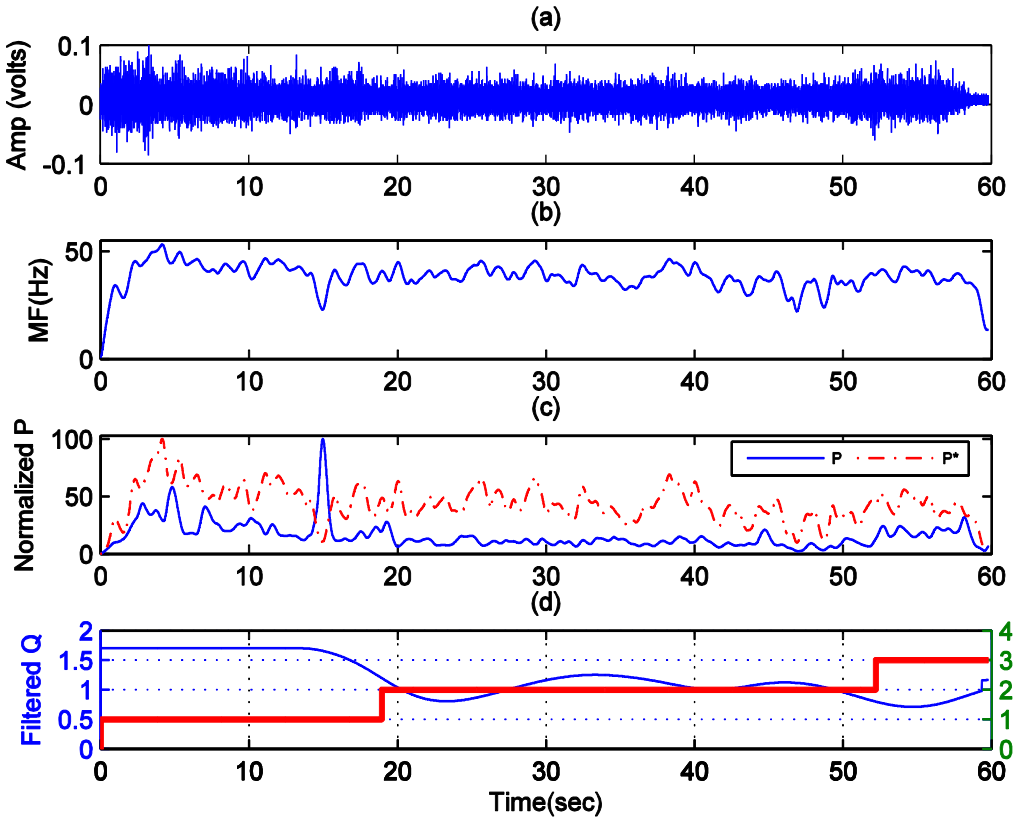

Figure 5.19 Rectus femoris muscle during 60% MVC constant force contraction of stroke subject 2. (a) Raw sEMG signal; (b) *MF*; (c) Signal power *P* and the estimated signal power *P**; (d) filtered *Q* value (left *Y*-axis) and discrete fatigue level (right *Y*-axis).

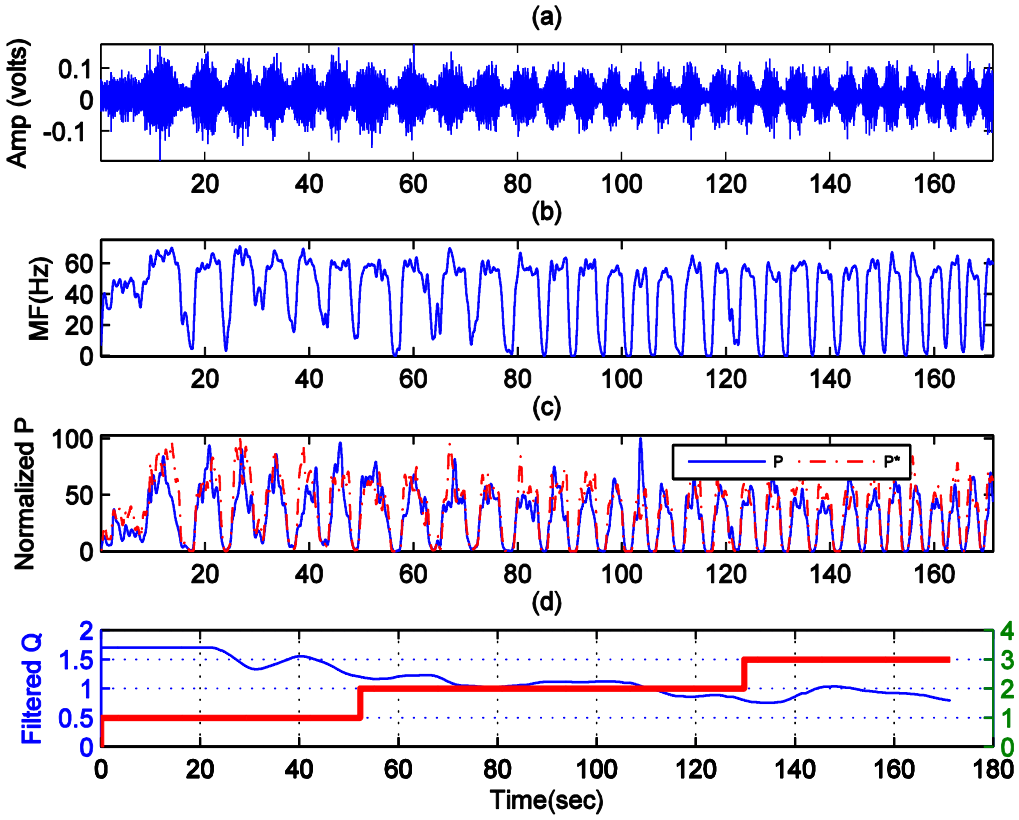

Figure 5.20 Biceps femoris muscle during varying force contraction of stroke subject 5. (a) Raw sEMG signal; (b) *MF*; (c) Signal power *P* and the estimated signal power *P**; (d) Filtered *Q* value (left *Y*-axis) and discrete fatigue level (right *Y*-axis).

5.4 Summary

In this chapter, a novel muscle fatigue detection approach is proposed. This method is developed based on the sEMG signal time-frequency analysis method CWT and the *MF*-*P* relationship. The performance and efficiency of the proposed method have been evaluated using the sEMG signals recorded from fatigue contraction experiments. The decrease in the relative change ratio *Q* value leads to the fatigue levels shifting to high levels for both constant force contractions and varying force contractions. Although the proposed fatigue detection algorithm has a slow response, the fatigue levels are still viable to indicate the fatigue state as the muscle fatigue in human body is a slow progress. These fatigue levels are quantified by correlating the fatigue levels with the MVCs during the fatigue tests in reference to MVCs without fatigue. The fatigue level quantification

adapts the fatigue levels to the muscle maximal capacity, which reflects the fatigue estimation as close as the real physiological fatigue changes of human body.

Same approach has been implemented to detect stroke patients muscle fatigue using sEMG signals from the affected leg muscles under constant force contraction and varying force contraction. Although the stroke patient sEMG signals are far different from healthy subjects, the preliminary results from a small number of stroke subjects still demonstrate that the proposed method is feasible for detecting fatigue for not only healthy subjects but also stroke patients. Further real-time implementation of the proposed approach will be presented in next chapter.

CHAPTER 6

REAL-TIME IMPLEMENTATION

6.1 Introduction

In recent decades, stroke has become a leading cause of chronic and serious disabilities. Because of hemiparesis and one-side motor impairment of the body, neurological impairments after stroke often affect the patient's ability to perform daily activities. In addition, nearly two thirds of stroke survivors experience a limitation in walking. Usually, physical rehabilitation therapists are involved to assist the stroke patients to regain movement functions. Research studies have found that high intensity, task-oriented rehabilitation training enables to enhance the walking ability of patients after stroke and regain the muscle motor function, particularly for those with moderate walking deficits [134]. For rehabilitation training, robotic exoskeletons and assistive devices have been widely developed for a variety of applications.

Devices such as the AutoAmbulator (Motorika, USA), LOPES [135] and ALEX [136], are designed as automated lower extremities gait training. These devices are commonly controlled to generate an assistive torque/force by a prescribed trajectory to move the patient's legs. Lokomat [137] is designed for stroke patients gait training with an advanced body weight support system, a robotic gait orthosis and a treadmill. It adjusts the shape of the desired stepping trajectory based on the participant's interaction forces, as well as the robot impedance. However, these rehabilitation devices move the patient's

legs through a fixed gait trajectory and there is no cycle-to-cycle variation in the kinematics and bio-signal feedback. Hybrid Assistive Limb (HAL) [138] is a wearable robot designed for assisting the elderly and stroke patients. The latest HAL-5 exoskeleton is controlled by sEMG signals to trigger the movement and drive the motor to assist movement-deficient elderly and disabled persons. There are many other lower extremity assistive devices designed for aiding people, such as RoboKnee [139] and Quasi-Passive Exoskeleton [140]. For these devices, multiple actuation systems and HMI are applied. However, due to limitations in price, size and portability, most of these devices are not suitable for casual indoor or home usage. Therefore, it would be advantageous to have a portable rehabilitation device give the users walking assistance for both hospital and home use.

To solve these problems of the current devices, a novel rehabilitation robotic device is designed by our group especially for providing assistive torque for stroke patients' lower limbs. The hardware design for this device is presented briefly in this chapter first. Then the proposed approach which is able to estimate muscle force is implemented real-time on the rehabilitation device. In addition, on-line tests on the force measurement setup and level walking are performed. Isometric and dynamic fatigue contraction experimental trials are performed to validate the feasibility of the proposed fatigue assessment approach in real-time.

6.2 Lower Limb Rehabilitation Device

A novel lower extremity rehabilitation device, as shown in Figure 6.1, is designed to aid in the flexion and extension motion of the wearer's hip and knee joint in the sagittal plane. This device consists of a lightweight adjustable anthropomorphic frame and actuator modules attached at the joints. Its adjustable frame is derived from the anthropometrical data provided in [141], to ensure it fit a wide range of users. Orthotic cuffs are used as the interface between the device frame and the user.

The actuator module is powered by a frameless direct drive high torque DC motor with a harmonic drive at a 50:1 gear ratio, which could deliver up to 50 Nm of maximum momentary torque and a continuous torque of 35 Nm. The maximum output speed can reach to 15.3 rad/s.

Optical incremental encoder at 1000 counts/rev is also equipped at the pre-reduction stage of each actuator module to measure the hip angle θ_h and knee angle θ_k. sEMG sensors are incorporated with the detection of user's intention. Mechanical stops at each joints limits the range of the motion of each joint to ensure that the device moves within the range of motion of a normal human for safety reasons. This range of motion is set to be slightly smaller than the normal human motion range. For the hip joint, the motion ranges from $-15°$ to $130°$, while it changes from $0°$ to $-130°$ for the knee joint. A summary of the rehabilitation device is tabulated in Table 6.1.

Table 6.1 Specifications of the Rehabilitation Device.

Actuator Module	**Parameters**	
Maximum output speed	877 °/s	
Maximum continuous torque	35 Nm	
Power	347 W	
Range of motion (Sagittal)	**Flexion**	**Extension**
Hip	130 °	*-15* °
Knee	*130* °	*0* °

A real-time reconfigurable embedded control and acquisition system, which consists of a real-time processor, a user-reconfigurable field programmable gate array (FPGA), and analog and digital I/O are used for the signal processing and the low-level motor control. A digital servo drive at each actuator module performs close-loop current control to control the torque output at each actuated joint. Desktop computer can communicate with the controller via network cable for high-level control and monitoring. Controller area network (CAN) bus communication at 1 Mbits/s is implemented between the controllers and the digital servo drive. All the electronics can be fitted into a small backpack for

portability. The internal electrical block diagram of the whole system schematic is shown in Figure 6.2.

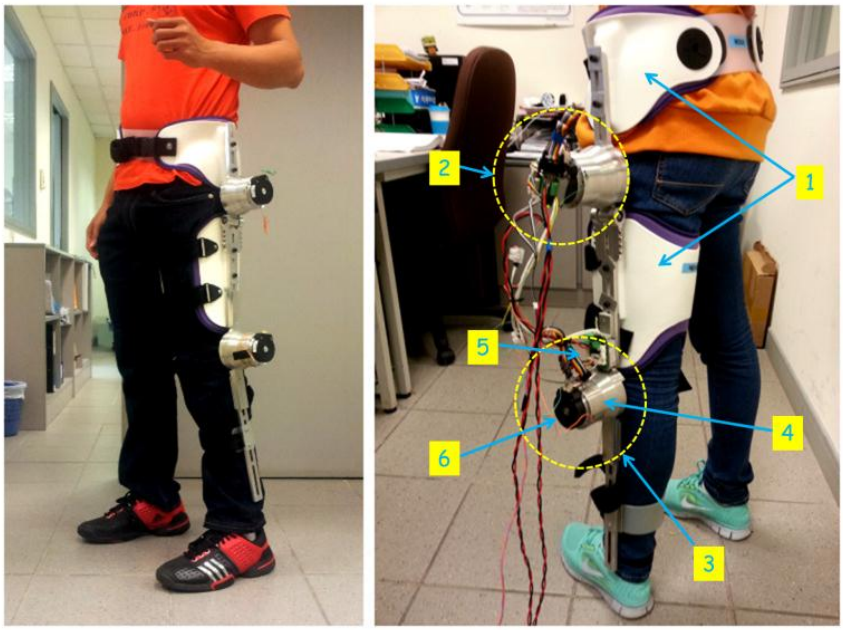

Figure 6.1 Lower extremities rehabilitation device prototype with users. 1: Orthotic cuffs; 2: Hip joint actuator module; 3: Knee joint actuator module; 4: DC motor and harmonic drive housing; 5: Digital servo drive; 6: Incremental encoder.

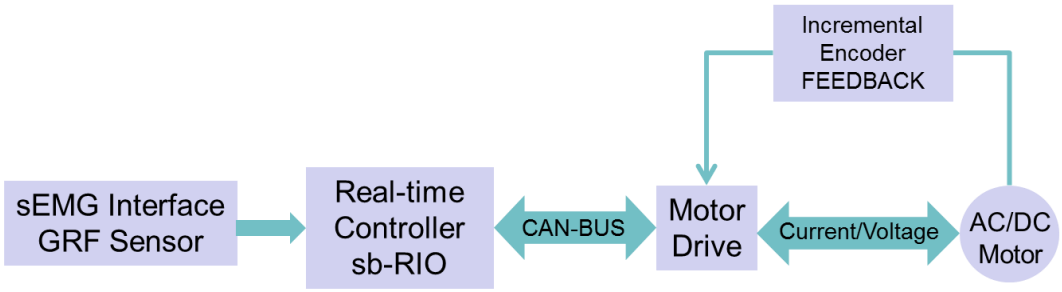

Figure 6.2 Block diagram illustrating control system architecture of the rehabilitation device.

6.3 Real-time Implementation of Force Estimation Algorithm

The proposed method for predicting muscle force has been validated to be feasible and efficient using the off-line sEMG signals recorded from biceps brachii, triceps brachii, rectus femoris and biceps femoris. To test the feasibility on the rehabilitation device, the

developed method is implemented real-time. Different testing trials were performed on the force measurement setup and the rehabilitation device. The details of the trials are described in the following subsections and the performance of the force estimation results are also presented.

6.3.1 Online Tests on Force Measurement Setup

During the online tests, sEMG signals and the measured force data are recorded at a sampling rate of 10 KHz using a USB data acquisition (DAQ) device (National Instruments). The skin preparation, the electrodes attachments, and the warm-up exercises are all same as the details described in Chapter 3 (Subsection 3.2.2). During the experiments, the subjects were seated comfortably on a chair with their back in a vertical position. All the muscle contractions were performed by elbow or knee flexion/extension at a joint angle of 90-degree. Graphs depicting the actual applied force and the estimated force from the CWT-based algorithm were displayed real-time on a computer screen facing the subjects.

The proposed CWT-based force estimation algorithm was implemented in LabView (National Instruments). During the Labview implementation, some signal processing parameters of the proposed algorithm were modified to achieve good muscle force estimation performance. For example, in MATLAB off-line implementation, the sEMG signal and the measured force were recorded at a sampling rate of 10K Hz, and the signals were downsampled to 5000 Hz in order to reduce the size of data. Whereas, during the real-time implementation, the sampling rate was downsampled to be 2500 Hz. In addition, some filters parameters were changed. To smoothen the *MF* signal, a low-pass filter was implemented to filter out the high frequency spikes. This low-pass filter was selected to be a 4^{th} order Bessel filter with 3 Hz cut-off frequency. This filter cut-off frequency is lower than the one used in off-line signal processing. It was selected according to the real-time signal processing performance. We tried a few cut-off frequencies by comparing the filtered signal shape and time lag. No additional filters are involved to filter the estimated force as the predicted force results are observed to be

appropriately smooth. These mentioned modifications on the proposed method were chosen by repetitive results performance comparison.

Four muscles, biceps brachii, triceps brachii, rectus femoris and the biceps femoris were involved in the first online test by performing contraction tasks separately. During the contraction trials, each subject exerted the muscle contraction force, following the shape of a half-sinusoidal signal by pulling or pushing the handle of the force measurement setup (Figure 3.2 and Figure 4.11). Precise tracking performance was not required for a successful experiment. Actually, the purpose of the target tracking was to ensure that subjects would exert the contraction forces at a roughly constant frequency. Subjects took a few minutes (followed by a 3 minutes rest) to become familiar with the tracking task as none had any prior experience.

The peak force target was up to 40% MVC and the forces were exerted by only performing joint flexion or extension. To avoid the influence of muscle fatigue induced from long-term muscle contraction, only five to six flexion/extension contractions were performed during each trial. The period of each repeated cycle was limited approximately to two seconds.

The graphic user interface of the real-time implementation is illustrated in Figure 6.3. In the left column, the top block is the raw sEMG signal. The bottom block depicts the measured force and the estimated force in one graph. The red curve is the applied force measured from force sensor, while the white curve shows the estimated force calculated using the CWT-based algorithm. The right column is the scalogram of CWT, which represents the signal energy distribution. The highest energy during one varying force contraction cycle is distributed in the red color area. In addition, the corresponding frequency and time of this dominant energy distribution can be observed in this demo graph.

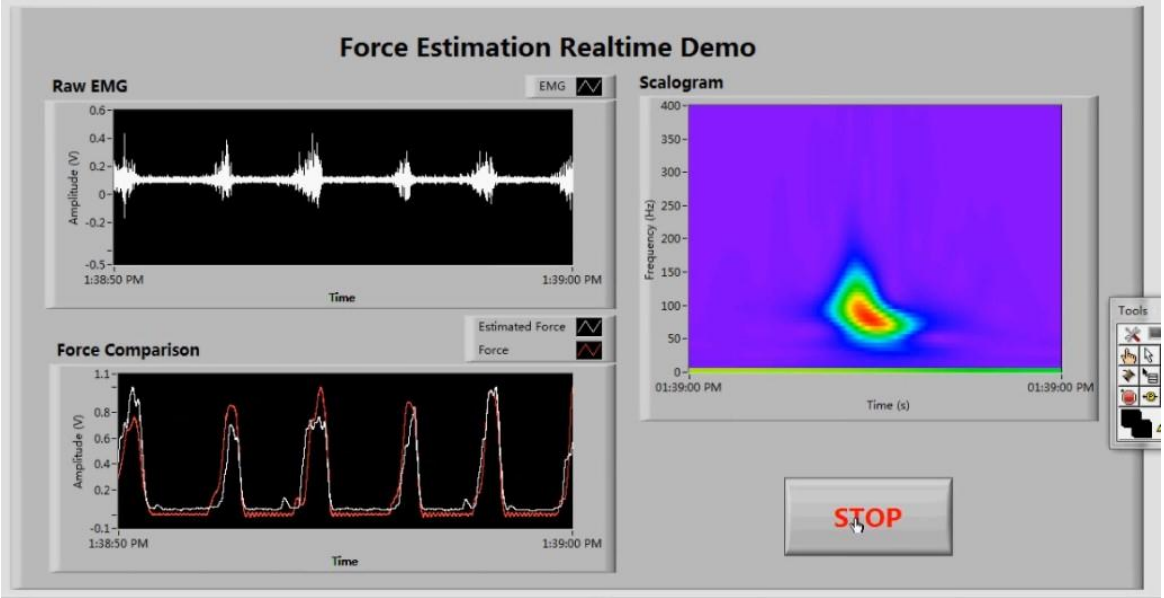

Figure 6.3 Real-time force estimation implementation user interface.

Figure 6.4 shows the estimated force results calculated online from the four muscles of healthy Subject 8. The actual applied forces measured by the force sensors are also plotted to compare the performance with the estimated force. Good similarity in the signal shape can be observed between the estimated force and the measured force.

The CC values and RMSE are calculated using the same method as in Chapter 4 between the estimated force and the measured force, and the corresponding results are tabulated in Table 6.2.

For the involved four muscles, the CC values are high (p<0.05). The average correlation coefficients values are above 0.9535 ± 0.0201 throughout all the muscles, reflecting similar shapes between the estimated force and measured force. In addition, the RMSEs are low, and the minimum averaged value is 0.1071 ± 0.0304 obtained from biceps brachii among all the measured muscle groups.

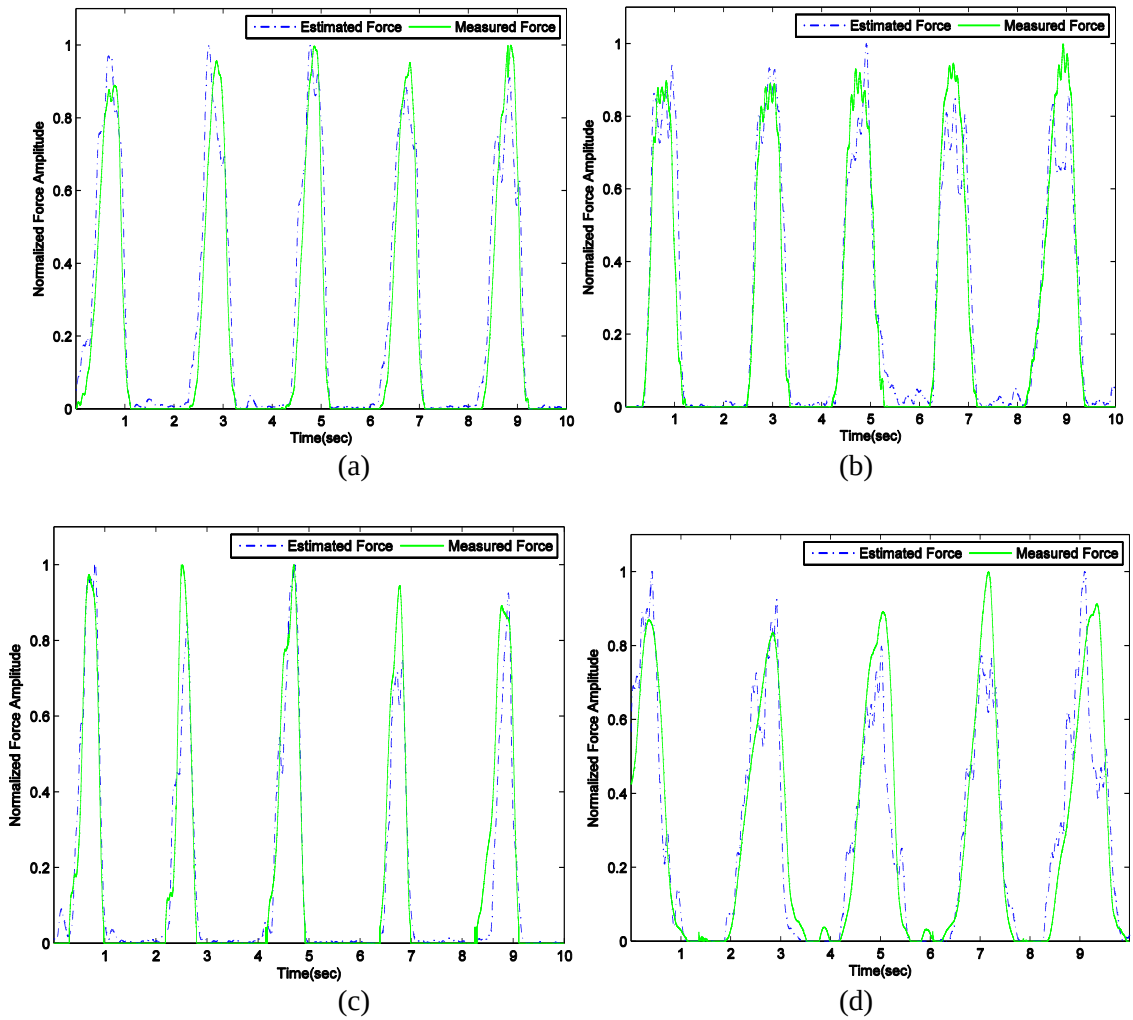

Figure 6.4 Real-time force estimation results using the proposed CWT-based approach. (a) biceps brachii, elbow flexion; (b) triceps brachii, elbow extension; (c) rectus femoris, knee extension; (d) biceps femoris, knee flexion.

Table 6.2 Averaged correlation coefficients and RMSE of four muscles from real-time implementation.

Muscle Groups	Correlation Coefficients	RMSE
Biceps Brachii	0.9614 ±0.0212	0.1071 ±0.0304
Triceps Brachii	0.9535 ±0.0201	0.1333 ±0.0358
Rectus Femoris	0.9614 ±0.0244	0.1259 ±0.0577
Biceps Femoris	0.9630 ±0.0149	0.1224 ±0.0316

The T_f values are also calculated using the same approach as Chapter 4 (Subsection 4.3.3). Even though for every single contraction, the estimated force does not lead the measured force, the T_f ranges from 8.8 ms to 70.4 ms for those contraction cycles where the estimated force leads the measured one. Figure 6.5 shows the statistical analysis results of T_f during real-time implementation for the four measured muscle groups. The negative T_f values demonstrate the estimated force lags the measured force. The T_f results indicate that it is feasible and efficient for the CWT-based algorithm to be implemented in real-time with some parameters modifications.

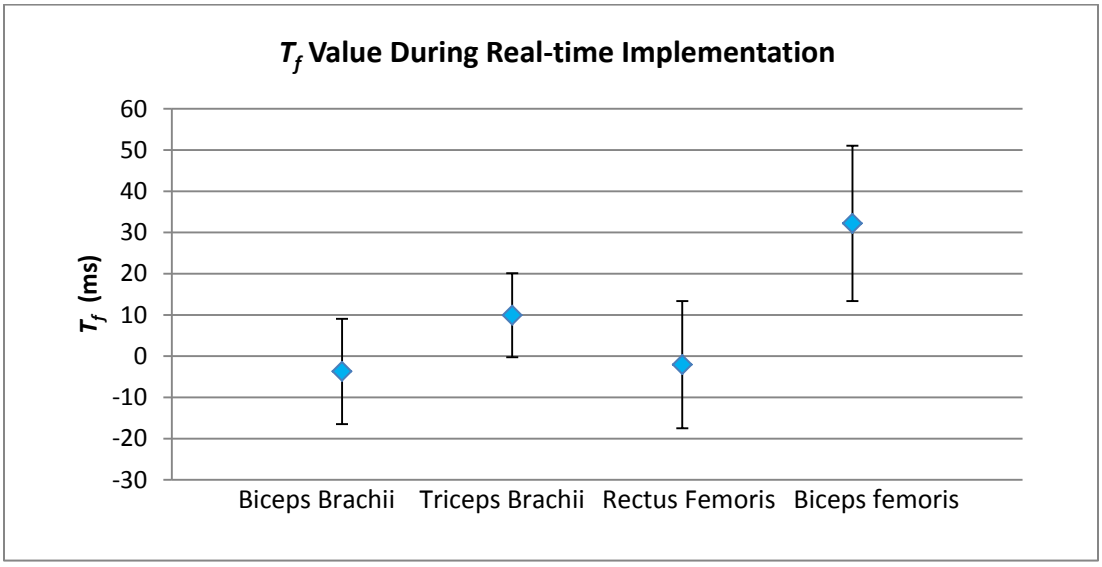

Figure 6.5 T_f calcualted during real-time implementation for all measured muscle groups. (Negative values demonstrate the estimated force lags the measured force).

6.3.2 Online Tests on Level Walking

Results from the online force estimation tests showed good similarity in shape and long T_f as compared to the actual measured forces, we then followed up with another online test of level walking on a treadmill. sEMG signals were recorded from the lower extremity muscles, rectus femoris and biceps femoris. The CWT-based algorithm works online to predict muscle force during walking using sEMG signals. During the experiments, the subjects were asked to walk on a treadmill at different walking speed, 1.5 km/h, 2 km/ h, 2.5 km/h, 3 km/h, 3.5 km/h, 4 km/h, 4.5 km/h and 5 km/h. Another higher speed of 8 km/h was also involved in this experiment. At this high speed, the

subjects had to perform a running activity. Figure 6.6 shows the recorded sEMG signals and the estimated force under different walking and running velocity. The estimated force is normalized to the maximum force value. In each figure, plot (a) is the sEMG signal recorded from rectus femoris, plot (b) is the sEMG signal recorded from biceps femoris. The last two plots, plot (c) and plot (d) are the estimated forces from rectus femoris and biceps femoris respectively.

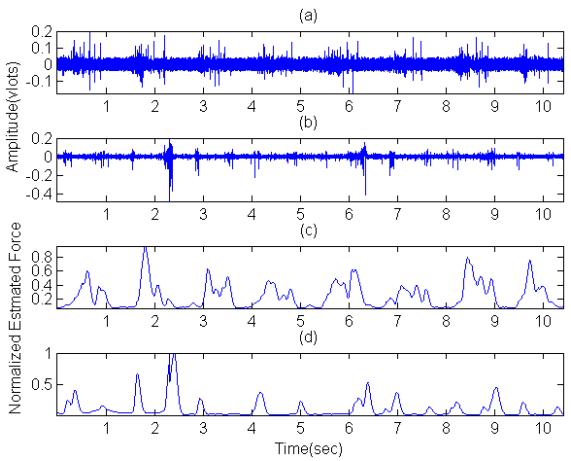

(A) Walking speed 1.5 km/h;

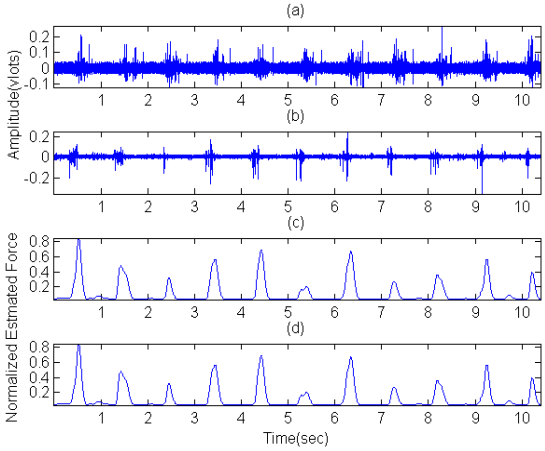

(B) Walking speed 2 km/h;

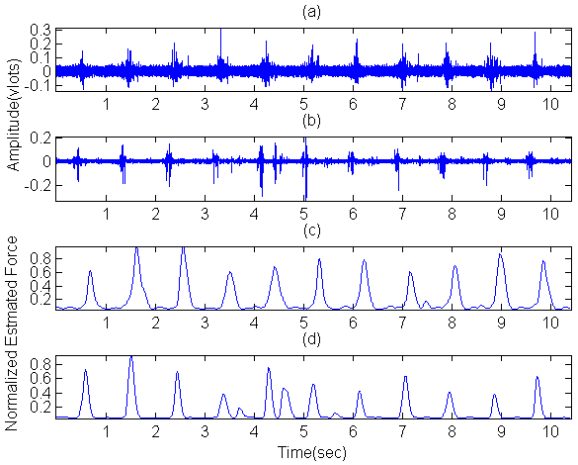

(C) Walking speed 2.5 km/h;

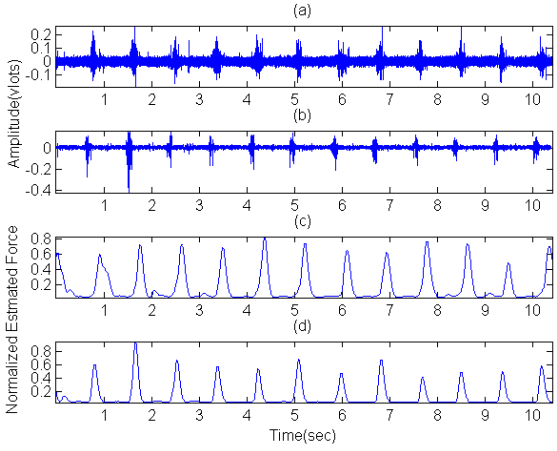

(D) Walking speed 3 km/h;

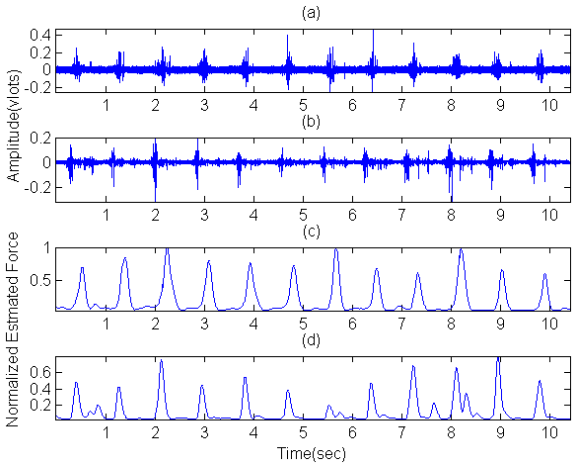

(E) Walking speed 3.5 km/h;

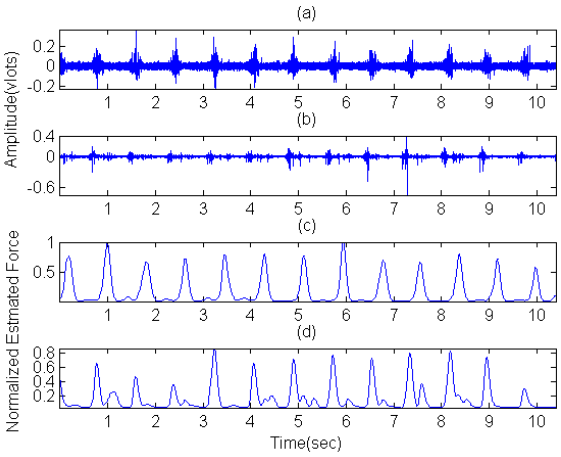

(F) Walking speed 4 km/h;

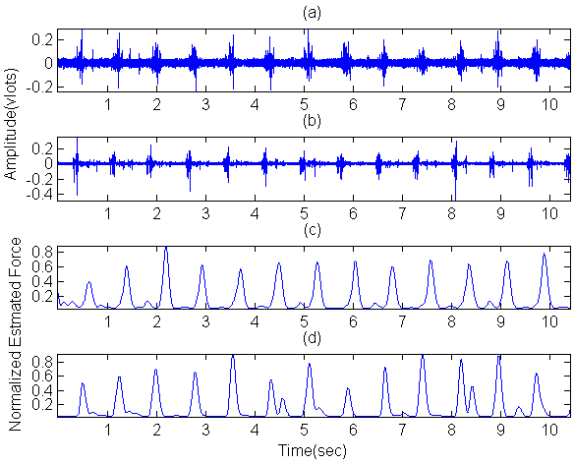

(G) Walking speed 4.5 km/h;

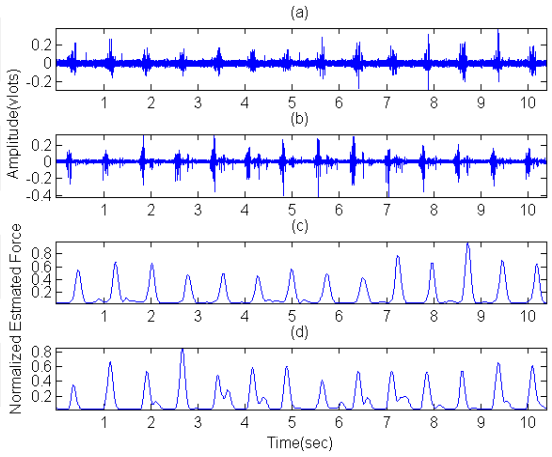

(H) Walking speed 5 km/h;

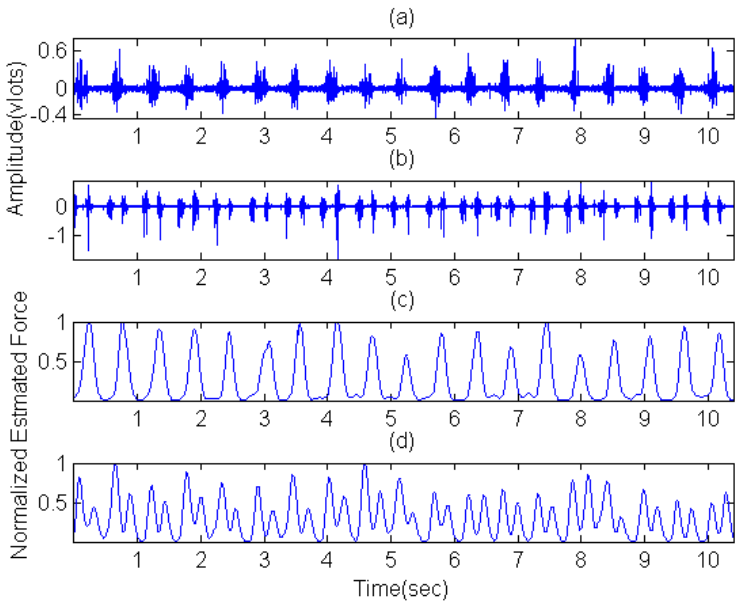

(I) Running speed 8 km/h;

Figure 6.6 Muscle force estimation results on level walking and running at different speed.

From these plots, the sEMG signal amplitude is very small when the walking speed is low. For the low walking speed, the force estimation results are not quite smooth, since the small sEMG amplitude can easily be contaminated by the baseline noise and movement artifacts. As the walking speed increases, the sEMG amplitude becomes larger and the human intention can be detected in a smooth shape and generally simultaneously or before the muscles contract. Results also demonstrate that the force estimation algorithm yields good prediction results for running activity. As we are interested in estimating force/torque at the knee joint for the application in rehabilitation device, the force estimation approach shows its potential feasibility from these plots in Figure 6.6. In addition, the force estimation results show the proposed CWT-based force estimation method is robust under a wide range of walking speeds.

6.3.3 Online Tests on Rehabilitation Robotic Device

To test the feasibility and efficiency of the proposed force estimation approach on rehabilitation device, the algorithm was implemented in a real-time embedded controller

(National Instruments, NI sbRIO-9612). Different trials were performed to test the performance with a lower extremities rehabilitation device to control the knee joint.

Subjects performed the experiments while sEMG signals were recorded from the rectus femoris in real-time. To make the subjects familiarize with the device and the experimental tasks, warm-up exercises were carried out before the experiments. This helped these inexperienced subjects to perform independent movements and proper operations on the device. To confirm the effects of assistance as physically sensed by its users, repetitive squatting and sit-stand motion experiments were conducted by mounting the device on subjects. Two trials were performed in the experiments:

- ***Trial 1:*** Subjects were asked to perform the two legged squatting by knee extension and flexion with around 6 seconds per cycle.
- ***Trial 2***: 6 cycles of the repetitive sit-stand were performed by the subjects in 30 s.

Figure 6.7 illustrates the signal flow with sEMG signal controlling the knee joint. Raw sEMG signals were acquired by the analog input at the sampling frequency of 10 KHz. The normalized estimated force was amplified by a proper selected gain. Then the signal was transmitted as a desired assistive torque via CAN-bus to the digital servo driver to actuate the motor. The transmission speed of the CAN bus was set to 1 Mbits/s. Raw sEMG signals, the normalized estimated force, hip and knee joint position data were measured and displayed on the LabView user interface for online monitoring and data recording.

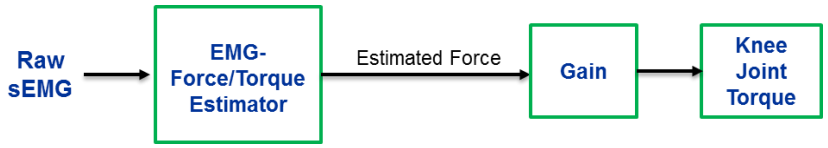

Figure 6.7 Signal flow of sEMG control structure of the real-time implementation of the device.

During the experiments, to ensure the safety of the subjects, low gain was selected to be 3 and the torque for the motor was set to be 25 Nm. Figure 6.8 and Figure 6.9 illustrate the online data measured during repetitive squatting and sit-stand trials. The knee joint is

controlled by the estimated force/torque. The positions change with the estimated force/torque. The hip joint positions are also recorded by the encoders. For the sit-stand motion, the knee and hip joint angles reach the mechanical joint limit when the subjects sit down.

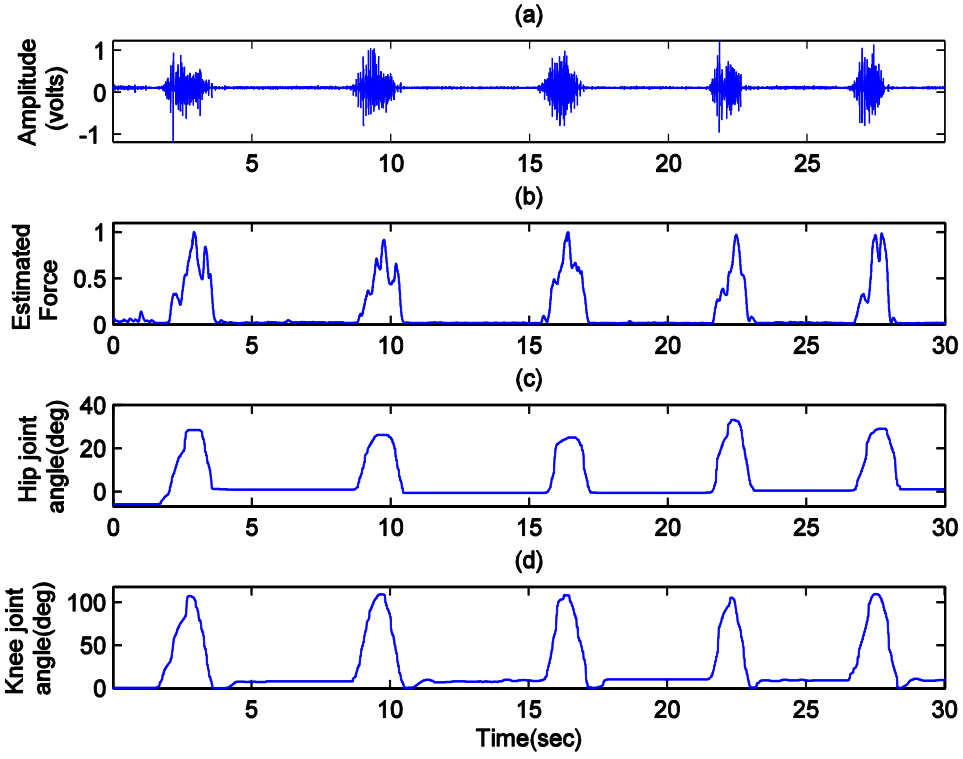

Figure 6.8 Muscle force estimation method real-time implementation on rehabilitation device during repetitive squatting. (a) Raw sEMG signal from rectus femoris muscles; (b) Estimated muscle force/torque; (c) Hip joint angle; (d) Knee joint angle.

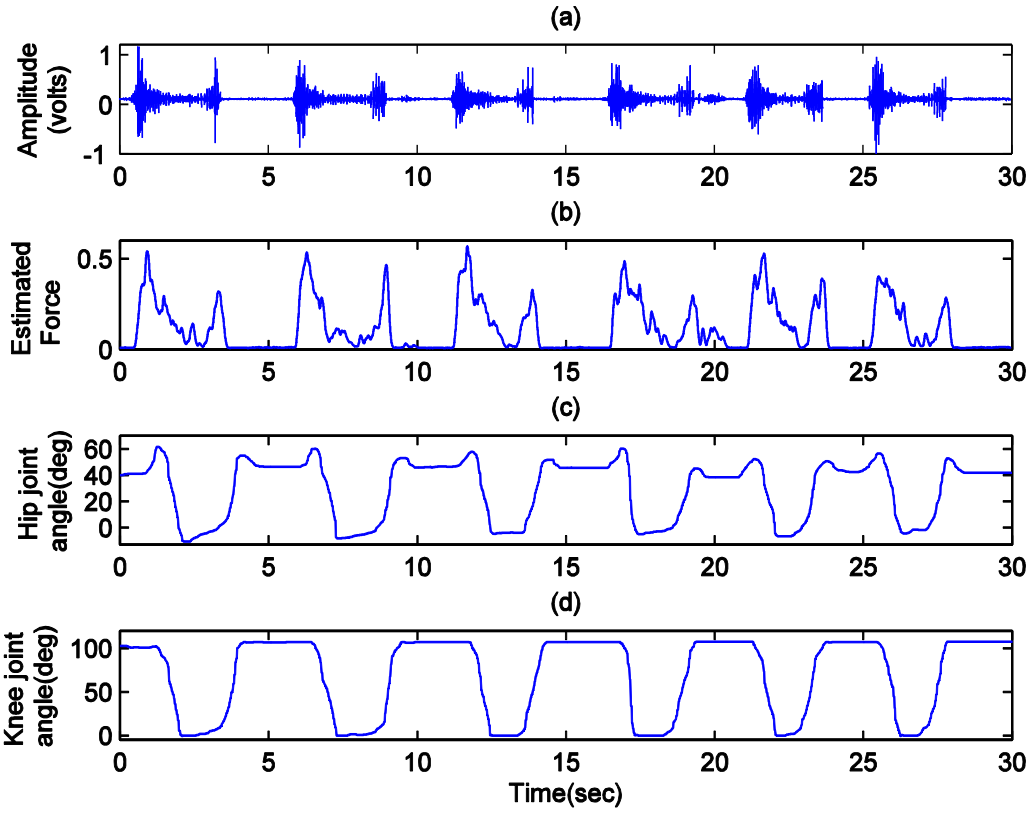

Figure 6.9 Muscle force estimation method real-time implementation on rehabilitation device during repetitive sit-stand. (a) Raw sEMG signal from rectus femoris muscles; (b) Estimated muscle force/torque; (c) Hip joint angle; (d) Knee joint angle.

From the figures, it can be observed that the knee joint is controlled by the estimated force/torque. Meanwhile, the force/torque is estimated by the proposed CWT-based approach concurrent or faster than the muscles. This information ensures the prompt delivery of the estimated force to the motor, which is very important for developing an active and intuitive rehabilitation device. In addition, from the feedback of the subjects, they felt that there was significant assistance from the device while performing the given tasks as the device was able to provide assistive torque according to the subject's intention.

6.4 Fatigue Detection Algorithm Real-time Implementation

For our rehabilitation device, sEMG signals are used to detect the human intention so as to command the control system to provide assistive torque, which makes the device

active and intuitive. However, human muscles can fatigue even with the external assistance from the device, and human performance may be decrease dramatically. When fatigued, human tends to be more error prone and it might lead to accidental injury. Therefore, during rehabilitation gait training, accidents and injuries can be avoided by continuously monitoring the progression of muscle fatigue, warning the users in advance. Hence, knowledge of muscle fatigue is useful for the improvement of a rehabilitation device control system. In addition, based on the previous chapter's study, the estimated fatigue levels can be applied to moderate the output torque of the device.

The proposed muscle fatigue detection approach (described in Subsection 5.3.1) has been investigated and validated using the off-line recorded sEMG signals from upper arms and legs muscles. To investigate the feasibility of the algorithm with online data, the proposed method was implemented in real-time. In this section, the details of the experimental trails are presented, and the fatigue detection results are illustrated in figures. As the fatigue detection approach is an online implementation, but the rehabilitation device is still under development, we alternatively tested the fatigue detection approach with separate setup to experiment with online fatigue contractions.

6.4.1 Online Tests on Fatigue Contraction

During the online tests, the data collection setup is same as Chapter 3 (Subsection 3.2.2). The proposed approach was implemented using LabView (National Instruments). The *MF* and signal power *P* were calculated from CWT. The relative changes of *P* and *P** were obtained by employing the same method as the off-line computation.

During the off-line data validation, the shifting transition thresholds of the fatigue levels are 0.4, 0.8, 1.2 and 1.6 (Subsection 5.3.1), which describe the fatigue levels into four levels. All the fatigue contraction trials end when the subjects feel exhausted and cannot continue any further, which demonstrates the fatigue levels have almost reached to the highest fatigue level. Therefore, in this real-time implementation, to make the estimated fatigue levels demonstrate the fatigue progress as close as the true physiological changes

under fatigue, the threshold values for fatigue level transitions were modified to be 1, 1.2, 1.4 and 1.6 respectively for the 4 fatigue levels. These threshold values were chosen because the filtered *Q* value decreases much slower in real-time when compared to the off-line filtered *Q*.

Three muscles, biceps brachii, rectus femoris and biceps femoris were involved in the online tests by performing different contraction tasks separately. Before the fatigue contraction, the subjects exerted MVCs for at least three times. The submaximal force values used in the following trials were calculated from the averaged MVC values.

The fatigue contractions were divided into isometric contraction and dynamic muscle contraction. During the isometric contraction trials, each subject exerted the muscle contraction at 60% MVC and maintained the force level until exhaustion. The forces were exerted by performing joint flexion or extension while pulling or pushing the handles of the force measurement setup. To avoid the influence of muscle fatigue between trials and to avoid injuries from over-fatigue, each trial was conducted on different days to ensure that the muscles are fully recovered from the previous trial.

Figure 6.10 illustrates the raw sEMG signal, *MF* and the corresponding fatigue detection results from biceps brachii under isometric contraction from different healthy subjects. As shown in this figure, *MF* keeps decreasing as the increasing progress of muscle fatigue. In Figure 6.10 (c), the filtered *Q* declines as the muscle fatigue levels increase. In this figure, the Subject 4's (Figure 6.10 (A)) filtered *Q* shows a fast and straightforward decrease and the fatigue levels reach to the 4^{th} fatigue level in 55 seconds. Whereas, from Figure 6.10 (B), the filtered *Q* fluctuates at the initial few seconds. The fatigue levels start to shift to level 2 in approximate 77 seconds and keep on shifting to higher fatigue level in the following 20 seconds. Figure 6.11 shows the real-time fatigue detection results from lower extremity muscles, rectus femoris and biceps femoris. From the results, the *MF* and filtered *Q* changing trends are general same as the biceps brachii. The overall estimated fatigue levels keep increasing until they reach to the highest fatigue level before the contraction trial ends.

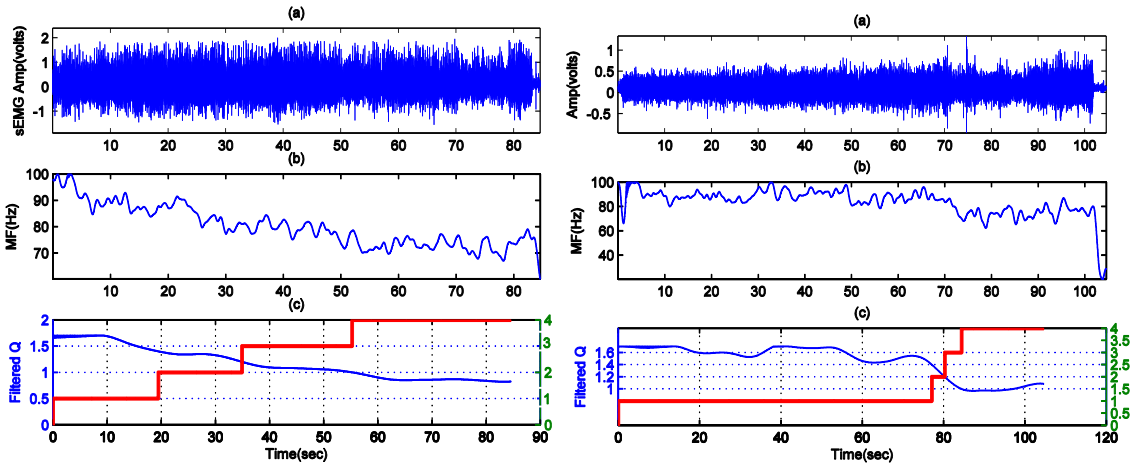

(A) (B)

Figure 6.10 Real-time implementation results of muscle fatigue estimation method during isometric contraction. (a) Raw sEMG signal from bicep brachii muscle; (b) *MF*; (c) Filtered *Q* (blue curve corresponding to the left *Y*-axis) and discrete fatigue level (red curve corresponding to the right *Y*-axis). (A) is fatigue results from Subject 4 and (B) is fatigue results from Subject 8.

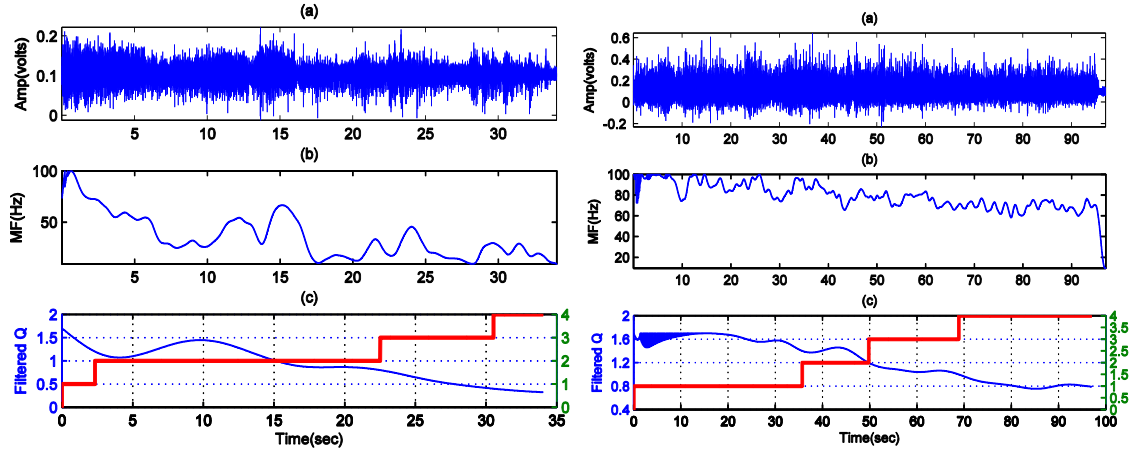

(A) (B)

Figure 6.11 Real-time implementation results of muscle fatigue estimation method during constant force muscle contraction. (a) Raw sEMG signal; (b) *MF*; (c) Filtered *Q* (blue curve corresponding to the left *Y*-axis) and discrete fatigue level (red curve corresponding to the right *Y*-axis). (A) is fatigue results from Subject 3's rectus femoris and (B) is fatigue results from Subject 8's biceps femoris.

Another fatigue contraction trial was completed by performing the squatting in a fixed position. During this trial, sEMG signal was recorded from rectus femoris muscle. The knee angle between thigh and shank was kept approximate 110 degree. The subjects were asked to keep the squatting posture and stop the contraction until they felt exhausted and cannot continue any further. Figure 6.12 shows the sEMG signal, normalized *MF* and the fatigue detection results of this kind of fatigue contraction.

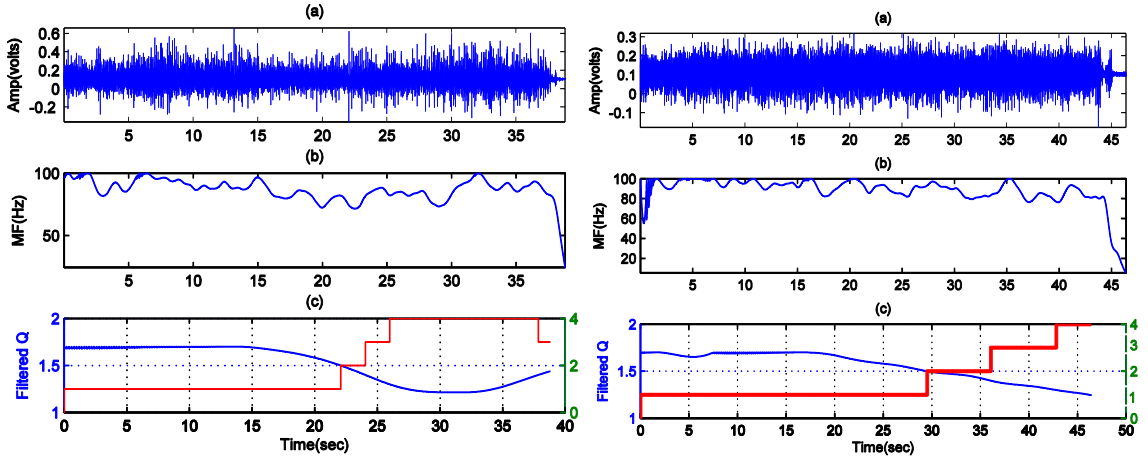

Figure 6.12 Real-time implementation results of muscle fatigue estimation method during squatting. (a) Raw sEMG signal; (b) *MF*; (c) filtered *Q* (blue curve corresponding to the left *Y*-axis) and discrete fatigue level (red curve corresponding to the right *Y*-axis). (A) is fatigue results from Subject 4' rectus femoris and (B) is fatigue results from Subject 8's rectus femoris.

The last trial for real-time fatigue detection validation was the dynamic muscle contraction performed by biceps brachii. During this dynamic muscle contraction, the subjects performed the elbow flexion and extension while holding a 2 kg dumbbell. The contraction started at the position of 90 degree between the forearm and upper arm, and the angle between upper arm and trunk was kept at 0 degree. Then the subjects exerted force by rising up the dumbbell during the elbow flexion until the elbow joint angle decreased to the minimum. One cycle of dynamic contraction was completed by increasing the joint angle back to the starting position. Repetitive dynamic cycles were performed until exhaustion. The raw sEMG signal, *MF* and estimated fatigue levels of one example are illustrated in Figure 6.13.

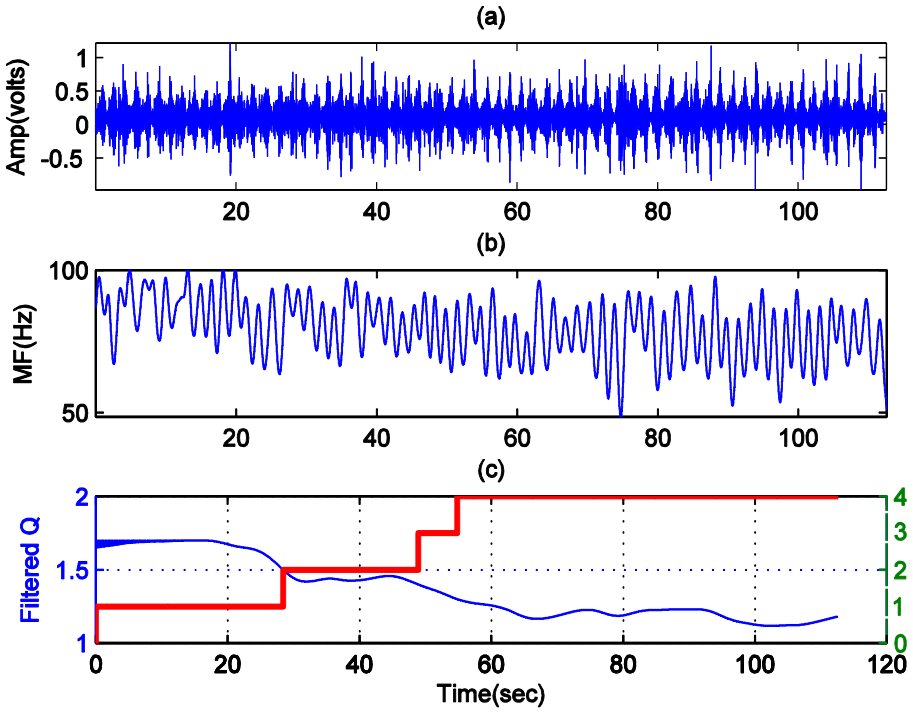

Figure 6.13 Real-time implementation results of muscle fatigue estimation during dynamic contraction (biceps brachii). (a) Raw sEMG signal; (b) *MF*; (c) Filtered *Q* (blue curve corresponding to the left *Y*-axis) and discrete fatigue level (red curve corresponding to the right *Y*-axis).

From the all the above figures, the filtered *Q* keeps decreasing which induces the muscle fatigue levels shifting up the higher levels. Although the fatigue detection algorithm in real-time shows a slow response, the fatigue levels are still viable to indicate the fatigue state as the muscle fatigue in human body is a slow progress.

6.5 Summary

In this chapter, the newly developed lower limb rehabilitation device is first briefly introduced. This device is designed to aid in the flexion and extension motion of the wearer's hip and knee joint by providing assistive torque actively, during level walking or stairs climbing for stroke patients. Then the proposed CWT-based force estimation method and the fatigue detection method described in Chapter 4 and Chapter 5 are implemented in real-time to validate the efficiency and feasibility using online data.

The online force estimation results demonstrate high correlation coefficient (CC>0.9535) when comparing with the measured force, which implies similar shape as the measured force can be obtained from this approach. When this method is implemented to the rehabilitation device, the knee joint is controlled by the estimated force/torque and the positions change with the estimated force. The results also indicate that the device is able to provide assistive torque according to the human's intention. Moreover, it also ensures the intuitive and effortless control from the user's perspective when using sEMG signals as HMI.

The fatigue assessment approach based on CWT is implemented and tested in real-time. Online validation tests are performed during isometric contractions, squatting and dynamic contractions, respectively. The general estimated fatigue levels keep rising with the increasing progress of muscle fatigue. Even though these discrete fatigue levels probably not represent the true fatigue progress accurately, the general trends of these increasing levels are an important reference to track the muscle state.

CHAPTER 7

CONCLUSION AND FUTURE WORKS

7.1 Conclusion

The main objectives of this research were to investigate the relationships between sEMG signal features and muscle force using time-frequency analysis, and to explore novel approaches to estimate muscle force and detect muscle fatigue. In addition, real-time implementation of force estimation and fatigue detection methods are carried out to test and validate the feasibility of the algorithms using online sEMG signals.

An initial investigation on the correlation between sEMG features and muscle force was first carried out. Three relationships were established, the amplitude-force, *MF*-force and the relationships between frequency parameter and signal energy distribution (*MF-P* relationship). Regression fitting results showed that these relationships were nonlinear with high R^2 values. Both signal amplitude and *MF* were found to increase nonlinearly with an increasing exerted force, with the former generally consistent with observations reported by previous literatures [33-37]. In particular, one significant contribution of this thesis is in being the first to successfully establish a relationship between *MF* and force with the frequency domain features. In addition, the *MF*-force relationship provides a simple way to quantitatively estimate the force exerted by muscles through the analysis of the sEMG signal. The establishment of the *MF-P* relationship in this thesis reveals the

correlation between signal frequency spectral changes and signal energy distribution in the frequency domain.

The influence of different electrode locations on these relationships was examined by displacing the electrode locations along muscle fibers. The linear regression and statistical analysis results revealed that the relationships were nonlinear. Although the maximum displacement for each set of the electrodes was 1 cm, the new *MF*-force relationships and *MF*-*P* relationships, showed higher R^2 values as the second electrode location was in the innervation zone.

New approaches for estimating muscle force using sEMG signals from healthy subjects and stroke patients were proposed and evaluated in this work. From the off-line sEMG signal validation results, the force/torque exerted by the four muscle groups (biceps brachii, triceps brachii, rectus femoris and biceps femoris) can be estimated using both time-domain and time-frequency analysis approaches. On average, high correlation coefficients between the estimated force and measured force were observed from the CWT-based method for all measured muscle groups. In addition, the estimated force leads the measured force by $T_f = 75.4 \pm 23.7$ ms. These findings from the developed approaches of this study are of crucial importance in terms of predicting human muscle intention in advance or concurrently. The major advantage of the force estimation approach developed in this study over conventional approaches is that the muscle force can be predicted using sEMG signals before the force exerted by muscles are recorded, both in healthy subjects and stroke patients. This contribution has a large potential for application, especially in the development of active rehabilitation devices.

A new muscle force prediction method was also developed based on CWT and ANN. The force estimation results demonstrated high correlation coefficients between the estimated force and the measured force for both healthy subjects and stroke patients. The important contribution of this approach is that it avoids deriving complex and specific polynomials with different inputs signals from different subjects. This approach is more suitable for stroke patients force estimation compared to the CWT-based approach.

A novel muscle fatigue detection approach was also developed based on time-frequency analysis for both healthy and stroke subjects. Validation with sEMG signals recorded during isometric and varying force contractions demonstrated the effectiveness and reliability in assessing muscle fatigue for both type of contractions. The estimated fatigue levels were being the first to be obtained, indicating the changes within muscles during fatigue contractions. The fatigue levels deliver indicative information of muscle fatigue with the slow response of this approach. In addition, quantification of the fatigue levels by mapping the fatigue levels to the percentage of muscle maximal capacity was proposed. This quantification to the maximum voluntary contractions (MVCs) is substantial since it presents the fatigue assessment much closer to the real physiological fatigue changes. The quantified fatigue levels provide valuable information concerning the muscle state, possibly offering a general standard to avoid injury during variety muscle contractions. In addition, the fatigue detection algorithm for stroke patients showed the feasibility in tracking the patients' affected muscle state.

The proposed muscle estimation and fatigue detection methods were implemented and tested using on-line sEMG signals. High correlation coefficients between the online estimated force and measured force were achieved. When the CWT-based force estimation approach was implemented on the lower limb rehabilitation device, the real-time experimental results showed that the device provided assistive torque to users according to their intention. When implementing the fatigue detection algorithm in real-time, validation results were consistent with the off-line fatigue detection results. The major advantage of the fatigue assessment approach proposed in this study that surpasses most current methods is that it can be used to detect fatigue with both off-line data and in real-time for constant force and dynamic contractions. In addition, this approach is of considerable importance since it provides significant application potential in assessing muscle fatigue in real-time for rehabilitation device.

7.2 Future Works

Although this thesis has reported the successful estimation of muscle force and assessment of muscle fatigue with both healthy subjects and stroke patients using the proposed approaches, there are still some limitations. More works can be done to further improve on the current approaches. The following aspects are recommended for further study:

- Although CWT has been proved to be the most computational and storage efficient method when compared to STFT, WVD and CWD, CWT is unlikely to provide precise estimation of the low frequency components with short-time duration or narrow-band high frequency components. In wavelet transform, the basic functions are derived from a single mother wavelet by two operations of dilation and translation. To avoid the problems in using CWT, a new time-frequency analysis approach like the chirplet transform, which accomplishes the time-frequency plane feature extraction based on the rotation of the TF plane, can be investigated in future studies. Chirplet transform has been introduced to improve energy concentration for signals whose components are not aligned with either the time or the frequency axis. Currently, very few studies use this transform to analyze sEMG signals. Muscle force and fatigue estimation studies based on chirplet transform may be an interesting area for the future work.

- To achieve more robust results for the proposed force estimation and fatigue detection methods for stroke patients, more patients are still needed. Even though validation results from the limited number of patients achieved successful force and fatigue estimation, more stroke patients with different severities should be encouraged to participate in future studies to ensure that the proposed methods are suitable for a wide variety of patients.

- The current data collection from stroke patients focuses only on the affected legs with the differences between the affected legs and un-affected legs not compared. If the

force estimation and fatigue detection results from both legs are compared, it will be helpful in exploring more effective approaches.

- Even though the proposed methods have been shown to be feasible using sEMG signal from dynamic contractions both offline and online, it is still necessary to modify the present force measurement setup to be suitable for measuring force from varying angles instead of constant angles.

- Implementation of the proposed fatigue detection approach can be carried out on the lower limb rehabilitation device allowing compensation torque by the device to be adjusted based on the muscle fatigue levels and control algorithms.

BIBLIOGRAPHY

[1] R. F. M. Kleissen, J. H. Buurke, J. Harlaar *et al.*, “Electromyography in the biomechanical analysis of human movement and its clinical application,” *Gait & Posture,* vol. 8, no. 2, pp. 143-158, 1998.

[2] J. Basmajian, “Research foundations of EMG biofeedback in rehabilitation,” *Biofeedback and Self-regulation,* vol. 13, no. 4, pp. 275-298, 1988-12-01, 1988.

[3] T. M. Lubecki, F. J. Bai, C. M. Chew *et al.*, "Development of intuitive human-machine interface based on Electromyography for assistive robot (KAAD)." pp. 908-913.

[4] P. Contessa, A. Adam, and C. J. De Luca, “Motor unit control and force fluction during fatigue,” *J. Appl. Physiol,* vol. 207, pp. 235-243, 2009.

[5] R. M. E. a. J. Duchateau, “Muscle fatigue: What, why and how it influences muscle function,” *J. Physiol,* vol. 586, pp. 11-23, 2008.

[6] R. H. Fitts, “Cellular mechanisms of muscle fatigue,” *J. Appl Physiol,* vol. 74, no. 1, pp. 49-94, 1994.

[7] R. Merletti, and P. Parker, “Physiology, engineering, and noninvasive applications,” *Electromyography,* 2005.

[8] D. C. Basmajian J, *Muscles alive: their function revealed by electromyography*: Baltimore: Williams & Wilkins, 1985.

[9] D. G. Lloyd, and T. F. Besier, “An EMG-driven musculoskeletal model to estimate muscle forces and knee joint moments in vivo,” *Journal of Biomechanics,* vol. 36, no. 6, pp. 765-776, 2003.

[10] D. A. Winter, *Biomechanics and motor control of human movement*: Wiley, 2009.

[11] M. Shaughnessy, K. M. Michael, J. D. Sorkin *et al.*, “Steps after stroke: capturing ambulatory recovery,” *Stroke,* vol. 36, no. 6, pp. 1305-7, 2005.

[12] D. H. Sutherland, “The evolution of clinical gait analysis part l: kinesiological EMG,” *Gait & Posture,* vol. 14, no. 1, pp. 61-70, 2001.

[13] J. Basmajian, C. Gowland, M. Finlayson *et al.*, “Stroke treatment: comparison of integrated behavioral-physical therapy vs traditional physical therapy programs,” *Archives of Physical Medicine and Rehabilitation,* vol. 68, no. 5 Pt 1, pp. 267, 1987.

[14] G. Colombo, M. Wirz, and V. Dietz, “Driven gait orthosis for improvement of locomotor training in paraplegic patients,” *Spinal Cord,* vol. 39, no. 5, pp. 252-255, 2001.

[15] E. R. Kandel, J. H. Schwartz, and T. M. Jessell, *Principles of neural science*: McGraw-Hill New York, 2000.

[16] R. Burke, “Motor units: anatomy, physiology, and functional organization,” *Comprehensive Physiology*, 2011.
[17] P. Konrad, “The ABC of EMG: A Practical Introduction to Kinesiological Electromyography,” 2005.
[18] T. Moritani, D. Stegeman, and R. Merletti, “Basic physiology and biophysics of EMG signal generation,” *Electromyography: Physiology, engineering, and noninvasive applications*, pp. 1-25, 2004.
[19] C. J. De Luca, “The use of surface electromyography in Biomechanics,” *J. Appl. Biomech,* vol. 13, pp. 135-163, 1997.
[20] C. J. De Luca, and Z. Erim, “Common drive of motor units in regulation of muscle force,” *Trends in neurosciences,* vol. 17, no. 7, pp. 299-305, 1994.
[21] D. Farina, R. Merletti, and R. M. Enoka, “The extraction of neural strategies from the surface EMG,” *Journal of Applied Physiology,* vol. 96, no. 4, pp. 1486-1495, 2004.
[22] C. J. D. Luca, “Surface Electromyography: Detection and Recording,” *Delsys Incorporated*, 2002.
[23] B. Gerdle, S. Karlsson, S. Day *et al.*, "Acquisition, processing and analysis of the surface electromyogram," *Modern Techniques in Neuroscience Research*, pp. 705-755: Springer, 1999.
[24] E. D. Toffola, D. Sparpaglione, A. Pistorio *et al.*, “Myoelectric manifestations of muscle changes in stroke patients,” *Arch Phys Med Rehabil,* vol. 82, no. 5, pp. 661-5, 2001.
[25] M. Zwarts, G. Bleijenberg, and B. Van Engelen, “Clinical neurophysiology of fatigue,” *Clinical Neurophysiology,* vol. 119, no. 1, pp. 2-10, 2008.
[26] C. Disselhorst-Klug, T. Schmitz-Rode, and G. Rau, “Surface electromyography and muscle force: Limits in sEMG–force relationship and new approaches for applications,” *Clinical Biomechanics,* vol. 24, no. 3, pp. 225-235, 2009.
[27] D. Farina, R. Merletti, and D. Stegeman, “Biophysics of the generation of EMG signals,” *Electromyography: Physiology, engineering, and noninvasive applications,* pp. 81-105, 2004.
[28] V. T. Inman, H. J. Ralston, J. B. De C.M. Saunders *et al.*, “Relation of human electromyogram to muscular tension,” *Electroencephalography and Clinical Neurophysiology*, vol. 4, no. 2, pp. 187-194, 1952.
[29] O. C. J. Lippold, “The relation between integrated action potentials in a human muscle and its isometric tension,” *The Journal of physiology,* vol. 117, no. 4, pp. 492, 1952.
[30] B. Bigland, and O. Lippold, “The relation between force, velocity and integrated electrical activity in human muscles,” *The Journal of physiology,* vol. 123, no. 1, pp. 214-224, 1954.
[31] H. A. DeVries, “" Efficiency of electrical activity" as a physiological measure of the functional state of muscle tissue,” *American Journal of Physical Medicine & Rehabilitation,* vol. 47, no. 1, pp. 10-22, 1968.
[32] H. Milner-Brown, and R. Stein, “The relation between the surface electromyogram and muscular force,” *The Journal of physiology,* vol. 246, no. 3, pp. 549-569, 1975.

[33] S. Karlsson, and B. Gerdle, "Mean frequency and signal amplitude of the surface EMG of the quadriceps muscles increase with increasing torque — a study using the continuous wavelet transform," *Journal of Electromyography and Kinesiology,* vol. 11, no. 2, pp. 131-140, 2001.
[34] H. Onishi, R. Yagi, K. Akasaka *et al.*, "Relationship between EMG signals and force in human vastus lateralis muscle using multiple bipolar wire electrodes," *Journal of Electromyography and Kinesiology,* vol. 10, no. 1, pp. 59-67, 2000.
[35] V. Hermans, A. J. Spaepen, and M. Wouters, "Relation between differences in electromyographic adaptations during static contractions and the muscle function," *Journal of Electromyography and Kinesiology,* vol. 9, no. 4, pp. 253-261, 1999.
[36] W. Herzog, J. Sokolosky, Y. T. Zhang *et al.*, "EMG-Force Relation in Dynamically Contracting Cat Plantaris Muscle," *Journal of Electromyography and Kinesiology,* vol. 8, no. 3, pp. 147-155, 1998.
[37] B. A. Alkner, P. Tesch, and H. E. Berg, "Quadriceps EMG/force relationship in knee extension and leg press," *Medicine and science in sports and exercise,* vol. 32, no. 2, pp. 459-463, 2000.
[38] A. Guimaraes, W. Herzog, M. Hulliger *et al.*, "EMG-force relationship of the cat soleus muscle studied with distributed and non-periodic stimulation of ventral root filaments," *Journal of experimental biology,* vol. 186, no. 1, pp. 75-93, 1994.
[39] A. L. Hof, and J. van den Berg, "Linearity between the weighted sum of the EMGs of the human triceps surae and the total torque," *Journal of Biomechanics,* vol. 10, no. 9, pp. 529-539, 1977.
[40] J. J. Woods, and B. Bigland-Ritchie, "Linear and non-linear surface EMG/force relationships in human muscles: an anatomical/functional argument for the existence of both," *American Journal of Physical Medicine & Rehabilitation,* vol. 62, no. 6, pp. 287-299, 1983.
[41] D. G. Bell, "The influence of air temperature on the EMG/force relationship of the quadriceps," *European journal of applied physiology and occupational physiology,* vol. 67, no. 3, pp. 256-260, 1993.
[42] K. E. I. J. O. Häkkinen, and P. A. A. V. O. V. Komi, "Electromyographic changes during strength training and detraining," *Medicine and science in sports and exercise,* vol. 15, no. 6, pp. 455-460, 1982.
[43] J. Vredenbregt, Rau, G., "Surface Electromyography in relation to force, muscle length, and endurance.," *New Developments in Electromyography and Clinical Neurophysiology,* vol. Vol. 1, pp. 607-622, 1973.
[44] B. Gerdle, K. HENRIKSSON‐LARSÉN, R. Lorentzon *et al.*, "Dependence of the mean power frequency of the electromyogram on muscle force and fibre type," *Acta Physiologica Scandinavica,* vol. 142, no. 4, pp. 457-465, 1991.
[45] R. Baratta, M. Solomonow, B.-H. Zhou *et al.*, "Methods to reduce the variability of EMG power spectrum estimates," *Journal of Electromyography and Kinesiology,* vol. 8, no. 5, pp. 279-285, 1998.
[46] T. Moritani, and M. Muro, "Motor unit activity and surface electromyogram power spectrum during increasing force of contraction," *European journal of applied physiology and occupational physiology,* vol. 56, no. 3, pp. 260-265, 1987.
[47] G. B., and N. E. E. a. L. Brundin, "The behaviour of mean power frequency of the surface electromyogram in biceps brachii with increasing force and during fatigue.

With special regard to the electrode distance," *Electroencephalogr Clin Neurophysiol,* vol. Vol. 30, pp. 483-489, 1990.

[48] J. S. Petrofsky, and A. R. Lind, "Frequency analysis of the surface electromyogram during sustained isometric contractions," *European journal of applied physiology and occupational physiology,* vol. 43, no. 2, pp. 173-182, 1980.

[49] M. Solomonow, C. Baten, J. Smit *et al.*, "Electromyogram power spectra frequencies associated with motor unit recruitment strategies," *Journal of Applied Physiology,* vol. 68, no. 3, pp. 1177-1185, 1990.

[50] M. Bilodeau, S. Schindler-Ivens, D. Williams *et al.*, "EMG frequency content changes with increasing force and during fatigue in the quadriceps femoris muscle of men and women," *Journal of Electromyography and Kinesiology,* vol. 13, no. 1, pp. 83-92, 2003.

[51] E. A. Clancy, S. Bouchard, and D. Rancourt, "Estimation and application of EMG amplitude during dynamic contractions," *IEEE engineering in medicine and biology,* vol. 20, no. 6, pp. 47-54, 2001.

[52] J. R. Potvin, and S. H. Brown, "Less is more: high pass filtering, to remove up to 99% of the surface EMG signal power, improves EMG-based biceps brachii muscle force estimates," *Journal of electromyography and kinesiology: official journal of the International Society of Electrophysiological Kinesiology,* vol. 14, no. 3, pp. 389, 2004.

[53] D. G. Lloyd, and T. S. Buchanan, "A model of load sharing between muscles and soft tissues at the human knee during static tasks," *J Biomech Eng,* vol. 118, no. 3, pp. 367-76, 1996.

[54] A. Erdemir, S. McLean, W. Herzog *et al.*, "Model-based estimation of muscle forces exerted during movements," *Clinical Biomechanics,* vol. 22, no. 2, pp. 131-154, 2007.

[55] J. F. Soechting, and M. Flanders, "Evaluating an integrated musculoskeletal model of the human arm," *J Biomech Eng,* vol. 119, no. 1, pp. 93-102, 1997.

[56] M. A. Nussbaum, and D. B. Chaffin, "Lumbar muscle force estimation using a subject-invariant 5-parameter EMG-based model," *Journal of Biomechanics,* vol. 31, no. 7, pp. 667-672, 1998.

[57] W. Lin, and T. S. Buchanan, "Prediction of joint moments using a neural network model of muscle activations from EMG signals," *Neural Systems and Rehabilitation Engineering, IEEE Transactions on,* vol. 10, no. 1, pp. 30-37, 2002.

[58] F. Sepulveda, D. M. Wells, and C. L. Vaughan, "A neural network representation of electromyography and joint dynamics in human gait," *Journal of Biomechanics,* vol. 26, no. 2, pp. 101-109, 1993.

[59] S. H. Holzreiter, and M. E. Köhle, "Assessment of gait patterns using neural networks," *Journal of Biomechanics,* vol. 26, no. 6, pp. 645-651, 1993.

[60] M. M. Liu, W. Herzog, and H. H. C. M. Savelberg, "Dynamic muscle force predictions from EMG: an artificial neural network approach," *Journal of Electromyography and Kinesiology,* vol. 9, no. 6, pp. 391-400, 1999.

[61] C. Choi, S. Kwon, W. Park *et al.*, "Real-time pinch force estimation by surface electromyography using an artificial neural network," *Medical Engineering & Physics,* vol. 32, no. 5, pp. 429-436, 2010.

[62] J. J. Luh, G. C. Chang, C. K. Cheng *et al.*, "Isokinetic elbow joint torques estimation from surface EMG and joint kinematic data: using an artificial neural network model," *J Electromyogr Kinesiol,* vol. 9, no. 3, pp. 173-83, 1999.
[63] M. R. Al-Mulla, F. Sepulveda, and M. Colley, "A review of non-invasive techniques to detect and predict localised muscle fatigue," *Sensors (Basel),* vol. 11, no. 4, pp. 3545-94, 2011.
[64] B. K. Barry, and R. M. Enoka, "The neurobiology of muscle fatigue: 15 years later, Integrative and Comparative Biology," *Integrative and comparative biology,* vol. 47, no. 4, pp. 465-473, 2007.
[65] H. J. Green, "Mechanisms of muscle fatigue in intense exercise," *Journal of sports sciences,* vol. 15, no. 3, pp. 247-256, 1997.
[66] S. Boyas, and A. Guével, "Neuromuscular fatigue in healthy muscle: Underlying factors and adaptation mechanisms," *Annals of Physical and Rehabilitation Medicine,* vol. 54, no. 2, pp. 88-108, 2011.
[67] M. Cifrek, V. Medved, S. Tonković *et al.*, "Surface EMG based muscle fatigue evaluation in biomechanics," *Clinical biomechanics (Bristol, Avon),* vol. 24, no. 4, pp. 327-340, 2009.
[68] B. Bigland-Ritchie, E. F. Donovan, and C. S. Roussos, "Conduction velocity and EMG power spectrum changes in fatigue of sustained maximal efforts," *Journal of Applied Physiology,* vol. 51, no. 5, pp. 1300-1305, 1981.
[69] L. Arendt‐Nielsen, K. R. Mills, and A. Forster, "Changes in muscle fiber conduction velocity, mean power frequency, and mean EMG voltage during prolonged submaximal contractions," *Muscle & nerve,* vol. 12, no. 6, pp. 493-497, 1989.
[70] K. M. Calder, D. W. Stashuk, and L. McLean, "Physiological characteristics of motor units in the brachioradialis muscle across fatiguing low-level isometric contractions," *Journal of Electromyography and Kinesiology,* vol. 18, no. 1, pp. 2-15, 2008.
[71] A. Luttmann, M. Jäger, and W. Laurig, "Electromyographical indication of muscular fatigue in occupational field studies," *International Journal of Industrial Ergonomics,* vol. 25, no. 6, pp. 645-660, 2000.
[72] G. M. Hägg, "Comparison of different estimators of electromyographic spectral shifts during work when applied on short test contractions," *Medical and Biological Engineering and Computing,* vol. 29, no. 5, pp. 511-516, 1991.
[73] P. Welch, "The use of fast Fourier transform for the estimation of power spectra: a method based on time averaging over short, modified periodograms," *Audio and Electroacoustics, IEEE Transactions on,* vol. 15, no. 2, pp. 70-73, 1967.
[74] F. B. Stulen, and C. J. De Luca, "Frequency Parameters of the Myoelectric Signal as a Measure of Muscle Conduction Velocity," *Biomedical Engineering, IEEE Transactions on,* vol. BME-28, no. 7, pp. 515-523, 1981.
[75] M. Hagberg, "Work load and fatigue in repetitive arm elevations," *Ergonomics,* vol. 24, no. 7, pp. 543-555, 1981.
[76] M. Knaflitz, and P. Bonato, "Time-frequency methods applied to muscle fatigue assessment during dynamic contractions," *Journal of Electromyography and Kinesiology,* vol. 9, no. 5, pp. 337-350, 1999.

[77] S. Karlsson, Y. Jun, and M. Akay, "Enhancement of spectral analysis of myoelectric signals during static contractions using wavelet methods," *Biomedical Engineering, IEEE Transactions on*, vol. 46, no. 6, pp. 670-684, 1999.
[78] P. Bonato, G. Gagliati, and M. Knaflitz, "Analysis of myoelectric signals recorded during dynamic contractions," *Engineering in Medicine and Biology Magazine, IEEE*, vol. 15, no. 6, pp. 102-111, 1996.
[79] W. T. Cochran, J. W. Cooley, D. L. Favin *et al.*, "What is the fast Fourier transform?," *Proceedings of the IEEE*, vol. 55, no. 10, pp. 1664-1674, 1967.
[80] L. Cohen, *Time-frequency analysis*: Prentice Hall PTR New Jersey, 1995.
[81] M. Al-Mulla, F. Sepulveda, and M. Colley, "sEMG Techniques to Detect and Predict Localised Muscle Fatigue," *EMG Methods for Evaluating Muscle and Nerve Function, ISBN*, pp. 978-953, 2012.
[82] M. Cifrek, S. Tonković, and V. Medved, "Measurement and analysis of surface myoelectric signals during fatigued cyclic dynamic contractions," *Measurement*, vol. 27, no. 2, pp. 85-92, 2000.
[83] L. Cohen, *Time-Frequency Analysis*: Prentice Hall PTR, 1995.
[84] J. Duchene, D. Devedeux, S. Mansour *et al.*, "Analyzing uterine EMG: tracking instantaneous burst frequency," *Engineering in Medicine and Biology Magazine, IEEE*, vol. 14, no. 2, pp. 125-132, 1995.
[85] C. DeCusatis, and P. K. Das, *Wavelets and subbands: fundamentals and applications*: Birkhauser, 2002.
[86] A. Teolis, *Computational signal processing with wavelets*, Boston: Birkhäuser 1988.
[87] Agostino Abbate, C. M. DeCusatis, and P. K. Das, *Wavelets and Subbands: Fundamentals and Applications*, Boston: Birkhauser, 2002.
[88] B. Boashash, *Time-Frequency Signals Analysis: Methods and Applications*: Longman Cheshire, 1992.
[89] S. Karlsson, Y. Jun, and M. Akay, "Time-frequency analysis of myoelectric signals during dynamic contractions: a comparative study," *Biomedical Engineering, IEEE Transactions on*, vol. 47, no. 2, pp. 228-238, 2000.
[90] J. S. Karlsson, B. Gerdle, and M. Akay, "Analyzing surface myoelectric signals recorded during isokinetic contractions," *Engineering in Medicine and Biology Magazine, IEEE*, vol. 20, no. 6, pp. 97-105, 2001.
[91] M. González-Izal, A. Malanda, E. Gorostiaga *et al.*, "Electromyographic models to assess muscle fatigue," *Journal of Electromyography and Kinesiology*, vol. 22, no. 4, pp. 501-512, 2012.
[92] M. Gonzalez-Izal, A. Malanda, I. Navarro-Amezqueta *et al.*, "EMG spectral indices and muscle power fatigue during dynamic contractions," *Journal of Electromyography and Kinesiology*, vol. 20, no. 2, pp. 233-240, 2010.
[93] G. V. Dimitrov, T. I. Arabadzhiev, K. N. Mileva *et al.*, "Muscle fatigue during dynamic contractions assessed by new spectral indices," *Medicine and science in sports and exercise*, vol. 38, no. 11, pp. 1971, 2006.
[94] R. Boostani, and M. H. Moradi, "Evaluation of the forearm EMG signal features for the control of a prosthetic hand," *Physiological measurement*, vol. 24, no. 2, pp. 309, 2003.

[95] D. Moshou, I. Hostens, G. Papaioannou *et al.*, "Dynamic muscle fatigue detection using self-organizing maps," *Applied Soft Computing,* vol. 5, no. 4, pp. 391-398, 2005.
[96] P. S. Sung, U. Zurcher, and M. Kaufman, "Gender differences in spectral and entropic measures of erector spinae muscle fatigue," *J. Rehabil. Res. Develop,* vol. 45, pp. 1431-1439, 2008.
[97] D. Farina, F. Leclerc, L. Arendt-Nielsen *et al.*, "The change in spatial distribution of upper trapezius muscle activity is correlated to contraction duration," *Journal of Electromyography and Kinesiology,* vol. 18, no. 1, pp. 16-25, 2008.
[98] A. Troiano, R. Merletti, and L. Mesin, "Assessment of force and fatigue in isometric contractions of the upper trapezius muscle by surface EMG signal and perceived exertion scale," *Gait & Posture,* vol. 28, pp. 179-186, 2008.
[99] S. M. Pincus, "Approximate entropy as a measure of system complexity," *Proceedings of the National Academy of Sciences,* vol. 88, no. 6, pp. 2297-2301, 1991.
[100] H.-B. Xie, J.-Y. Guo, and Y.-P. Zheng, "Fuzzy Approximate Entropy Analysis of Chaotic and Natural Complex Systems: Detecting Muscle Fatigue Using Electromyography Signals," *Annals of Biomedical Engineering,* vol. 38, no. 4, pp. 1483-1496, 2010/04/01, 2010.
[101] H.-B. Xie, Y.-P. Zheng, J.-Y. Guo *et al.*, "Cross-fuzzy entropy: a new method to test pattern synchrony of bivariate time series," *Information Sciences,* vol. 180, no. 9, pp. 1715-1724, 2010.
[102] J.-Y. Kim, M.-C. Jung, and J. M. Haight, "The sensitivity of autoregressive model coefficient in quantification of trunk muscle fatigue during a sustained isometric contraction," *International Journal of Industrial Ergonomics,* vol. 35, no. 4, pp. 321-330, 2005.
[103] D. T. MacIsaac, P. A. Parker, K. B. Englehart *et al.*, "Fatigue estimation with a multivariable myoelectric mapping function," *Biomedical Engineering, IEEE Transactions on,* vol. 53, no. 4, pp. 694-700, 2006.
[104] D. R. Rogers, and D. T. MacIsaac, "Training a multivariable myoelectric mapping function to estimate fatigue," *Journal of Electromyography and Kinesiology,* vol. 20, no. 5, pp. 953-960, 2010.
[105] D. R. Rogers, and D. T. MacIsaac, "EMG-based muscle fatigue assessment during dynamic contractions using principal component analysis," *Journal of Electromyography and Kinesiology,* vol. 21, no. 5, pp. 811-818, 2011.
[106] M. R. Al-Mulla, F. Sepulveda, and M. Colley, "Evolved pseudo-wavelet function to optimally decompose sEMG for automated classification of localized muscle fatigue," *Medical engineering & physics,* vol. 33, no. 4, pp. 411-417, 2011.
[107] M. Al-Mulla, F. Sepulveda, M. Colley *et al.*, "Statistical class separation using sEMG features towards automated muscle fatigue detection and prediction." pp. 1-5.
[108] J. L. Young, and R. F. Mayer, "Physiological alterations of motor units in hemiplegia," *Journal of the Neurological Sciences,* vol. 54, no. 3, pp. 401-412, 1982.
[109] C. E. Hafer-Macko, A. S. Ryan, F. M. Ivey *et al.*, "Skeletal muscle changes after hemiparetic stroke and potential beneficial effects of exercise intervention

strategies," *Journal of rehabilitation research and development,* vol. 45, no. 2, pp. 261, 2008.
[110] B. Bigland‐Ritchie, and J. J. Woods, "Changes in muscle contractile properties and neural control during human muscular fatigue," *Muscle & nerve,* vol. 7, no. 9, pp. 691-699, 1984.
[111] U. M. Svantesson, K. S. Sunnerhagen, U. S. Carlsson *et al.*, "Development of fatigue during repeated eccentric-concentric muscle contractions of plantar flexors in patients with stroke," *Archives of Physical Medicine and Rehabilitation,* vol. 80, no. 10, pp. 1247-1252, 1999.
[112] N. A. Riley, and M. Bilodeau, "Changes in upper limb joint torque patterns and EMG signals with fatigue following a stroke," *Disability & Rehabilitation,* vol. 24, no. 18, pp. 961-969, 2002.
[113] W. F. Brown, "Functional compensation of human motor units in health and disease," *Journal of the Neurological Sciences,* vol. 20, no. 2, pp. 199-209, 1973.
[114] Y. Hara, K. Akaboshi, Y. Masakado *et al.*, "Physiologic decrease of single thenar motor units in the F-response in stroke patients," *Archives of Physical Medicine and Rehabilitation,* vol. 81, no. 4, pp. 418-423, 2000.
[115] Y. Hara, Y. Masakado, and N. Chino, "The physiological functional loss of single thenar motor units in the stroke patients: when does it occur? Does it progress?," *Clinical Neurophysiology,* vol. 115, no. 1, pp. 97-103, 2004.
[116] http://seniam.org/sensor_location.htm.
[117] E. A. Clancy, E. L. Morin, and R. Merletti, "Sampling, noise-reduction and amplitude estimation issues in surface electromyography," *Journal of Electromyography and Kinesiology,* vol. 12, no. 1, pp. 1-16, 2002.
[118] L. Cohen, *Time Frequency Analysis: Theory and Applications*: Prentice Hall, 1995.
[119] http://person.hst.aau.dk/enk/ST8/wavelet_tutotial.pdf.
[120] P. Coorevits, L. Danneels, D. Cambier *et al.*, "Correlations between short-time Fourier- and continuous wavelet transforms in the analysis of localized back and hip muscle fatigue during isometric contractions," *Journal of Electromyography and Kinesiology,* vol. 18, no. 4, pp. 637-644, 2008.
[121] A. Phinyomark, C. Limsakul, and P. Phukpattaranont, "A novel feature extraction for robust EMG pattern recognition," *arXiv preprint arXiv:0912.3973*, 2009.
[122] C. J. De Luca, L. Donald Gilmore, M. Kuznetsov *et al.*, "Filtering the surface EMG signal: Movement artifact and baseline noise contamination," *Journal of Biomechanics,* vol. 43, no. 8, pp. 1573-1579, 2010.
[123] "http://en.wikipedia.org/wiki/Analysis_of_variance."
[124] C. Jensen, O. Vasseljen, and R. H. Westgaard, "The influence of electrode position on bipolar surface electromyogram recordings of the upper trapezius muscle," *European journal of applied physiology and occupational physiology,* vol. 67, no. 3, pp. 266-273, 1993.
[125] T. Corser, "Temporal Discrepancies in the Electromyographic Study of Rapid Movement," *Ergonomics,* vol. 17, no. 3, pp. 389-400, 1974/05/01, 1974.
[126] K. Hakkinen, and P. V. Komi, "Electromyographic and mechanical characteristics of human skeletal muscle during fatigue under voluntary and reflex conditions," *Electroencephalogr Clin Neurophysiol,* vol. 55, no. 4, pp. 436-44, 1983.

[127] R. M. Enoka, *Neuromechanics of human movement*: Human Kinetics Publishers, 2008.
[128] S. M. Kay, *Fundamentals of Statistical signal processing, Volume 2: Detection theory*: Prentice Hall PTR, 1998.
[129] W. I. Schöllhorn, "Applications of artificial neural nets in clinical biomechanics," *Clinical Biomechanics,* vol. 19, no. 9, pp. 876-898, 2004.
[130] E. Knutsson, "Gait control in hemiparesis," *Scandinavian journal of rehabilitation medicine,* vol. 13, no. 2-3, pp. 101, 1981.
[131] L. F. Teixeira-Salmela, S. Nadeau, I. Mcbride *et al.*, "Effects of muscle strengthening and physical conditioning training on temporal, kinematic and kinetic variables during gait in chronic stroke survivors," *Journal of Rehabilitation Medicine,* vol. 33, no. 2, pp. 53-60, 2001.
[132] A. R. Den Otter, A. C. H. Geurts, T. H. Mulder *et al.*, "Abnormalities in the temporal patterning of lower extremity muscle activity in hemiparetic gait," *Gait & Posture,* vol. 25, no. 3, pp. 342-352, 2007.
[133] T. M. Lubecki, B. Fengjun, C. Chee-Meng *et al.*, "Development of intuitive human-machine interface based on Electromyography for assistive robot (KAAD)." pp. 908-913.
[134] N. M. Salbach, N. E. Mayo, S. Wood-Dauphinee *et al.*, "A task-orientated intervention enhances walking distance and speed in the first year post stroke: a randomized controlled trial," *Clin Rehabil,* vol. 18, no. 5, pp. 509-19, 2004.
[135] J. F. Veneman, R. Kruidhof, E. E. G. Hekman *et al.*, "Design and Evaluation of the LOPES Exoskeleton Robot for Interactive Gait Rehabilitation," *Neural Systems and Rehabilitation Engineering, IEEE Transactions on,* vol. 15, no. 3, pp. 379-386, 2007.
[136] S. K. Banala, S. K. Agrawal, and J. P. Scholz, "Active Leg Exoskeleton (ALEX) for Gait Rehabilitation of Motor-Impaired Patients." pp. 401-407.
[137] R. Riener, L. Lunenburger, S. Jezernik *et al.*, "Patient-cooperative strategies for robot-aided treadmill training: first experimental results," *Neural Systems and Rehabilitation Engineering, IEEE Transactions on,* vol. 13, no. 3, pp. 380-394, 2005.
[138] T. Hayashi, H. Kawamoto, and Y. Sankai, "Control method of robot suit HAL working as operator's muscle using biological and dynamical information." pp. 3063-3068.
[139] J. E. Pratt, B. T. Krupp, C. J. Morse *et al.*, "The RoboKnee: an exoskeleton for enhancing strength and endurance during walking." pp. 2430-2435 Vol.3.
[140] C. J. WALSH, K. ENDO, and H. HERR, "A QUASI-PASSIVE LEG EXOSKELETON FOR LOAD-CARRYING AUGMENTATION," *International Journal of Humanoid Robotics,* vol. 04, no. 03, pp. 487-506, 2007.
[141] T. K. Chuan, M. Hartono, and N. Kumar, "Anthropometry of the Singaporean and Indonesian populations," *International Journal of Industrial Ergonomics,* vol. 40, no. 6, pp. 757-766, 2010.

LIST OF PUBLICATIONS

Journal Papers

[1]. Fengjun Bai, Tomasz Marek Lubecki, Chee Meng Chew, "Muscle Force Estimation with sEMG signals during Force-varying Muscle Contractions Using Wavelet Time-Frequency Analysis Method", in Biomedical Signal Processing and Control (Under review).

[2]. Fengjun Bai, Tomasz Marek Lubecki, Chee Meng Chew, "Novel Approach for Detecting Muscle Fatigue Using Continuous Wavelet Transform during Isometric and Dynamic Muscle Contractions", in Medical Engineering and Physics (Under review).

[3]. Fengjun Bai, Chee Meng Chew, "Stroke Patients Muscle Force Estimation with sEMG Signals during Varying Force Contractions: A Wavelet and ANN based Approach", in Biomedical Signal Processing and Control (Under review).

Conference Papers

[1]. Fengjun Bai, Tomasz Marek Lubecki, Chee Meng Chew, and Chee-Leong Teo, "Novel Time-Frequency Approach for Muscle Fatigue Detection Based on sEMG", in Biomedical Circuits and Systems (BioCAS), 2012 IEEE, pp. 364-67.

[2]. Fengjun Bai, Chee-Meng Chew, Jinfu Li, Bingquan Shen and Tomasz Marek Lubecki, "Muscle Force Estimation Method with Surface EMG for a Lower Extremities Rehabilitation Device", in IEEE international conference on rehabilitation robotics (ICORR), 2013.

[3]. Fengjun Bai, Chee-Meng Chew, "Muscle Force Estimation with Surface EMG during Dynamic Muscle Contractions: A Wavelet and ANN based Approach", in conference of the IEEE Engineering in Medicine and Biology Society (EMBC), 2013.

[4]. T. M. Lubecki, Bai Fengjun, Chew Chee-Meng, and Teo Chee Leong, "Development of Intuitive Human-Machine Interface Based on Electromyography for Assistive Robot (KAAD)," in System Integration (SII), 2011 IEEE/SICE International Symposium on, 2011, pp. 908-13.

[5]. F.J. Bai, C.M. Chew, T.M. Lubecki, B. Shen and J. Li, "Muscle Force Estimation using Continuous Wavelet Transform Analysis with Surface-Electromyography Signals", 2nd Singapore Rehabilitation Conference (SRC 2013).

[6]. B. Shen, J. Li, Bai Fengjun, C. M. Chew, "Motion Intent Recognition for Control of a Lower Extremity Assistive Device (Lead)", In Mechatronics and Automation (ICMA), 2013 IEEE International Conference on, 2023, pp. 926-31.

[7]. B. Shen, J. Li, Bai Fengjun, C. M. Chew, "Development and Control of a Lower Extremity Assistive Device for Gait Rehabilitation of Stroke Patients", in IEEE international conference on rehabilitation robotics (ICORR), 2013.